Effect of Temperature on Bond Strength of Reinforced Concrete Structure

By

Bappa Kumar Paul

A thesis report submitted to the Department of Civil Engineering, Khulna University of Engineering & Technology (KUET), Khulna, Bangladesh in partial fulfillment of the requirements for the degree of

Master of Science in Civil Engineering

Khulna University of Engineering & Technology
Khulna 9203, Bangladesh

April 2016

Declaration

This is to certify that the thesis work entitled “Effect of Temperature on Bond Strength of Reinforced Concrete Structure" has been carried out by Bappa Kumar Paul in the Department of Civil Engineering, Khulna University of Engineering & Technology, Khulna, Bangladesh. The above thesis work or any part of this work has not been submitted anywhere for the award of any degree or diploma.

Dr. Muhammad Harunur Rashid	Bappa Kumar Paul
Professor	Roll: 1201556

Approval

This is to certify that the thesis work submitted by Bappa Kumar Paul entitled " Effect of Temperature on Bond Strength of Reinforced Concrete Structure " has been approved by the board of examiners for the partial fulfillment of the requirements for the degree of Master of Science in Civil Engineering in the Department of Civil Engineering, Khulna University of Engineering & Technology, Khulna, Bangladesh in April 2016.

The Board of Examiners

1. _____ Chairman

Dr. Muhammad Harunur Rashid (Supervisor)
Professor
Dept. of Civil Engineering, KUET
Khulna 9203

2. _____

Dr. Muhammad Harunur Rashid Member
Head
Dept. of Civil Engineering, KUET
Khulna 9203

3. _____

Dr. Md. Keramat Ali Molla Member
Professor
Dept. of Civil Engineering, KUET
Khulna 9203

4. _____

Dr. Abu Zakir Morshed Member
Professor
Dept. of Civil Engineering, KUET
Khulna 9203

5. _____

Dr. Niamul Bari
Professor (External)
Dept. of Civil Engineering, RUET
Rajshahi

Acknowledgement

All praises belong to the God, the most kindhearted and bounteous to all His creatures and their actions.

The author would like to express his deepest appreciation to his supervisor Dr. Muhammad Harunur Rashid, Professor, Department of Civil Engineering, Khulna University of Engineering & Technology for his valuable advice, guidance, suggestion, patient and encouragement throughout the execution of this research program. His unfailing optimism and constant encouragement always prompted the author to overcome the difficulties in completing this research.

He would like to express his sincerely thanks to the Department of Civil Engineering in Khulna University of Engineering & Technology.

He is grateful and expresses special thanks to Milon Kanti Howlader, for his adorable attitude, exquisite inspiration and lend a hand in all stage of this project. Without his support, it was impossible to complete this research work within the time.

He gratefully expresses his acknowledgement to Grytan Sarkar, Masum Shaikh, Md. Ashiqur Rahman, and Md. Kamrul Ahsan for their mental support and encouragement.

Finally, He solemnly acknowledges his parents and brother, who gave him the utmost mental supports throughout his whole student life and make a way to build up his career in the field of Civil Engineering.

April 2016 Author

KUET, Khulna

Abstract

The study has been carried out to investigate the influence of temperature on bond behavior of reinforced concrete. The effects of casting temperature and curing temperature on various properties of concrete were investigated. Four different temperatures (20 ^{o}C, 30 ^{o}C, 45 ^{o}C and 60 ^{o}C) were maintained for this purpose. Locally available materials were used to prepare the specimens. To observe the effect of coating on bond stress, three different types of coating were used in this work such as red oxide, synthetic enamel paint and aluminum oxide. The study also investigates the temperature effect on corrosion of reinforced concrete. In this work, pullout test and electrochemical corrosion were performed as a major test program. To carry out these tests, 100 mm dia and 200 mm high cylindrical concretes were prepared. A 12 mm dia MS bar was placed vertically at the center concrete layer. Bond stress measurement under different temperatures and coatings were the major findings of this work. Test results explained that volume of void increased with the increment of temperature. Result of bond strength showed 20% better performance for lower casting and curing temperature compared to higher temperature. Application of coating on rebar surface did not give satisfactory result of bond stress compared to non-coated rebar. 20 ^{o}C temperature induced specimens increase the time of corrosion crack initiation and decrease the penetration rate than 60^{o}C temperature induced specimens. Coatings significantly showed a good agreements for corrosion effect on reinforced concrete. Among three coatings, aluminum oxide revealed better performance against pullout test and electrochemical corrosion test. Finally, it can be concluded that temperature at 20 ^{o}C gives significant bond stress and provides better protection for corrosion than 60 ^{o}C temperature.

Contents

List of Figure

List of Table

List of Abbreviation

R	Gas law constant
I	Current
F	Faraday's constant
W_i	Initial mass loss
W_f	Final mass loss
P	Compressive force
L	Length of concrete cylinder
A	Mass of oven-dried sample in air, g
B	Mass of surface-dry sample in air after immersion, g
C	Mass of surface-dry sample in air after immersion and boiling, g
D	Apparent mass of sample in water after immersion and boiling, g
T	Corrosion time
σ	Compressive strength
τ	Bond strength
d	diameter of concrete cylinder
ρ	Resistivity
g_1	Dry bulk density
g_2	Apparent density

CHAPTER I

Introduction

1.1 Background

Reinforced concrete is commonly used as a well composite material in Civil Engineering Project, where plain concrete carries compressive stress and reinforcing steel takes tensile stress. Composite member made with concrete and reinforcing steel gives better stiffness, strength and durability. Composite action of steel and concrete in reinforced concrete structure depends on bond at interface between steel and concrete.

There are many factors which influence the quality of concrete. Among them temperature has a remarkable effect on the performance of concrete structure. Cement hydration at higher temperature is accelerated at early ages, but decelerated later on (Kim and Soo ., 2010). When water come to contract with cement hydrates then the reactants dissolve first and produce ions in solution. The reactions take place on the outer face of the hydrating cement particle. With time, it arrives at the center of the cement grain and produces a porous layer on the outer side. The thickness of the encapsulated cement grain layers increase as the hydration proceeds and the cement grains come closer. At a certain stage friction is increased between hydrating grain as well as the paste becomes brittle (Soroka, 2004). Cement hydration is an exothermic reaction. With a rise in temperature, the rate of chemical reaction of cement hydration also increases. The high rate of hydration generates greater thickness of the layer that hinders further diffusion of water. As a result, hydration can cease even in the presence of sufficient water. It induces the non-uniform distribution of hydration product across the microstructure. It declines the rate of hydration with age of cement paste.

Ambient temperature directly influences the setting time. As a result of the accelerated hydration, initial and final setting times are both reduced with the rise in temperature (Soroka, 2004). Concrete which is placed at low environmental temperature develops higher ultimate strength, greater durability and is less susceptible to thermal cracking (ACI 306R-88). Under hot environmental conditions more water is required for a given mix to have the same slump

(consistency). A 25 mm decrease in slump was brought about by a 10°C increase in concrete temperature (Klieger, P., 1958). The rate of reaction at 35°C is about twice of that at 20°C which is, in itself, about twice of that at 10°C (Newman and Choo, 2003). Rate of evaporation also increases with temperature that is accelerated the concrete mixture to get stiffen and produces poor workable concrete mixture.

High ambient temperature also affects the long term concrete strength due to rapid setting, low workability and thermal cracking. Compressive strength is considered to be a significant parameter in bond behavior because the force between steel and concrete is transferred mainly by bearing and bond (Orangun, et al., 1977). Micro cracks are controlled by the tensile stresses of the concrete and bearing stresses are increased in the front of the ribs by high compressive strength. Bond stress is proportional to the compressive strength of concrete (Alavi-Fard and Marzouk, 2002).

All materials expand with temperature for its own thermal expansion coefficient. Like as, volume of water increase approximately 1% for every 20 ^{o}C raise from 4 ^{o}C where its density is maximum. So the volume of concrete is larger at the time of setting. Changes in temperature and moisture content of concrete induce volumetric deformation (Kianoush, et al., 2008). Concrete is a poor heat conductor. The rate of heat evolution due to hydration of cement is much greater than the rate of heat dissipation. The slope of heat evolution and dissipation both are higher at high temperature. The varying rate of heat generation and dissipation causes the interior of a concrete to get hotter than its surface. This generates thermal stresses in the concrete. Thermal cracking is a durability issue because it provides pathways for air and water to reach the reinforcing steel and initiate corrosion. Normal air contains remain 0·03% carbon dioxide (CO_2) by volume. As the temperature goes up, diffusivity of CO_2 increases due to increase energy. The capillary pore system of the cement paste allows air to penetrate into the concrete and the CO_2 of the air combines with the calcium hydroxide to give calcium carbonate ($CaCO_3$). The transformation of the $Ca(OH)_2$ to $CaCO_3$ lowers the pH of the pore water to less than 9 in a fully carbonated concrete (Soroka, 2004). The passive film protecting the reinforcement steel can be disrupted by two mechanisms: carbonation and chloride induced corrosion. Disruption of passive film initiates corrosion of reinforcing steel. The volume of corrosion products may be more than six times larger than the volume of iron. This expansion causes tensile stress in the hardened cement paste that leads to cracking, eventual loss of concrete cover, and serious deterioration of structural concrete. A 25 μm uniform corrosion on

the anodic length of reinforcement can produce crack of reinforced concrete (Pfeifer, 2000). Corrosion has a significant influence on the bonding performance of steel reinforced concrete. About 50% reductions in bond strength were observed associated with a 16% reduction in average cross-section due to corrosion (Kivell, et al., 2011). In addition to cracking, the reduction of the steel cross section, possible loss of steel ductility, and reduced bond strength are all possible consequences of reinforcement corrosion that can lead to serviceability problems and structural failures (Andrade and Alonso, 2001).

1.2 Objectives

The objectives of this research are as follow:

1. To investigate the effect of temperature on bond strength-slip relationship between reinforcing bar and concrete.
2. To find out the effect of temperature on corrosion of reinforced concrete.
3. To observe the effect of color coating of reinforcing bar on bond strength and corrosion
4. To assess the propagation of concrete crack due to corrosion at different temperatures.

1.3 Justification of Work

Atmospheric temperature is increasing day by day in this subcontinent. Temperature has great impact on freshly mixed concrete. Properties of concrete like as cement hydration, setting, workability are depend on temperature. These are the factor of mechanical properties of concrete. Otherwise, bond strength is the vital issue for composite materials. Also, in reinforced concrete structure, bond is function of bearing at steel concrete interface. And bearing stress is proportional to concrete strength. So, the research interest has been grown up to realize the temperature effect on concrete and its durability as well as the importance of bond behavior.

1.4 Scope and Limitations of This Study

This research work has been carried out by four different temperatures such as 20 ^{o}C, 30 ^{o}C, 45 ^{o}C and 60 ^{o}C. This study specially focused on the bonding performance of reinforced concrete under four different temperatures. Two different types of Portland cement and two different types of coarse aggregate have been used in this research work. Total 128 specific reinforced concrete cylinders have been made to perform this work. It also emphasized on the

steel corrosion of reinforced concrete for four different temperatures. Extent of corrosion, corrosion rate, current density, propagation of concrete crack have been measured in this work. Three types of color coating such as red oxide, synthetic enamel paint and aluminum oxide were used to execute the work. Those were applied on the surface of the reinforcing steel that have been added a new dimension in this study. Effectiveness of color coating on bond strength and corrosion of reinforced concrete have also been measured. This results can be insured the performance of those coating as an alternatives way to protect the reinforcing steel from severe environmental condition. This results also can be insured the bond behavior between steel and concrete.

Limitation of this work is to measure the corrosion crack of concrete with linear millimeter scale. For this reason, digital image analysis had to perform by AutoCAD software to determine sophisticated crack width that was time consuming job.

1.5 Organization of the Thesis

Chapter I: Introduction

It provides background of this study, objectives along with scope and limitations and methodology of this program.

Chapter II: Review of Literature

It focuses on the available literature related to the thesis topic that would help to understand the thesis. Brief discussions on several techniques and parameters, used to describe the temperature effect on strength properties of concrete, corrosion and corrosion techniques, bond stress and its mechanism, coating effect on bond performance of reinforced concrete were also reviewed in this chapter to conduct the study.

Chapter III: Methods and Materials

It describes the detailed methodology adopted to accomplish this study. Accelerated corrosion, pullout specimen features of the study area were also reviewed in this chapter. Also, the procedure for analyzing the results is explained in this chapter.

Chapter IV: Results and Discussion

It reveals the results and findings of the study including graphs and tables and their interpretations

Chapter V: Conclusions and Recommendations

It presents the summary of the thesis, the conclusions of the study and the recommendations provided for further extensions of the work.

CHAPTER II

Review of Literature

2.1 General

Before presenting the details of testing program, it is important to review the state of the art regarding temperature of concrete, temperature effect on strength properties of concrete, corrosion and corrosion process, environmental effect of corrosion on reinforced concrete, bond stress and its mechanism, bond strength parameter, failure type of bond, coating and coating effect on bond of reinforced concrete.

2.2 Temperature of Concrete

Portland cement hydration is affected by many variables, including chemical composition, the water/cement ratio, the presence of mineral additions and fineness. Yet another variable, however, is regarded to play a key role, bearing on early hydration kinetics and the properties of the hardened cement paste: that variable is temperature. Recommendation of ACI 318-02 (section 5.13), “Building code requirement for Structural Concrete” is “During hot weather, proper attention shall be given to ingredients, production methods, handling, placing, protection, and curing to prevent 'excessive concrete temperatures or water evaporation that could impair required strength or serviceability of the member of structure. Recommendation of ACI 305R-91 (section 1.2) "In the more general types of hot-weather construction, it is impractical to recommend a maximum limiting ambient or concrete temperature because circumstances vary widely. Accordingly, the effects of higher temperatures in concrete as mentioned in 2.2.1, and advise that at some temperature between about 75 and 100 ºF (24 and 38 ºC) there is a limit that will be found to be most favorable for best results in each hot weather operation, and such a limit should be determined for the work.

2.2.1 Hot weather concrete

Hot weather concrete tends to impair the quality of freshly mixed or hardened concrete by accelerating the rate of moisture loss and rate of cement hydration. Otherwise it can be

obtained high ambient temperature, high concrete temperature, low relative humidity, wind speed and solar radiation.

Potential problems for concrete in the freshly mixed state are likely to include:

- Increased water demand
- Increased rate of slump loss and corresponding tendency to add water at the job site
- Increased rate of setting, resulting in greater difficulty with handling, compacting, and finishing, and a greater risk of cold joints
- Increased tendency for plastic-shrinkage cracking and
- Increased difficulty in controlling entrained air content

Potential deficiencies to concrete in the hardened state may include:

- Decreased 28-day and later strengths resulting from either higher water demand, higher concrete temperature, or both at time of placement or during the first several days
- Increased tendency for drying shrinkage and differential thermal cracking from either cooling of the overall structure
- Decreased durability resulting from cracking
- Greater variability of surface appearance,
- Increased potential for reinforcing steel corrosion making possible the ingress of corrosive solutions and
- Increased permeability as a result of high water content, inadequate curing, carbonation, lightweight aggregates, or improper matrix-aggregate proportions

Other factors that should be considered along with climatic factors may include:

- Use of cements with increased rate of hydration
- Use of high-compressive-strength concrete, which requires higher cement contents
- Design of thin concrete sections with correspondingly greater percentages of steel, which complicate placing and consolidation of concrete
- Economic necessity to continue work in extremely hot weather and

2.2.2 Cold weather concrete

Cold weather is defined as a period when more than 3 consecutive days, the following conditions exist: a) average daily air temperature is less than 40 ^{o}F (5 ^{o}C) and b) the air temperature is not greater than 50 ^{o}F (10 ^{o}C) for more than one-half of any 24-hr period. The

average daily air temperature is the average of the highest and the lowest temperatures occurring during the period from midnight to midnight. Concrete may suffer permanent damage if its temperature falls below 0 °C before it is mature enough to resist disruption by freezing. BS 8110 goes on to say that the temperature of the concrete should at no point falls below 5 °C until it reaches a strength of 5 N/mm^2.

Potential problems for concrete in the freshly mixed state are likely to include:

- Water begins to freeze in capillaries of concrete at 28 ^oF
- Water expands up to 9% of its volume when it freezes causing cracks in the concrete mix.
- Up to 50% strength reduction can occur if concrete freezes before reaching 500 psi.
- Formation of ice crystals in concrete
- Increased thermal cracking
- Slower gain in strength
- Slower setting
- Delayed formwork removal

2.3 Temperature Effect on Concrete Strength Property

2.3.1 Setting and hardening

Process of cement setting and hardening can be depicted from three different points of view—

a) Phenomenological
b) Chemical and
c) Structural

Phenomenological point of view: It is concerned with the changes in the cement-water system (or the concrete) which are only perceptible to or evidenced by the senses.

Chemical point of view: It is concerned with the chemical reactions involved and the nature and composition of the reactions products.

Structural point of view: It is concerned with the structure of the set cement and with the possible changes in this structure with time (Soroka, 1979). Figure- 2.1 explains the setting and hardening procedure of the cement paste.

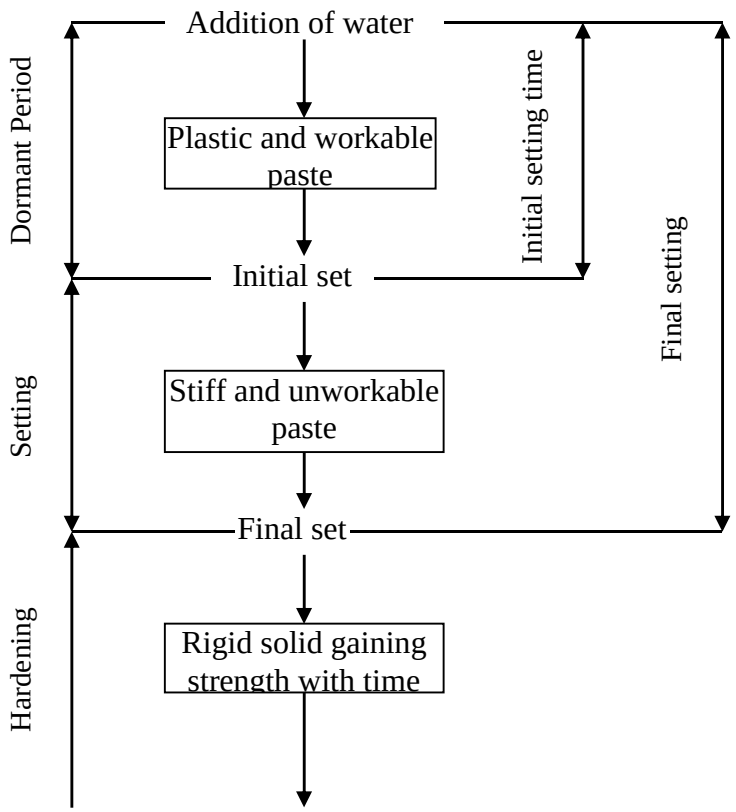

Figure 2.1: Schematic description of setting and hardening of the cement paste.

Mixing cement with water produces a plastic and workable mix, commonly referred to as a cement paste. These properties of the mix remain unchanged for some time, a period which is known as the dormant period. At a certain stage, however, the paste stiffens to such a degree that it loses its plasticity and becomes brittle and unworkable. This is known as the initial set, and the time required for the paste to reach this stage as the initial setting time. A setting period follows, during which the paste continues to stiffen until it becomes a rigid solid, i.e. final set is reached. Similarly, the time required for the paste to reach final set is known as final setting time. The resulting solid is known as the set cement or the hardened cement paste. The hardened paste continues to gain strength with time, a process which is known as hardening (Powers, 1962).

The initial and final setting times have a practical importance. The initial setting time determines the length of time in which cement mixers, including concrete, remain plastic and workable, and can be handled and used on the building site. Final setting time is required in order to allow the construction work to continue within a reasonable time after placing and finishing the concrete. Finally setting time is affected by ambient temperature. Low concrete

temperature has a major effect on the rate of cement hydration which results in slower setting time and rate of strength gain of concrete during cold weather typically delays finishing operations and form removal. As a result of the accelerated hydration, initial and final setting times are both reduced with the rise in temperature. It can be seen that a 14°C rise in temperature from 10 to 24°C reduced the initial setting time by 8 h while the same rise in temperature from 24 to 38°C reduced the latter by 5 h only (Tuthill and Cordon, 1955).

2.3.2 Hydration process

In contact with water the cement hydrates (i.e. combines with water) to give a porous solid usually defined as a rigid gel. Generally, chemical reactions may take place either by a through solution or by a topochemical mechanism. In the first case, the reactants dissolve and produce ions in solution. The ions then combine and the resulting products precipitate from the solution. In the second case, the reactions take place on the surface of the solid without its constituents going into solution. Hence, reference is made to topochemical or liquid-solid reactions. In the hydration of the cement both mechanisms are involved. It is usually accepted that the through-solution mechanism predominates in the early stages of the hydration, whereas the topochemical mechanism predominates during the later ones.

Consequently, the hydration products are deposited on the surface and form a dense layer which encapsulates the cement grains. As the hydration proceeds, the thickness of the layer increases, and the rate of hydration decreases because it is conditional, to a great extent, on the diffusion of water through the layer. That is, the greater the thickness of the layer, the slower the hydration rate explaining, in turn, the nature of the observed decline in the rate of hydration with time (Figure- 2.3). Moreover, it is to be expected that, after some time, a thickness is reached which hinders further diffusion of water, and thereby causes the hydration to cease even in the presence of a sufficient amount of water.

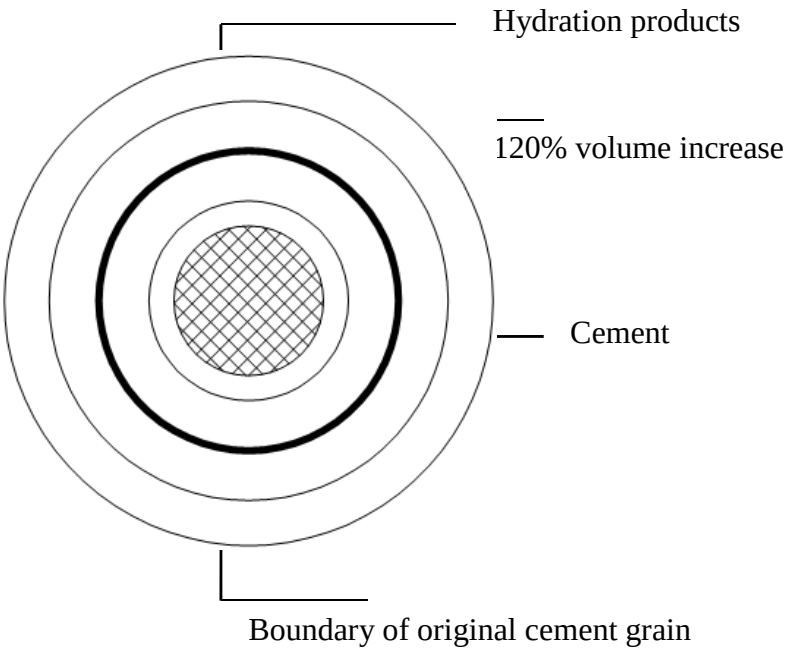

Figure 2.2: Schematic description of the hydration of a cement grain

The total volume of the hydration products is some 2·2 times greater than the volume of the un- hydrated cement (Fig. 2.2) and, consequently, the spacing between the cement grains decreases as the hydration proceeds. Nevertheless, for some time, the grains remain separated by a layer of water and the paste retains its plasticity and workability.

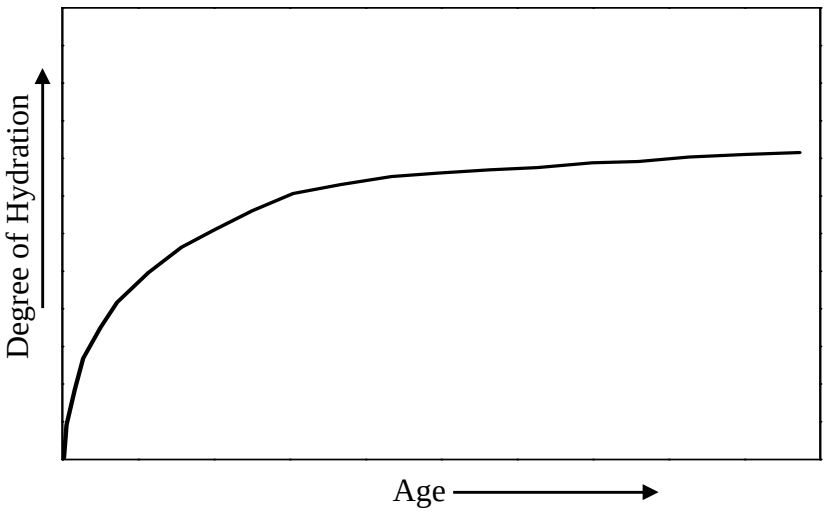

Figure 2.3: Schematic description of the relation between the degree of hydration and time.

As the hydration precedes the spacing between the cement grains further decreases, and at a certain stage friction between the hydrating grains is increased to such an extent that the paste becomes brittle and unworkable, i.e. initial set is reached. On further hydration, bonds begin to

form at the contact points of the hydrating grains, and bring about continuity in the structure of the cement paste. Consequently, the paste gradually stiffens and subsequently becomes a porous solid, i.e. final set is reached. The resulting solid is characterized by a continuous pore system usually known as capillary porosity. If water is available, the hydration continues and the capillary porosity decreases due to the formation of additional hydration products. It is to be expected that this decrease in porosity will result in a corresponding increase in the paste strength. Structure formation in the hydrating cement paste is schematically described in Figure- 2.4.

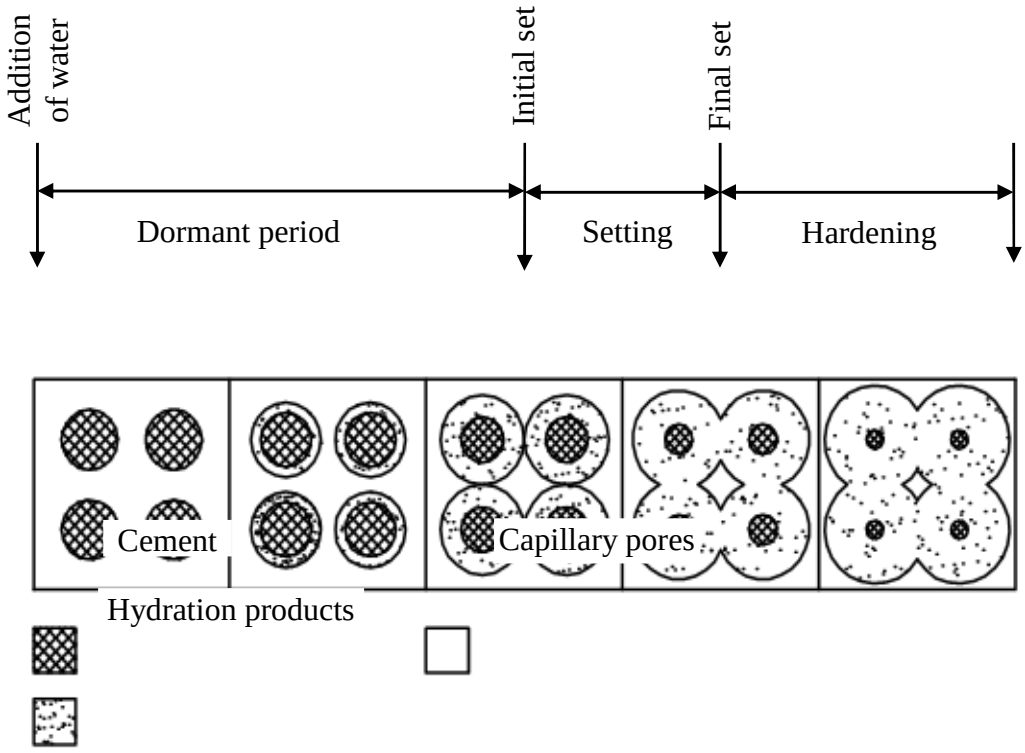

Figure 2.4: Schematic description of structure formation in a cement paste

The rate of chemical reactions, in general, increase with a rise in temperature, provided there is a continuous and uninterrupted supply of the reactants. This effect of temperature usually obeys the following empirical equation which is known as the Arrhenius equation:

$$\frac{d(\ln k)}{dT} = A / RT^2$$

in which k is the specific reaction velocity, T is the absolute temperature, A is a constant usually referred to as the energy of activation, and R is the gas law constant, i.e. R=8·314J/mol° C.

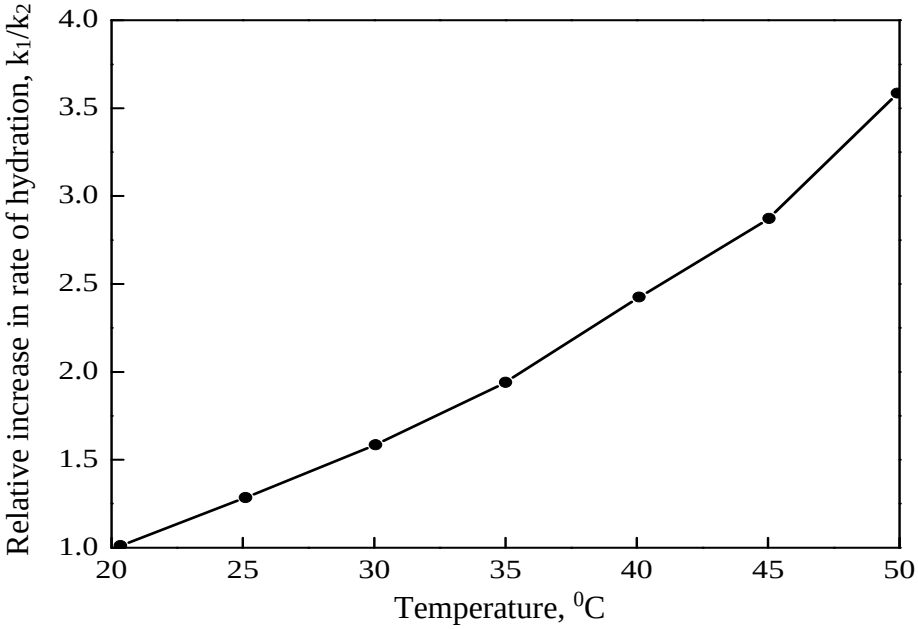

Figure 2.5: Effect of temperature on the hydration rate of Portland cement in accordance with the Arrhenius equation

It can be shown that, based on the former equation, the ratio between the rates of hydration k1/k2 at the temperatures T1 and T2, respectively, is given by the following equation:

$$2.303 \log (k1/k2) = - A/R (1/T_1 – 1/T_2)$$

In the temperature range above 20°C, the energy of activation for Portland cement may be assumed to equal 33500J/mol (Hansen and Pedersen, 1984). Solving the equation accordingly (Figure 2.5), it follows that the rise in the hydration temperature from T_1=20 °C to T_2=30, 40 and 50 °C, will increase the hydration rate by factors of 1·57, 2·41, and 3·59, respectively. That is, the accelerating effect of temperature on the hydration rate of Portland cement is very significant indeed. This expected accelerating effect of temperature is experienced, of course, in everyday practice and is supported by a considerable body of experimental data. It is clearly demonstrated, for example, in Figure 2.6 in which the degree of hydration is expressed by the amount of the chemically bound water. Indeed, this accelerating effect of temperature is well known and recognized, and is widely utilized to accelerate strength development in concrete.

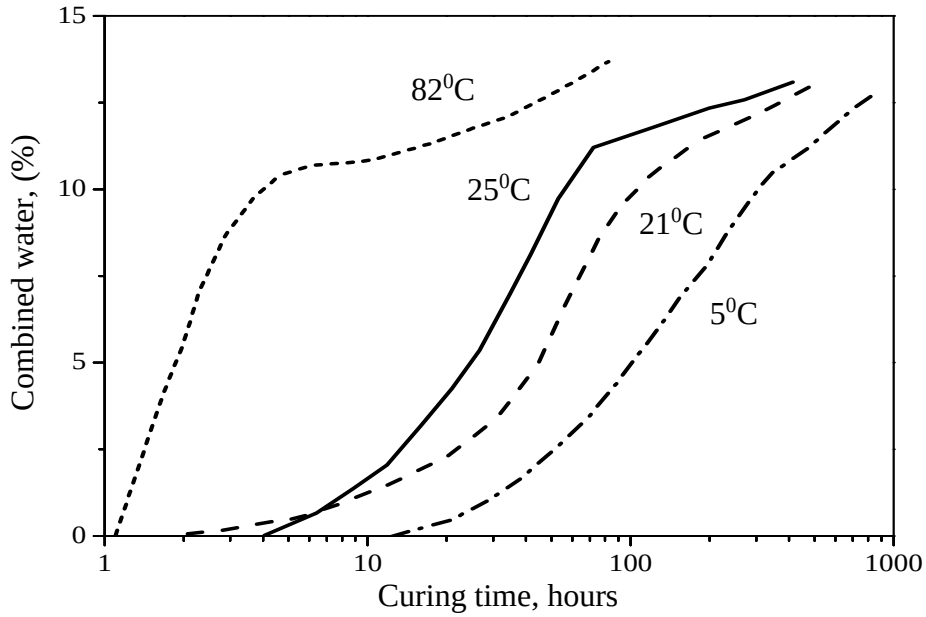

Figure 2.6: Effect of temperature on the rate of hydration.

The ultimate degree of hydration increases with temperature while other data indicate the opposite, i.e. that the ultimate degree of hydration decreases (Idorn, 1968).

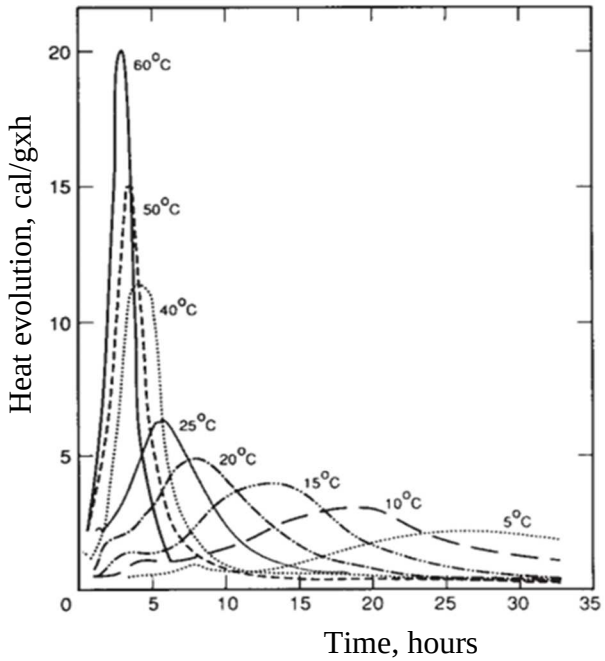

Figure 2.7: Effect of temperature on heat evolution in the hydration of C_3S (1 cal=4·2J)

Concrete is a poor heat conductor, and the rate of heat evolution due to the hydration of the cement is, therefore, much greater than the rate of heat dissipation and, consequently, the temperature inside the concrete rises. With time, however, the inner concrete cools off and

contracts, but this contraction is restrained to a greater or lesser extent. Restrained contraction results in tensile stresses, and this restraint may cause cracking if, and when, the tensile strength of the concrete at the time considered is lower than the induced stresses (Courtault and Longuet, 1982) .

2.3.3 Workability

The 'workability' of concrete may be defined as 'the property determining the effort required to manipulate a freshly mixed quantity of concrete with minimum loss homogeneity'. In this definition the term 'manipulate' is meant to include all the operations involved in handling the fresh concrete, namely, transporting, placing, compacting and also, in some cases, finishing. In other words, workability is that property which makes the fresh concrete easy to handle and compact without an appreciable risk of segregation.

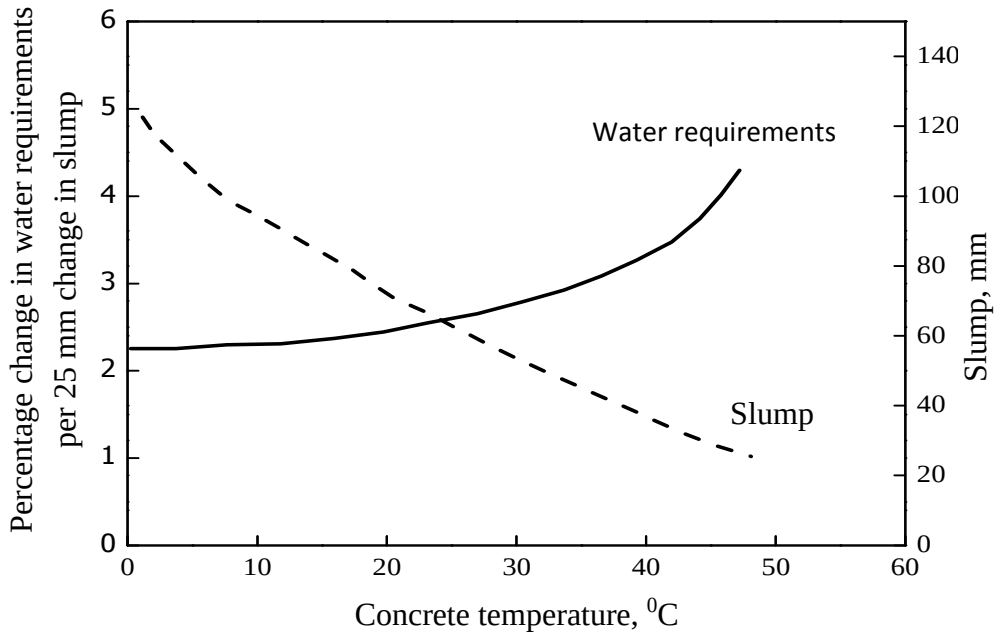

Figure 2.8: Effect of concrete temperature on slump and amount of water required to change slump

It is well known that under hot weather conditions more water is required for a given mix to have the same slump, i.e. the same consistency. Approximately a 25 mm decrease in slump was brought about by a 10 °C increase in concrete temperature. Alternatively, it is indicated in Figure 2.9 that the water demand increases by 6·5 kg/m^3 for a rise of 10 °C in concrete

temperature. An increase of 4·6 kg/m^3 for the same change in temperature has been reported by others (Yamamoto and Kobayashi, 1986).

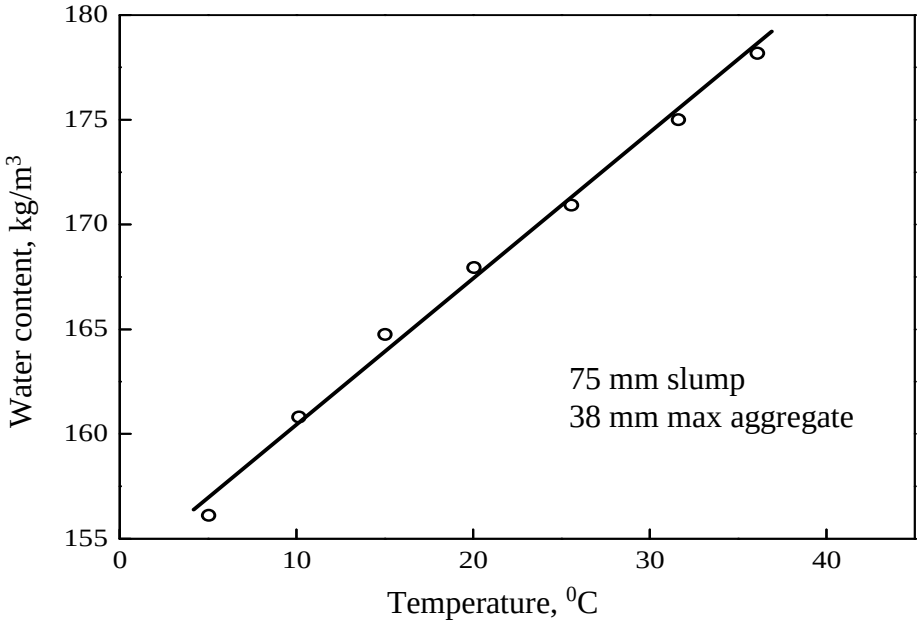

Figure 2.9: Effect of concrete temperature on the amount of water required to produce 75 mm slump in a typical concrete.

The effect of temperature on water demand is mainly brought about by its effect on the rate of the cement hydration (Mahter, 1987), and possibly also on the rate of water evaporation. The slump data of Figure- 2.8 and 2.9 refer to the initial slump, i.e. to the slump determined as soon as possible after the mixing operation is completed. Nevertheless, some time elapses between the moment the water is added to the mix and the moment the slump is determined. The cement hydrates during this period and some water evaporates. Consequently, the mix somewhat stiffens and its slump, therefore, decreases. As the rates of hydration and evaporation both increase with temperature, the associated stiffening is accelerated, and the resulting slump loss is, accordingly, increased. Hence, if a certain initial slump is required, a wetter mix must be prepared in order to allow for the greater slump loss which takes place when the concrete is prepared under higher temperatures. In other words, under such conditions, a greater amount of water must be added to the mix explaining, in turn, the increase in water demand with temperature.

2.3.4 Curing

The hardening of concrete is a chemical reaction – the rate of this reaction increases with temperature but so does the rate of evaporation from an exposed concrete surface. The rate of reaction at 35 °C is about twice that at 20 °C which is, in itself, about twice that at 10 °C (Newman and Choo, 2003). The ultimate strength of concrete cured at low temperature (e.g. in winter) is generally greater than that of concrete cured at a higher temperature (e.g. in summer); but extremes of temperature generally have a negative effect. The slow rate of reaction at low temperatures means the concrete must be cured for a longer period to achieve the desired degree of reaction. The fast rate of reaction at high temperatures gives relatively high early strengths but the long-term strength and durability are generally reduced (Newman and Choo, 2003).

The optimum temperature required to produce the maximum 28-day strength, based on small laboratory specimens, is said to be approximately 13 °C (Neville and Brooks, 1987) and ambient temperatures of 15–25 °C are generally considered to be most suitable for concreting operations. Concrete allowed to freeze before a certain minimum degree of hardening has been achieved will be permanently damaged by the disruption from the expansion of the water within the concrete as it freezes. This will result in irretrievable strength loss. Excessive evaporation from an exposed horizontal surface within the first approximately 24 hours after casting will result in plastic shrinkage cracking and a weak, dusty surface. An excessive temperature difference through the cross-section of an element will result in early thermal cracking due to restraint to contraction of the cooling outer layers from the warmer inner concrete. Inadequate curing will result in the properties of the surface layer of concrete, up to 30–50 mm, not meeting the intentions of the designer in terms of durability, strength and abrasion resistance (Newman and Choo, 2003).

2.3.5 Concrete strength

Temperature affects concrete strength through its effect on (i) the rate of hydration, (ii) the nature of concrete structure, and (iii) the rate of evaporation and the resulting drying out of the concrete. It may be noted that the preceding effects may be of a contradictory nature. Temperature, for example, accelerates hydration, and thereby the development of concrete strength. On the other hand, the increased rate of evaporation, associated with elevated temperatures, reduces the amount of water available, and thereby retards the rate of hydration and may even cause its complete cessation. Hence, in practice, the combined effect of

temperature on strength varies and depends on the specific conditions considered. The rate of cement hydration is considerably increased with the rise in temperature. As the strength of concrete depends on the porosity of the cement paste, and porosity, in turn, is determined by the degree of hydration, it is to be expected that the rate of strength development and concrete early-age strength will both increase with the rise in temperature as well. On the other hand, assuming that the effect of temperature on ultimate degree of hydration is small and provided the concrete is not allowed to dry, concrete later-age strength is not expected to be greatly temperature-dependent. That is, identical concretes, exposed to different temperatures, are expected to exhibit essentially the same later-age strength. It has been demonstrated, however, that while concrete cast and initially cured at high temperatures exhibits the expected increased early- age strength, its later-age strength is adversely affected when, in this context, 'early-age' generally refers to ages up to 7 days and 'later-age' to ages over, say, 28 days .

2.4 Corrosion

Corrosion of reinforcing steel is widely accepted as the primary cause of premature deterioration in the reinforced concrete structures. Corrosion is defined as the destruction or deterioration of a material because of its reaction with environment. In case of corrosion, formation of an oxide of iron due to oxidation of the iron atoms in solid solution is a well known example of electrochemical corrosion, commonly known as rusting. These oxides are loosely attached and spall off from the surface of steel. During the process of corrosion, weight of material decreases as depth of corrosion layer/pits increases. The magnitude of reinforcement corrosion has a significant effect on flexural strength, deformational behavior, ductility, bond strength and mode of failure of reinforced concrete structures (Shetty, et al., 2011).

The formation of the corrosion products of iron (i.e. rust) involves a substantial volume increase, i.e. the volume of the corrosion products, assuming they are mainly $Fe(OH)_3$, is some four times greater than that of the corroding iron. In reinforced concrete, such an expansion is subjected to volume restraint and, therefore, when rust is formed, pressure is exerted on the surrounding concrete. At some stage, this pressure may cause the cracking of the concrete cover over the reinforcement, and the corrosion is then aggravated due to the readily available oxygen and moisture, which are conditional for the corrosion process to precede. At a more advanced stage, spalling of the concrete cover occurs, and the unprotected reinforcement is exposed to

environmental factors. The continued corrosion of the reinforcement gradually reduces the cross-sectional area of the reinforcing bars (Wierig, 1984).

2.4.1 Different theories of corrosion

There are mainly three theories of corrosion. They are-

(i) acid theory

(ii) dry or chemical corrosion and

(iii) galvanic or electrochemical or wet corrosion

2.4.2 Classification of corrosion

There are different types of corrosions based on the reactions and physical states. It has been seen that there are several types of corrosion. They are-

1. General (Uniform) Corrosion
   a) Uniform thinning over the exposed surface
   b) Estimation of life expectancy with reasonable accuracy
2. Localized Corrosion
   a) Galvanic corrosion: Two dissimilar metals in contact in the presence of an electrolyte
   b) Pit corrosion: Corrosion in steel bars starts by forming a small pit. After that, the number of pits
      will increase with time and then the combination of these pits causes a uniform corrosion on the surface of the steel bars.
   c) Crevice corrosion: Special type of pitting with the geometry of crevice .Wide enough to permit entry of the liquid, but narrow enough to maintain a stagnant zone
   d) Selective leaching (Parting, De-alloying)
   e) Erosion corrosion: Acceleration of metal loss (mechanical wear) due to the relative movement between a fluid and a metal surface. Removal of passive surface film for corrosion resistance
   f) Inter-granular corrosion: Selective attack of grain boundary
3. Cracking
   a) Corrosion fatigue: Initiated at surface defects, pits, or irregularities
   b) Stress corrosion cracking: Combined action of static tensile stress and corrosion
   c) Hydrogen damage: Diffusion of atomic hydrogen into the metal collected at internal voids or laminations to form more voluminous molecular hydrogen.
4. Exfoliation: Leaves metals in a laminated, flaky, or blistered condition

2.4.3 Concrete resistivity

The electrical resistivity of concrete is a material property that is useful for monitoring and inspection of concrete structures with regard to reinforcement corrosion in combination with other non-destructive techniques. Concrete resistivity is a geometry-independent property that describes the electrical resistance, which is the ratio between a voltage applied on the specimen and resulting current in a unit cell. In concrete, the current is carried by ions in the pore solution. More pores water (wet concrete) as well as more and larger pores with a high degree of connectivity and a low tortuosity (high water-binder ratio) cause a lower resistance to ionic and electric flow. For a constant relative humidity and in stationary conditions, resistivity is increased by a lower water-binder ratio, extended curing time or the addition of supplementary cementtitious materials e.g. flies ash, blast furnace slag or silica fume. Resistivity is influenced by both moisture content inside the specimen and the porosity of the cement matrix. As it was discussed before, moisture transport in concrete is relatively slow for the bulk specimen. In the surface (down to approx. 20 mm depth) the moisture content depends mostly on the environmental conditions (exposure) of the specimens. Temperature also has a significant impact in the behavior of concrete electrical resistivity. When temperature is low near or below freezing point, the mobility of ions is reduced. Therefore, ionic flow is decreased.

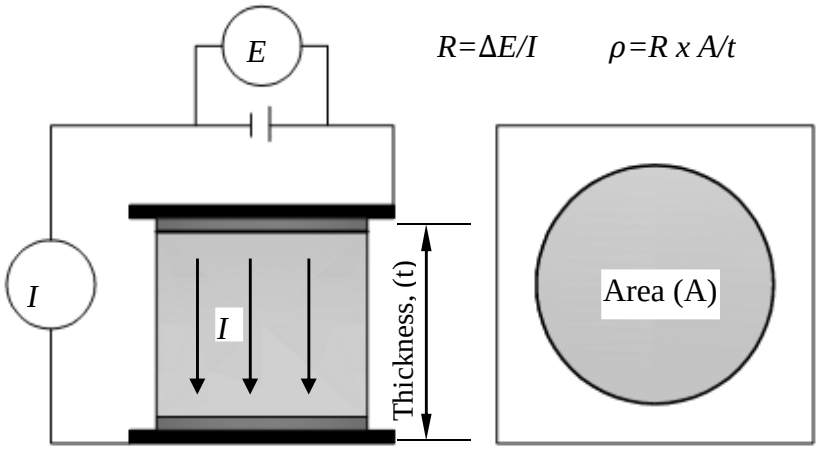

Figure 2.10: Measurement of concrete resistivity

The resistivity is calculated by using the formula

$$\rho = A \times R_2$$

With ρ as the concrete resistivity (Ωm), A is a cell constant which depends on the geometry of the specimen and the arrangement of steel reinforcement and R_2 is the electrical resistance measured with a voltmeter in AC to avoid electrode polarization.

2.4.4 Passive layer

Concrete is a high concentration of the oxides calcium, sodium, and magnesium. These oxides produce hydroxides that have a high alkalinity when water is added with a pH ranging from 12.6 to 13.8. At this pH level, a protective film is spontaneously formed during the early stages of cement hydration. This protective film is known as passive layer. This passive film may grow to a thickness of the order of 10^{-3} to 10^{-1} micro- ohm and contains hydrated iron oxides (Smith, 2007). The process by which steel in concrete is protected from corrosion by formation of passive layer due to high alkaline environment created by pore water is defined as passivation. Passive layer is dense and prevents the occurrence of corrosion. This layer will not remain for long. Two factors always have an effect in breaking it: the carbonation process and the permeability of chlorides to the steel reinforcement.

2.4.5 Corrosion process

Corrosion of reinforcing steel embedded in concrete is an electrochemical process that requires an anode, a cathode, an electrolyte, and an electrical connection between the anode and cathode for the transfer of electrons. Coupled anodic and cathodic reactions take place on the surface of the reinforcing steel. Concrete pore water acts as the electrolyte. And the body of reinforcement provides the electrical connection between the anode and cathode. Cathodes and anodes may be located on the same rebar (microcell) or on different bars (macro cell) that are electrically connected through metallic ties or chairs. After the passive layer is broken down, rust will appear instantly on the steel bar's surface. The chemical reactions are the same in cases of carbonation or of chloride attack. When the corrosion of the reinforced steel bars in concrete occurs, they melt in the void that contains water. The oxidation and reduction reactions that take place at the anode and cathode are called half cell reactions. At the anode, iron is oxidized and goes into solution as ferrous ions releasing its electrons.

$$Fe \longrightarrow Fe^{2+} + 2e^{-}$$

If the electron will be accumulated on the other part of the steel reinforcement but cannot accumulate with huge numbers in the same location, there is another reaction that uses the number of the electrodes with oxygen and water the cathodic reaction. Its equation is:

$$2e^{-} + H_2O + O_2 \longrightarrow 2OH^{-}$$

From this equation it is found that the presence of OH^- occurs due to cathodic reaction. The hydroxide ions increase the alkalinity and reduce the effect of carbonates or chlorides slightly. From this equation, it is important to know that water and oxygen are the main reason for the corrosion process. As shown in the preceding equations and Figure 2.11, the anodic and cathodic reactions are the first step in the process of producing corrosion as the hydroxide ions (OH^-) will react with ferrous iron (Fe^{2+}) as a result of chemical equation (2.1). This reaction will produce ferrous hydroxide, which will react with oxygen and water again and produce ferric hydroxide. This chemical reaction is shown graphically in Figure 2.11.

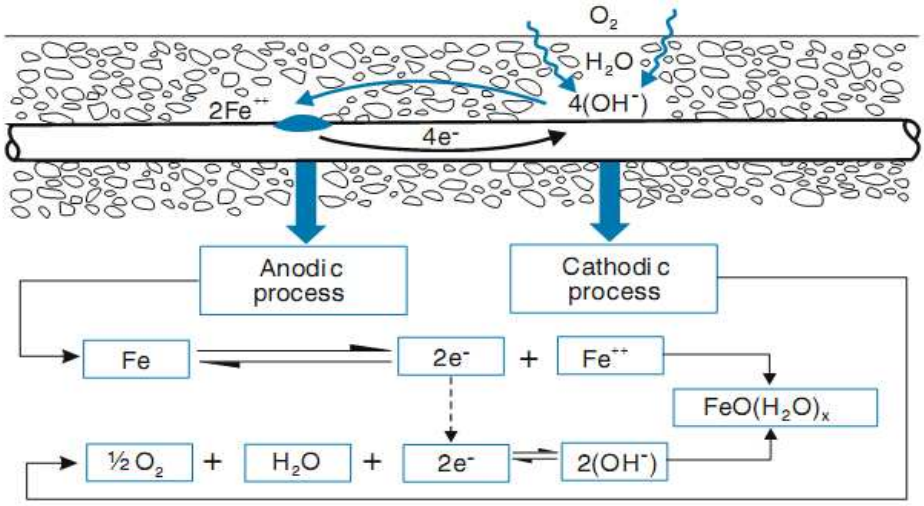

Figure 2.11: Corrosion process on a steel reinforcement surface.

$$Fe^{2+} + 2OH^- \longrightarrow Fe(OH)_2 \qquad 2.1$$

Ferrous hydroxide

$$4Fe(OH)_2 + O_2 + 2H_2O \longrightarrow 4Fe(OH)_3 \qquad 2.2$$

Ferric hydroxide

$$2Fe(OH)_3 \longrightarrow Fe_2O_3.H_2O + 2H_2O \qquad 2.3$$

Hydrated ferric oxide (rust)

The preceding chemical reactions show the transformation of steel from ferrous hydroxides ($Fe(OH)_2$). $Fe(OH)_2$ will react with oxygen and water to produce ferric hydroxides ($Fe(OH)_3$).With presence of water this ferric hydroxide form as hydrate ferric oxide (rust); its chemical term is $Fe_2O_3.H_2O$. The passive film protecting the reinforcement steel can be disrupted by two mechanisms: carbonation and chloride induced corrosion. Disruption of passive film initiates corrosion of reinforcing steel, initiating corrosion. The volume of corrosion products may be more than six times larger than the volume of iron (Mansfeld, 1981).

This expansion causes tensile stress in the hardened cement paste that leads to cracking, spalling, eventual loss of concrete cover, and serious deterioration of structural concrete. A uniform corrosion of 1 mil (25 μm) of reinforcement would cause cracks to develop (Pfeifer, 2000). A localized corrosion loss of 30 to 270 μm to crack concrete based on the anodic length and member dimensions (cover depth) (Torres-Acosta and Sagues, 2004). In addition to cracking, the reduction of the steel cross section, possible loss of steel ductility, and reduced bond strength are all possible consequences of reinforcement corrosion that can lead to serviceability problems and structural failures (Andrade and Alonso, 2001). In this stage, cracks on concrete start until the concrete cover falls; rust, with its brown color, can clearly be seen on the steel bar.

2.4.6 Physical effects of corrosion

With increasing corrosion the tensile stress in the concrete will reach a critical value and crack will be developed. During this process the volume of the corrosion products at initial cracking of concrete will occupy three volumes, namely the porous zone near the reinforcement, expansion of concrete due to rust pressure, and the space of the corroded steel. The corrosion process and its effect on a reinforced concrete structure are schematic illustrated in Figure 2.12. The result will be a reduced load carrying capacity of the structure primarily due to the reduced steel bar cross-section and the loss of bond between the steel bar and the surrounding concrete.

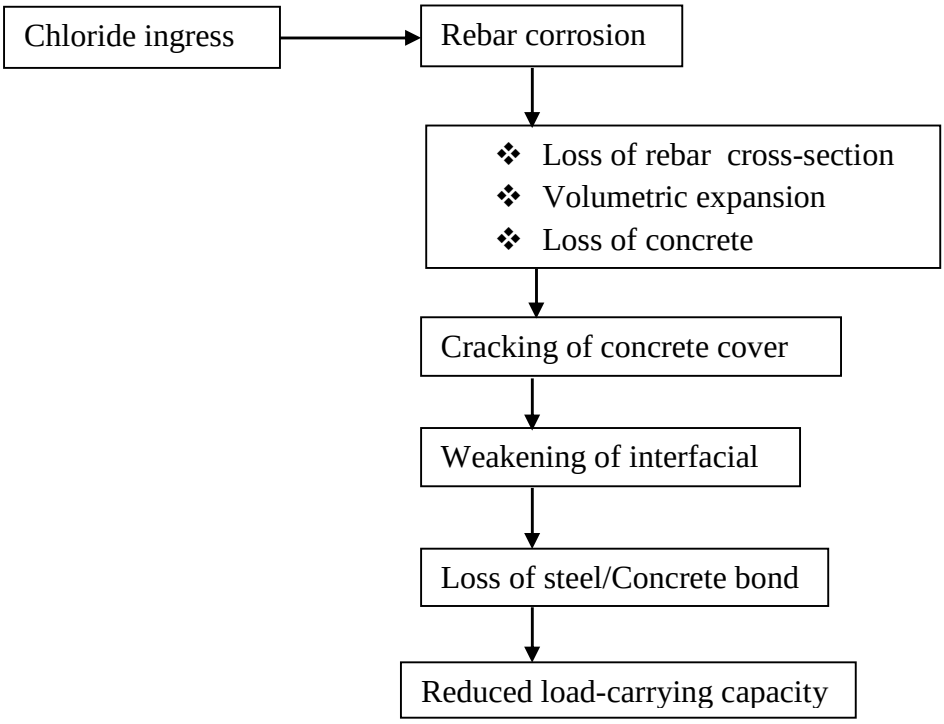

Figure 2.12: Effect of corrosion on reinforced concrete structure

2.5 Environmental Effect on Corrosion of Reinforced Concrete

The main causes of corrosion of steel in concrete are chloride attack and carbonation. These two mechanisms are unusual in that they do not attack the integrity of the concrete. Instead, aggressive chemical species pass through the pores in the concrete and attack the steel. This is unlike normal deterioration processes due to chemical attack on concrete. Other acids and aggressive ions such as sulphate destroy the integrity of the concrete before the steel is affected. Most forms of chemical attack are therefore concrete problems before they are corrosion problems. Carbon dioxide and the chloride ion are very unusual in penetrating the concrete without significantly damaging it. Accounts of (for instance) acid rain causing corrosion of steel embedded in concrete have been shown to attack the steel and not the concrete.

2.5.1 Carbonation

The process by which carbon dioxide in the atmosphere reacts with water in concrete pores to form carbonic acid and then reacts with alkalis in the pores, neutralizing them. This can then lead to the corrosion of the reinforcing steel. The high alkalinity of concrete is partly due to the presence of the alkalis Na_2O and K_2O of the cement and mainly to the presence of calcium hydroxide which is produced on the hydration of the Alite and the Belite. Normal air contains some 0·03% carbon dioxide (CO_2) by volume. The capillary pore system of the cement paste allows air to penetrate into the concrete and the CO_2 of the air combines with the calcium hydroxide ($Ca(OH)_2$) to give calcium carbonate ($CaCO_3$) in accordance with the following expression:

$$CO_2 + H_2O \longrightarrow H_2CO_3 \qquad 2.4$$

Gas water Carbonic acid

$$H_2CO_3 + Ca(OH)_2 \longrightarrow CaCO_3 + 2H_2O \qquad 2.5$$

Carbonic acid pore solution

Due to the neutralization of alkalis, carbonation and diffusion of other acidic gases, such as SO_2 and NO_2, cause a decrease in the pH of concrete pore solution, which is typically between 12.5 and 13.6. A reduction of pH to a lower level may cause loss of passivity and initiate corrosion of reinforcement. Different studies stated different limits of pH for the stability of passive film. The pH level lower than 9.5 would commence corrosion of steel reinforcement as shown in Table 2-1. The protective film tends to be stable in the absence of chloride ions as long as the pH of concrete pore solution stays above 11.5 (Berkely and Pathmanaban, 1990).

Table 2.1: State of reinforcement corrosion at various pH levels

pH of Concrete	State of Reinforcement corrosion
Below 9.5	Commencement of steel corrosion
At 8.0	Passive film of the steel surface disappears
Below 7	Corrosion occurs

The carbonation process occurs quickly when the concrete cover is not very thick. It may also occur when the concrete cover over the steel bars is thick because the carbonation transformation will happen as a result of the existence of pore voids open in the concrete that assist the quick propagation of CO_2 inside the concrete. The carbonation process can occur when the alkalinity in voids is relatively small. This happens when the cement content is small and water-to-cement (w/c) ratio is high and also due to a bad curing process during construction. Carbonation moves inside concrete according to the diffusion theory: The diffusion rate is in inverse proportion to the distance between the steel bars and the concrete surface, which is the concrete cover thickness:

$$\frac{dx}{dt} = D_0/x$$

Where,

x = the distance from the concrete surface

t = the time

Do = the diffusion rate, which depends on the quality of the concrete

2.5.2 Factors affecting rate of carbonation

It is self-evident that the rate of carbonation is determined by the rate of CO_2 diffusion into the concrete. In turn, this diffusion depends on concrete porosity and its moisture content and temperature.

2.5.2.1 Relative humidity

Water content is the amount of free water existing in the pores of the solid matrix. It is an essential factor affecting the reactivity and diffusivity of carbon dioxide. The water takes part in the salvation and hydration of the CO_2. It also dissolves the Ca^{2+} ions from the solid that will react to form the $CaCO_3$ (Fernández and Bertos, 2005). With insufficient water, the CO_2 and calcium hydroxide will not be fully ionized, whereas too much water limits the reaction due to

the blockage of the pores in the solid as the diffusivity of CO_2 is 10^4 times smaller in water than in air. Due to the differences of porosity and CO_2 uptake capacity, different cementtitious systems require different water contents in order to achieve the same degree of carbonation (Lange, et. al., 1996).

The water content of a porous material depends on its pore structure as well as external relatively humidity. When exposed to an environment with certain relative humidity, moisture exchanges occur between the atmosphere and the pores until a balance is formed. The free water left in the solid material tends to form a liquid film on the wall of large pores and fill the space of small pores. When the external relative humidity is zero, the water content in the cementtitious material is also zero and carbonation reactions cannot proceed. When the external relative humidity is 100%, the material is fully saturated, as all the pores are filled with water which blocks the diffusion pathway of CO_2. Therefore the external relative humidity has a considerable and important influence on the rate and ultimate extent of carbonation (Verbeck, 1958). For most cementtitious materials, carbonation is more rapid at an external relative humidity of 50%-60%. At 50%-60% relative humidity, the equilibrium water content in the solid tends to reach optimum for the carbonation reaction (Goñi and Guerrero, 2003).

2.5.2.2 Temperature

As temperature goes up, the diffusivity of CO_2 increases due to increased energy (Song, et al., 2006). However, the solubility of carbon dioxide and calcium hydroxide decrease with increasing temperature and the decreasing solubility's cause a decrease in the carbonation rate. The optimum reaction temperature for the highest carbonation rate is found to be at 20 ºC for lime mortar. For lightweight concrete waste, the uptake of CO_2 increased with increasing temperature up to 60 ºC (at atmospheric pressure) (Liu, et al., 2001).

2.5.2.3 Partial pressure of CO_2

Slight increases of CO_2 partial pressure in the atmosphere will accelerate the rate of reaction and influence the strength development. However, experimental work shows that increases in pressure from 1 to 2 atom have been found to increase the rate of the carbonation reaction for compacted cement mortars, whilst a further increase to 4 atom had little effect (Young, et. al., 1974).

2.5.3 Chloride attack

Chlorides can attack concrete from more than one source. The first source is from inside the concrete during the casting process; the second is to move concrete from outside to inside. When casting takes place, chlorides exist in concrete as a result of the following:

a) using seawater in the concrete mix
b) using calcium chloride in additives required to accelerate setting time
c) aggregate that contains chlorides that can be washed well
d) additives that have a higher chloride content than that defined in the specification
e) water used in the concrete mix that has a higher number of chloride ions than that allowed in the specifications

Chlorides can propagate inside concrete from the external environment by:

a) concrete exposed to seawater spray or continuous exposure to salt water
b) using salt to melt ice
c) presence of chlorides in chemical substances that attack the concrete structure, such as salt storage

2.5.3.1 Chloride attack mechanism

The chloride ion attacks the passive layer but, unlike carbonation, there is no overall drop in pH. Chloride act as catalysts to corrosion when there is sufficient concentration at the rebar surface to break down the passive layer. They are not consumed in the process but help to break down the passive layer of oxide on the steel and allow the corrosion process to proceed quickly. This is illustrated in Figure 2.13.

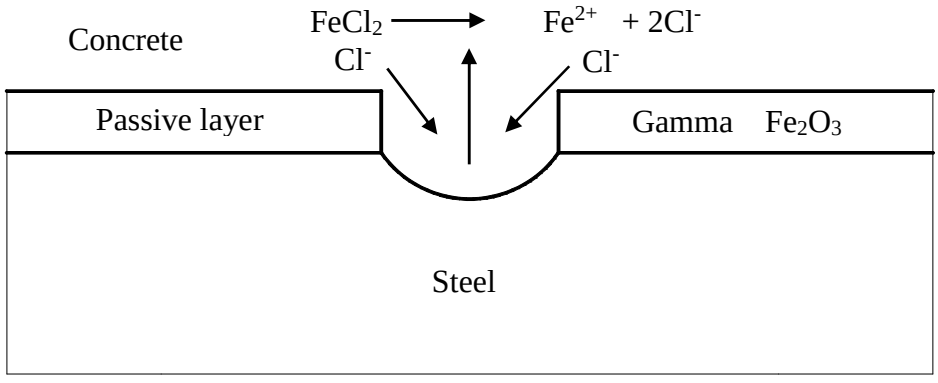

Figure 2.13: The breakdown of the passive layer and 'recycling' chlorides

Obviously a few chloride ions in the pore water will not break down the passive layer, especially if it is effectively re-establishing itself when damaged. There is a 'chloride threshold' for corrosion given in terms of the chloride/hydroxyl ration. It has been measured in laboratory tests with calcium hydroxide solutions. When the chloride concentration exceeds 0.6 of the hydroxyl concentration, corrosion is observed. This approximates to a concentration of 0.4% chloride by weight of cement of chlorides are cast into concrete and 0.2% they diffuse in.

2.5.4 Factor affecting the rate of chloride attack

2.5.4.1 Porosity of concrete cover

The time it takes chloride concentration to reach the critical content of 0·4% at a certain distance from the surface, increases with the decrease in concrete porosity or, alternatively, the distance at which the critical content is reached at a given time, increases with the increase in concrete porosity. It follows that the W/C ratio and length of curing would affect, similarly, chloride penetration (Al-Amoudi, et al., 1991). Accordingly, it may be again concluded that in order to control chloride penetration, a well-cured concrete cover, made with a low W/C ratio, should be provided over the rebar.

2.5.4.2 Temperature

Accordingly, the diffusion rate of the chlorides is expected to increase with temperature, and the relation between the logarithm of the diffusion coefficient and the reciprocal of temperature is expected to be linear. In a hot environment the time it takes the chlorides to reach the rebar's level is shorter than in a moderate environment. Again, the rate of chloride penetration decreases with a decrease in the W/C ratio (Page, et al., 1981).

2.5.4.3 Oxygen penetration

The reactions at the cathode involve the consumption of oxygen. Hence, the corrosion process depends on the presence of oxygen, and the rate of corrosion, on the rate of the oxygen supply at the cathode. The oxygen originates in the air surrounding the concrete, and the amount available at the rebar's level depends on the rate of oxygen diffusion through the concrete cover. Hence, similar to the rates of CO_2 and chloride diffusion, the rate of oxygen diffusion depends on porosity of the concrete cover, and decreases, accordingly, with the decrease in the

W/C ratio and the efficiency of curing. It is evident that the rate of oxygen diffusion decreases with a decrease in W/C ratio and increase of the cover thickness.

2.5.4.4 Environmental factors on rate of corrosion

The environmental factors which affect the rate of corrosion process are mainly temperature and relative humidity. The rate of corrosion increases with the rise in temperature when effect of temperature is considered. This effect of temperature is indicated in Figure 2.14 in which the rate of corrosion is measured by the intensity of the corrosion current.

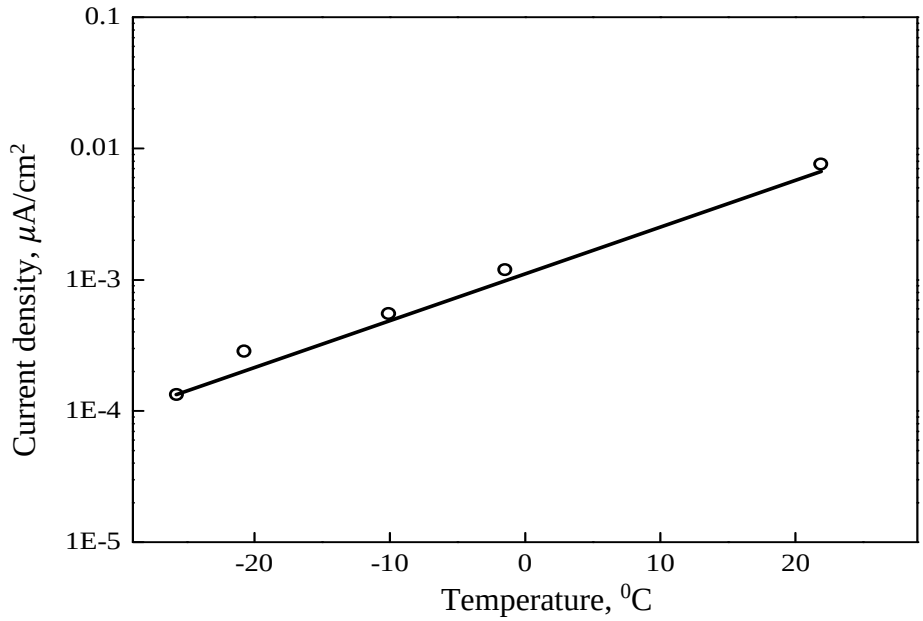

Figure 2.14: Effect of temperature on corrosion rate at 100% RH (W/C = 0.9, carbonated concrete)

Other data, presented in Figure 2.14, suggest the very same conclusion, namely, that the rate of corrosion becomes significant only when the relative humidity reaches 85%. Moreover, it is also clearly evident from Figure 2.15 that the effect of temperature on the rate of corrosion is negligible at the lower range of relative humidity. It becomes significant, however, at 85% RH and, indeed, very significant at 95% RH.

The preceding conclusions are of practical importance, implying that the risk of corrosion in a hot, dry environment is rather limited and, in this respect, it has been suggested that no corrosion is to be expected when the relative humidity remains below 70% .On the other hand, intensive corrosion is to be expected in a hot, wet environment. This may be also the case in

marine environment of arid zones because, in such an environment, the moisture content in the air may be high enough to induce corrosion which is further aggravated by the presence of chlorides (Raphael and Shalon, 1971). Finally, drying periods promote carbonation, whereas wet periods promote corrosion if carbonation has reached the reinforcement.

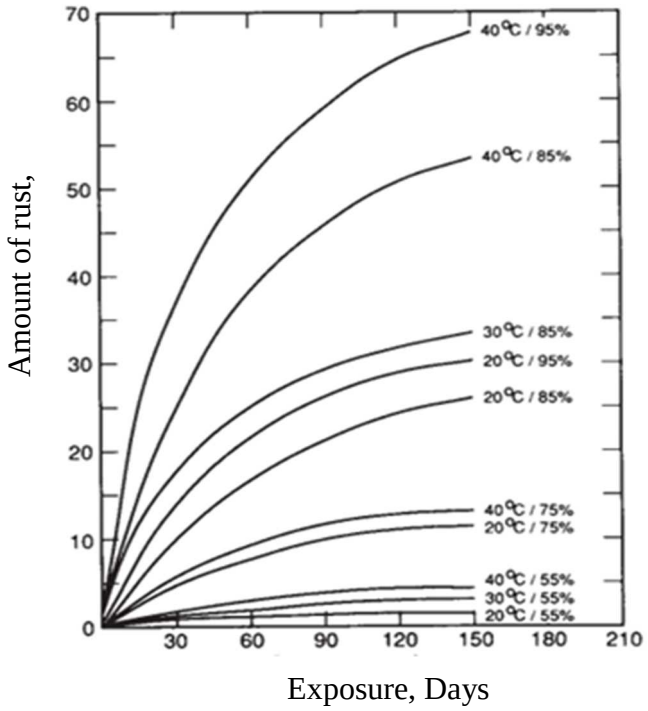

Figure 2.15: Effect of temperature and relative of rate of corrosion (Raphael and Shalon, 1971).

Therefore, the corrosion risk increases with increasing time of the dry periods. That means that climates with long dry and short wet periods may require a higher quality of concrete cover than climates with short dry and long wet periods. The risk of chloride-induced corrosion increases considerably after carbonation of concrete, because initially bound chlorides are released after carbonation and thus increase the amount of free 'corrosive' chlorides. As a rule, all processes involved are accelerated with increasing temperature. When choosing concrete composition, future changes of environmental conditions, resulting from, for example, change in use, should be considered.

2.6 Bond Stress

Bond stress is defined as the shear stress at the steel-concrete interface which modifies the steel stress by transferring the load between the steel and the surrounding concrete. Bond

stress can be calculated as the stress per nominal unit area of the bar surface. Also, bond stress can be measured by the rate of change of steel stress in the bar. Thus, there will not be any change in bar stress without bond stress or vice versa.

2.6.1 Bond mechanism

An efficient and reliable force transfer from the reinforcement to the surrounding concrete depends on three mechanisms; namely, adhesion, friction and mechanical interlocking as shown in Figure 2.16 where V_a is the adhesion, V_b is the mechanical anchorage due to bearing of the lug and V_f is the frictional resistance.

Adhesion: Adhesion is the chemical bond between the bar and the concrete which is related to the shear strength at the steel-concrete interface. For a small load, the basic resisting mechanism is the chemical adhesion; however when a deformed bar moves with respect to the surrounding concrete due to increase in the loads, the chemical adhesion along the bar surface is lost.

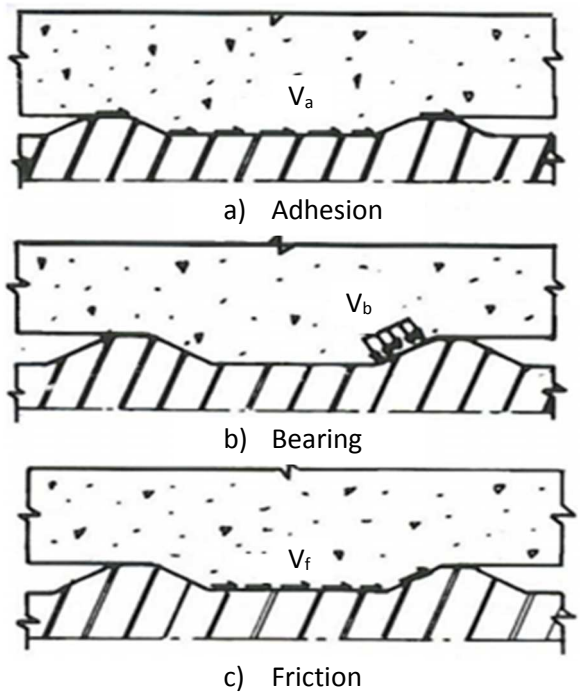

Figure 2.16: Idealized forced transfer mechanism

Friction: Friction is the force resisting the parallel displacement between two surfaces sliding against each other. Friction plays a significant role in force transfer between the

concrete and the steel bar. Friction can contribute up to 35% of the ultimate strength governed by the splitting of the concrete cover (Treece and Jirsa, 1989).

Mechanical interlocking: For deformed steel bars, bond depends primarily on mechanical interlocking between the ribs and the concrete keys. In addition, the mechanical interlocking of the deformed steel bar depends on the geometry of the ribs along the steel bar. As the ultimate bond strength is reached, shear cracks begin to form in the concrete between the ribs as the interlocking forces induce large bearing stresses around the ribs, and slip occurs. Therefore, the bar ribs restrain the slip movement by bearing against the concrete keys. The slip of a deformed bar may occur in two ways, either through pushing the concrete away from the bar by the ribs, i.e. wedging action, or through crushing of the concrete by the ribs.

Perfect bond for reinforced concrete members provides complete compatibility of strains between concrete and steel. However, in reality, perfect bond occurs only in the regions where negligible stress transfers between concrete and steel. Whereas, in the regions where high stress transfers along the steel concrete interface, such as in the vicinity of cracks, the bond stress is related to the relative displacement between reinforcing steel and the surrounding concrete. Therefore, strain compatibility does not exist between reinforcing steel and surrounding concrete near cracks. The relation between bond stress and the relative displacement between reinforcing bar and concrete is due to strain incompatibility and the crack propagation is known as bond-slip as shown in Figure 2.17.

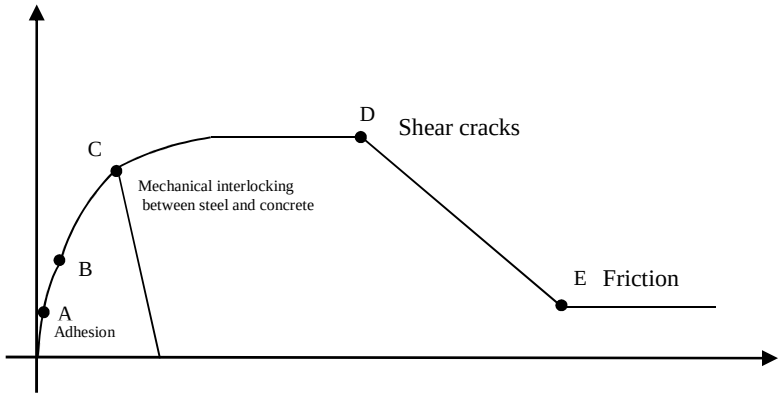

Figure 2.17: Typical bond stress-slip relationship

Initially, with uncracked concrete, bond stress is assured by the chemical adhesion between the steel and the concrete up to the point A as shown in Figure 2.17 where the slip is

relatively negligible. As mentioned earlier, once a deformed bar moves with respect to the surrounding concrete, surface adhesion is destroyed as a consequence of the wedging action of the ribs which pushes the concrete away from the steel.

With the onset of slippage between the reinforcing steel and the concrete, bond resistance will be developed by friction and mechanical interlocking between the bar and the surrounding concrete. However, the bearing of the lugs become significant for the bond between steel and concrete. The concentrated bearing forces in front of the lugs will split into two directions: Parallel components to the bar axis represents the bond stresses and the radial (perpendicular) components to the bar axis represents the circumferential tensile stresses. When these tensile stresses exceed the tensile strength of the concrete internal cracks develop around the bar, and the deformation of concrete resulting from generated stresses tend to pull the concrete away from the reinforcing bar in the vicinity of a major crack. Therefore, at point B in Figure 2.17, the stiffness of the concrete is reduced and longitudinal splitting cracks are initiated by the inclined compressive forces spreading from the lugs into concrete. The internal cracks reach the concrete surface at point C, and the bond resistance will drop to zero if sufficient confinement is not provided. Thus bond failure due to splitting occurs (Lundgren, 2005). However, with the presence of sufficient confinement, the load can be increased further and pull out failure will occur instead of splitting failure. At point D, shear cracks will initiate in the concrete keys between ribs which correspond to the point of maximum bond resistance. The bond resistance is decreased with the increasing slip due to spreading of shear cracks through the concrete. Hence the frictional resistance of concrete along the failure surface remains the only mechanism that exists at point E.

2.6.2 Factors affecting the bond strength

Bond strength between the steel and concrete depends on several factors such as concrete and steel strengths; bar size and profile; concrete cover thickness; embedment length of steel; spacing of bars; stirrups; temperature; corrosion etc. A brief description of some of these factors that influence the bond strength at steel-concrete interface is presented in the following sections.

2.6.2.1 Concrete strength

Compressive strength is considered to be a significant parameter in bond behavior because the force between steel and concrete is transferred mainly by bearing and bond

(Orangun, et al., 1977). The slope of the bond stress distribution varies considerably over the splice length with a higher concrete strength when compared to that with lower concrete strengths (Tepfers, 1973) . Since bond failure can occur by tensile splitting and shearing off of the concrete, the compressive strength is considered to be a significant key in bond behavior. It has been found that the bond of high strength concrete is proportional to the compressive strength of concrete (Alavi-Fard and Marzouk, 2002). However, test result indicates that the square root has proven to be adequate as long as concrete strengths remain below about 55 MPa, while for high strength concrete, it is observed that $f_c'^{1/4}$ provides the best fit for the effect of compressive strength on the concrete contribution to bond strength for bars not confined by transverse reinforcement and $f_c'^{3/4}$ provides a good fit for the effect of compressive strength on the concrete contribution to bond strength for bars confined by transverse reinforcement (Darwin, 2000). The tensile and compressive stresses of concrete contribute to the development of bond stresses. For example, micro cracks are controlled by the tensile stresses of the concrete, while bearing stresses induce high compressive stresses in front of the ribs. A slip range of 0.01 to 1 mm, the bond stress is proportional to the concrete compressive strength, based on the pullout test results, with concrete strengths varying from 16 to 50 MPa; However, for very small slip less than 0.01 mm, and for high slip larger than 1 mm, the effect of the concrete compressive strength is less important and proportional to $f_c'^{2/3}$ (Martin, 1982).

2.6.2.2 Concrete cover thickness and bar spacing

Bond strength increases with increasing cover thickness and bar spacing (ACI Committee 408, 2003). The concrete cover and the bar spacing significantly influence the type of bond failure (Tepfers, 1973). Splitting tensile failure occurs with small concrete cover and bar spacing, while pullout failure occurs with large concrete cover and bar spacing. For most structural members, splitting failure is expected and can occurs between the bars, between the bars and the free surface, or both, while pullout failure can occurs with some splitting if the member has significant transverse reinforcement to confine the anchored steel.

2.6.2.3 Bar profile

The stress transfer between the reinforcing bar and the surrounding concrete depends on the resistance to relative motion or slippage between the concrete and the surface of the embedded

steel bar due to the bond at steel-concrete interface. It is well known that this mechanism of stress transfer is the base of the theory of reinforced concrete (Shetty, et al., 2011).

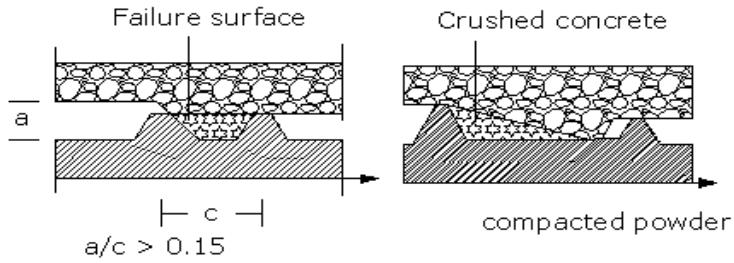

Figure 2.18: Failure Mechanism at the Ribs of Deformed Bars.

The steep face angle Figure 2.18 stated that the bond of deformed bars is developed mainly by the bearing pressure of the bar ribs against the concrete. Pullout tests showed that for bars with steep rib face angle α (larger than about 40 degrees with the bar axis) slip occurs only by the compression of the concrete in front of the bar rib, while in bars with flat ribs, i.e., the angle α is small, slip occurs with the ribs sliding relative to the concrete as the rib tends to push the concrete away from the bar. This wedging action can be a major cause of longitudinal splitting along the bar. For $45° < \alpha < 70°$, the deformations must reverse in direction on each side of the bar (Park and Paulay, 1975).

2.6.2.4 Casting position and concrete confinement

The load-bond slip relationship for deformed bars is primarily affected by the quality of the concrete on the font of the bar ribs. The quality of the concrete in the region depends on its relative position of casting. Soft and spongy layer of concrete can form under the ribs in case of casting perpendicular to the bar length

2.6.2.5 Corrosion effect

Corrosion affects the bond strength, the slight formation of the corrosion product of a corroding bar at first increase radial stress between the bar and the concrete and hence increases the fractional component of bond. However, further corrosion will lead to the development of longitudinal cracking and a reduction in the resistance to the bursting forces generated by the bond action. Some suggest that a firmly adherent layer of rust may contribute to an enhancement in bond strength at early stages of corrosion, at more advance stages of corrosion,

weak and friable material between bar and concrete will certainly be at least partially responsible for reductions in bond strength (Hassan, 2003). Corrosion has a significant influence on the bonding performance of steel reinforcing in concrete with over 50% reductions in bond strength observed associated with 16% reduction in average cross-section due to corrosion (Kivell, et al., 2011). The maximum bond stress will reduce the corrosion proceeds, and its reduction rate will become larger when the thickness of cover concrete is large. It is considered that the internal cracks due to corrosion make the bond strength lower in case of splitting failure of concrete.

2.6.3 Bond failure

There are two general types of failure mechanisms associated with concrete–steel bond: splitting failure and pullout failure.

Splitting Failure: A splitting failure occurs when the reinforcing bars are not well confined and the radial force exceeds the capacity of the surrounding concrete. The type of splitting failure that occurs depends on the relative differences among bar spacing, bottom or top cover, and side cover. A side-split failure occurs if the side cover is less than the top cover or half of the bar spacing, and a V-notch failure occurs if half of the bar spacing and the side cover are both greater than the top cover. An intermediate type of failure, a face-and-side-split failure, occurs if the top and side covers are approximately equal. Splitting failures have also been found to depend on the bar size, bar spacing, concrete strength, use of lightweight concrete, and the casting position of the bar.

Pullout Failure: A pullout failure occurs when reinforcing bars are well confined and the embedment or splice lengths are insufficient to develop yield and strain hardening of the steel. These failures are characterized by a series of cracks developing along a shear plane connecting the peaks of the reinforcement deformations. The failure pattern indicates that resistance to pullout is controlled by the capacity of concrete in shear, and the friction and adhesion components are of much less importance than with a splitting failure.

2.7 Coating Effects on Concrete–Steel Bond

Epoxy-coated bars have been commercially available for over 20 years; however, PVC- and nylon-coated bars are not yet commercially available. Consequently, there has been numerous research has been carried out regarding the bond behavior of epoxy-coated reinforcing bars but relatively few researches have included bond testing of other epoxy organic coatings.

Therefore, the following discussion regarding coating effects on concrete–steel bond will focus entirely on the test results of epoxy-coated bars.

The greatest concern regarding the use of epoxy coating for reinforcement in structural concrete has been its effect on bond between the concrete and the reinforcement. The ability of steel to transfer forces to the concrete through bond action is critical to the short- and long-term performance of concrete structures. Following are several factors that may affect the bond behavior of epoxy-coated reinforcement:

a) Adhesion is prevented because the layer of epoxy acts as a bond breaker between the steel and the hydrating cement.
b) Friction is reduced because the epoxy coating reduces the microscopic irregularities caused by mill scale.
c) Mechanical properties of the coating are different than those of concrete and steel and may change the state of stress in the concrete surrounding the bar.
d) Thicker coatings tend to be uneven, which typically decreases the effective height of the bar deformations.

2.7.1 Differences in bar deformation geometry

Pullout tests have been used to determine the effects of differences in rib geometry on the bond strength of epoxy-coated bars. A series of tests was performed that evaluated the influence of bar rib face angle, rib spacing, rib height, and concrete strength. In this study, specially machined coated reinforcing bars were tested in an eccentric pullout specimen. The results of these tests were compared with tests of similarly machined uncoated bars. These tests indicated that coated bars slipped more than did uncoated bars, regardless of the test variable. With all other test variables held constant, the relative bond strength of the coated bars increased as the rib face angle increased, rib spacing decreased, and rib height increased. These trends appeared to be independent of differences in concrete strength. Even though variations in bar geometry and concrete strength can produce significant differences in bond strength results, these variables appear to have no effect in the evaluation of coatings for comparison purposes only. A series of pullout tests, using different bar sizes, various bar deformation patterns, and different concrete strengths, was performed to determine differences in stress transfer between coated and uncoated bars. In these tests, it was found that the bond strength of epoxy-coated bars was lower than that of uncoated bars by approximately 10%–25%. This decrease in the pullout resistance of epoxy-coated bars did not appear to be influenced by any of the parameters

considered. Therefore, direct comparisons of relative bond behavior can be made between coated and uncoated bars, provided that there are no differences in rib geometry, concrete strength, and transverse reinforcement among specimens.

2.7.2 Loss of adhesion

The lack of adhesion between epoxy-coated reinforcement and concrete has been well documented. Autopsies were performed of several failed spliced beam specimens with epoxy-coated and uncoated reinforcement (Treece and Jirsa, 1989). These autopsies showed no indication that concrete adheres to epoxy-coated reinforcement. The concrete in direct contact with the epoxy-coated bars had a smooth, glassy surface and the coated bars appeared clean, with no concrete residue left on the deformations. The autopsies of similar specimens with uncoated reinforcement indicated that adhesion had occurred. The concrete surface in direct contact with uncoated bars was dull and rough and the uncoated bars that were removed had concrete particles firmly attached to the shaft, with large deposits on the sides of the deformations.

2.7.3 Loss of friction

A series of tests was performed that compared the frictional characteristics of a mill-scale steel-concrete interface with that of a fusion- bonded, epoxy-coated steel-concrete interface. Specimens were rectangular concrete prisms, each of which was cast between two steel plates. Half of the steel plates were coated with epoxy and half were left uncoated. The specimens were compressed during testing to impose a normal stress on the steel–concrete interface. A horizontal force was applied to create shear stress along the interface. This force was steadily increased until the maximum load was achieved. These sandwich specimens failed by shear along the concrete-steel plate interface. The results of these tests indicate that there are two components to friction: a frictional component and an adhesion component. The observed frictional components are similar for coated and uncoated bars; however, there is no adhesion for coated bars. At low values of normal stress, the maximum applied shear for the coated steel decreased by approximately 40%, as compared with the uncoated steel. The difference between coated and uncoated bars decreased as the applied normal stress increased (Treece & Jirsa, 1989).

2.7.4 Comparison of coated and uncoated reinforcement bond forces

With the loss of adhesion and friction, bearing on the bar deformations is the only component that contributes to the development of coated bars. A comparison of the resulting bond forces for uncoated and epoxy-coated bars is shown in Figures 2.19 and Figure 2.20. The friction and bearing force vectors can be added to determine the resultant force. As can be seen in Figures 2.19 and Figure 2.20, friction is beneficial to bond because it decreases the angle of the resultant force, which results in a smaller radial splitting force. The use of epoxy-coated bars increases the angle of the resultant bond force and causes higher radial splitting force. This indicates that epoxy-coated bars will have less bond capacity because they are more likely to experience a premature splitting failure than are uncoated bars.

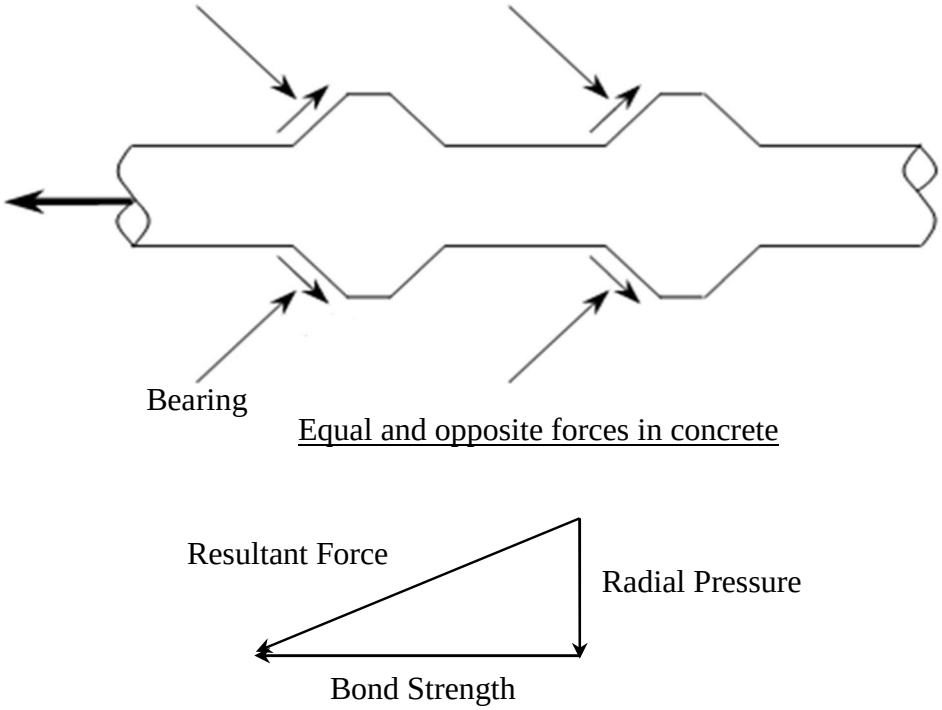

Figure 2.19: Uncoated Reinforcement Bond Forces

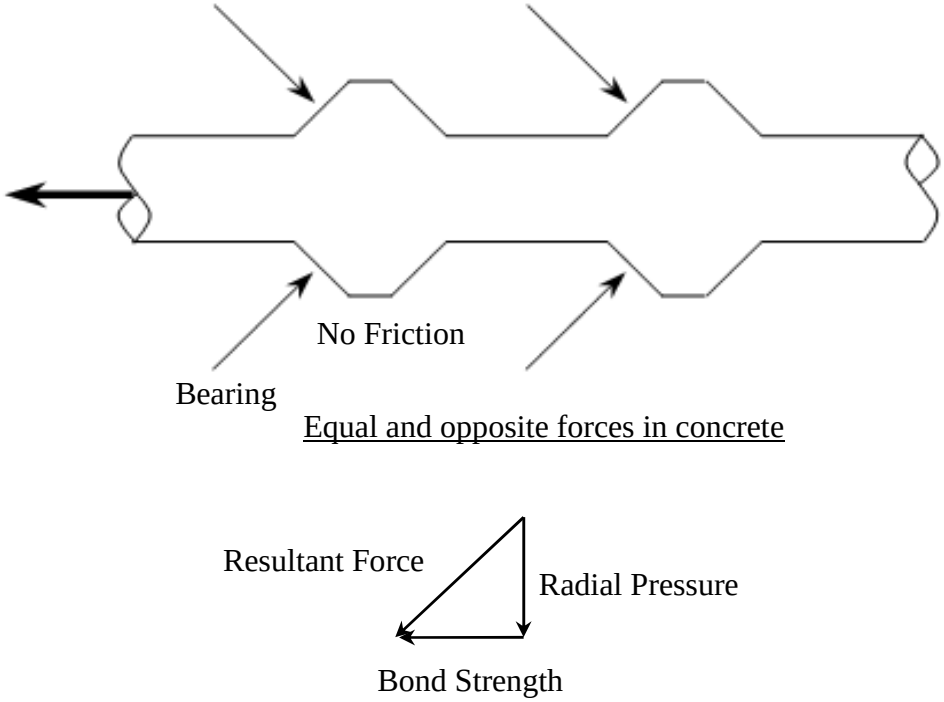

Figure 2.20: Coated Reinforcement Bond Forces

2.7.4.1 Pullout resistance

Pullout-type specimens have been used extensively in an attempt to quantify the difference in bond capacity between epoxy-coated and uncoated reinforcement. Several independent research programs have used various pullout specimens to evaluate the decrease in bond strength of epoxy-coated reinforcement (Kayyali, 1995).The results of these studies vary; however, the average pullout strength of epoxy-coated reinforcement was less than was the average pullout strength of uncoated reinforcement. In general, the pullout strength for epoxy-coated reinforcement was reduced to about 80%–95% of the pullout strength for uncoated reinforcement. This decrease in bond was also demonstrated in a series of pullout tests in which coated and uncoated bars were instrumented with strain gauges (Cusens and Yu, 1993). The strain gradient along the length of the bar was measured and found to be less for coated bars than for uncoated bars. The decrease in strain gradient indicates that forces are not transferred into coated reinforcing as efficiently as they are into uncoated reinforcement.

CHAPTER III

Methods and Materials

3.1 General

The purpose of this chapter is to elaborate the description of material properties, specimen's details and test setup. Two different types of Portland cement and coarse aggregate were used in the work. Also, accelerated electrochemical corrosion test was performed on reinforced concrete to measure the propagation of corrosion. Performance of coating effect on bond stress and corrosion of MS bar in concrete was also investigated in this work. Three different coating materials were used to achieve this goal. Under four different temperature, casting, curing and electrochemical corrosion test have been executed.

3.2 Material Property

3.2.1 Bar properties

In this work, deform shaped MS bar was used. Length and diameter of MS bar for all specimens were same. Diameter of reinforcing bars was 12 mm. Average yield stress of this bar was 530 MPa and ultimate stress was 622 MPa. Length of each bar was 325 mm. One end of the bars was threaded about 75 mm to carry out the bond strength test. A prepared reinforcing bar are shown in Figure 3.1.

Figure 3.1: Reinforcing bar specimen for pullout test

3.2.2 Coating

In this work, three different types of color coating were used. These were red oxide, aluminum oxide and synthetic enamel paint. Thicknesses of different color coating are presented in Table 3.1. It was measured by using digital Vernier scale shown in Figure 3.2. Accuracy of this scale is 0.01 mm. At first, reinforcing bar was cleaned by sand paper. Then, Vernier reading was

noted at three different places within a rib. After that coating material was applied over this Re-Bar. Thickness of the coating was measured by Vernier scale after 5 days of its application. Average thickness of color coatings is calculated using the measured data.

Table 3.1: Thickness of different coating

Name of coating		Observed thickness (mm)			Average coating thickness (mm)	Net average thickness =1000*(Avg. Difference Value)/2 (µm)
		Reading -01	Reading -02	Reading -03		
Aluminum Oxide	With coating	13.28	13.31	13.27	0.04333	21.67
	Without coating	13.23	13.27	13.23		
Red oxide	With coating	12.48	12.53	12.34	0.12333	61.58
	Without coating	12.34	12.40	12.24		
Synthetic Enamel Paint	With coating	13.06	12.93	12.98	0.10333	51.67
	Without coating	12.95	12.84	12.87		

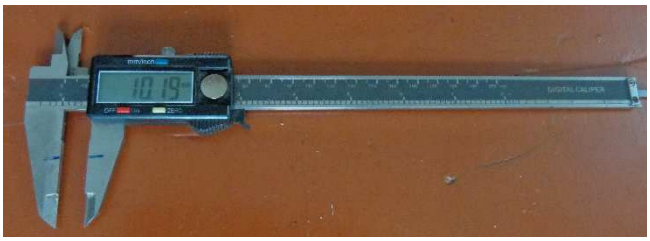

Figure 3.2: Typical picture of Vernier scale

3.2.3 Cement

Two different type of cement have been used in this research work. One is ordinary Portland cement. Specification of this cement is ASTM C-150, Type-I, CEM -I, 53.5 N. Composition of this cement is 95-100% clinker, and 0-5% gypsum. Another one is Portland composite cement. Specification of this cement is ASTM C-595, CEM II/B-M (S-V-L), 42.5N. Composition of this cement is 65-79% clinker; 21-35% slag, fly ash and limestone and 0-5% gypsum.

3.2.4 Aggregate

Two different types of coarse aggregate were used in this work. One type of coarse aggregate was crushed burn brick. Another type was crushed stone. There were four type of mixing batch based on cement type and coarse aggregate. That was identified by Batch-A, Batch- B, Batch-C and Batch-D. River bed sand was used as fine aggregate for all batches. Properties of fine and coarse aggregate are shown in Table 3.2.

Table 3.2: Properties of fine and coarse aggregate

Properties		Fine aggregate (River bed sand)	Coarse Aggregate	
			Crushed burn brick	Crushed stone
Maximum Aggregate size (mm)		--	19	19
Unit weight (kg/m^3)	Loose condition	1338	896	1315
	Compact condition	1520	1013	1495
Absorption (%)		3.10	8.2	1.2
Specific Gravity		2.64	2.04	2.34
Fineness modulus		2.72	--	--

3.2.5 Mix proportion

Two different types of cement like as ordinary Portland cement and Portland composite cement and two different types of coarse aggregate such as crushed burn brick and crushed stone were used in this work. The mix proportion of the concrete was 1 (cement): 1.4 (fine aggregate): 2.5 (coarse aggregate) by volume and water to cement ratio (W/C) was 0.5. The concrete was mixed by manual method. Weight of mixing materials for 1 m^3 concrete are given in Table 3.3.

Table 3.3: Amount of mixing materials for 1 m^3 concrete.

Batch Name	Cement (kg)		Fine aggregate (kg)	Coarse aggregate (kg)		Water (Litter)
	OPC	PCC		Crushed Brick	Crushed Stone	
OB	295	-	435	516	-	147
PB	-	295	435	516	-	147
OS	295	-	435	-	763	147
PS	-	295	435	-	763	147

3.2.6 Test matrix

Total 256 samples like as Figure 3.3 were casted to fulfill the objectives of the work. Two samples were made for an each test. Specific 128 samples were subdivided by two sets according to test method. Number of 64 samples were made for bond strength test. And rest part of samples was made for accelerated corrosion test. Two sets were equal in same parameters. This 64 samples also subdivided into 4 groups with respect to 4 different temperature (20 ^{o}C, 30 ^{o}C, 45 ^{o}C and 60 ^{o}C). Each group had total 16 samples. These 16 samples were casted with two different cement types. Also the number of 8 samples were prepared according to two type of coarse aggregate. Finally, rest of specific 4 samples were made with non- coated and three different coated MS bar.

Identification of a particular specimen for pullout test and corrosion test without referencing table are shown in below.

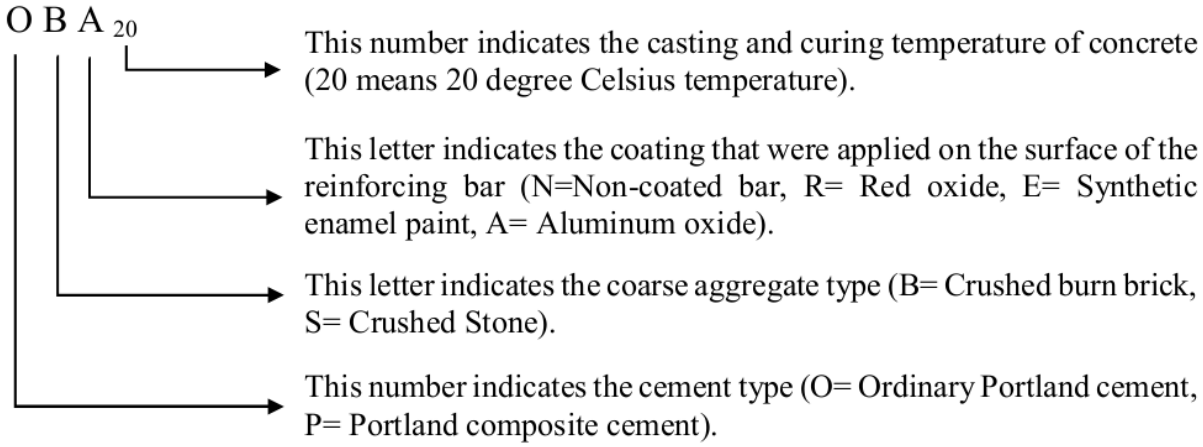

As example, specimen name PSN_{30} means (P = Portland composite cement; S= Crushed stone; N= Non- coated rebar; 30= 30^{o}C Temperature).

3.3 Specimens for Pullout Test

3.3.1 Specimen details

In order to examine the bond strength of the reinforced concrete, specimens were prepared for pull out test. By using the concept of ASTM C 900-01, pullout test specimen has been designed and concreted. The details of the specimens are shown in Figure 3.3.

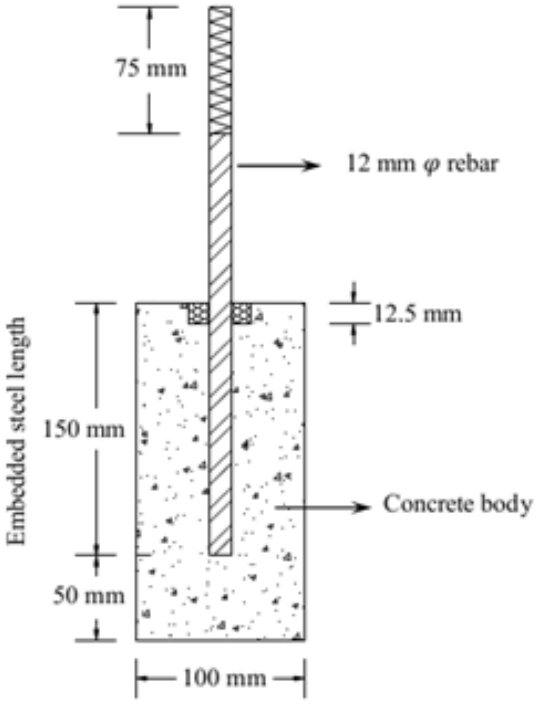

Figure 3.3: Typical specimens

Each specimen had a 325 mm long reinforcing bar. Diameter of the bar was 12 mm. About 150 mm of these bars was embedded into the concrete. 75 mm from top of the bars were threaded to lock the specimens for testing. Specimens had cylindrical in shape. Diameter and length of the specimen was 100 mm and 200 mm respectively. Reinforcing bar was placed into the concrete at 90 degree angle with the top surface of concrete. To achieve this, a special frame was prepared which is shown in Figure 3.5. A small size of circular cork sheet was placed at top of the concrete during casting. It was used to reduce the tension failure at the top face of concrete cylinder at the period of bond test. Its diameter was 40 mm and thickness was 12.5 mm.

3.3.2 Bar preparation

To observe the coating effect on bond stress and corrosion, a thin layer of color coating was applied on the surface of the bar. At first, bars were cleaned by sand paper. After that, bars were treated by a thin layer of coating. Three different types of coating such as Red oxide, Synthetic enamel paint, Aluminum oxide were used to treat the bars. Surface of thread area was free from coating. Coated and non-coated rebar are shown in Figure 3.4.

None coated bar Red oxide coated bar

Synthetic enamel paint coated bar Aluminum oxide coated bar

Figure 3.4: Re-bar surface preparation

3.3.3 Formwork and concrete placement

Cylindrical molds were used to cast the specimens. Two different semi-circular cylindrical metal parts were attached by nut and bolt. This completed cylindrical mold was positioned on a base plate. It was also fastened with nut and bolt. Two specimens were casted at same time and total 8 specimens were prepared in one day. At first, reinforcing bars were kept in a frame to set it vertical with base. It was fixed by attached nut of the frame. After this a single sized cork sheet was joined with the steel bar and it was poisoned at right place. Cylindrical steel mold was set into that frame and centered it with reinforcing bar. Finally, the interior surface of mold was treated by lubricating oil. Arrangement of reinforcing bar and cylindrical mold are shown in Figure 3.5.

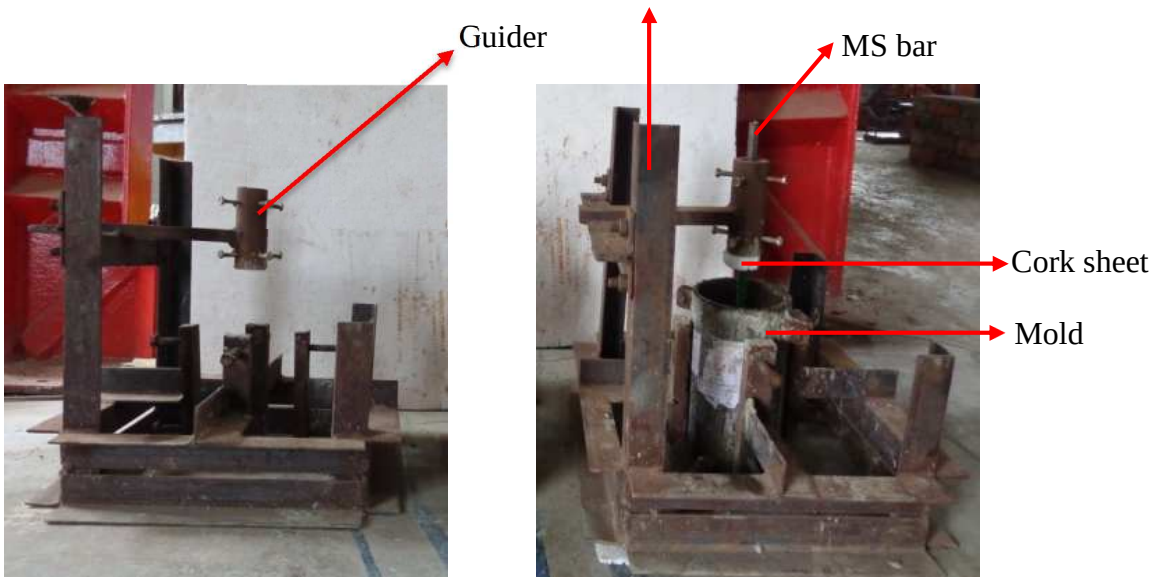

Figure 3.5: Formwork of specimens.

Concrete was mixed by manual method. It was mixed according to the mix proportion. Concrete mixture was compacted by tamping after placing into mold with 16 mm plain rod according to ASTM C31. Top surface was trowel finished. Concrete placement into the mold is shown in Figure 3.6.

Figure 3.6: Placement of concrete into the mold

3.4 Temperature Control Program

Control of casting and curing temperature is very important to full fill the objectives of this work. There were four different temperatures (20 ^{o}C, 30 ^{o}C, 45 ^{o}C, and 60 ^{o}C). For 20 ^{o}C temperature, room temperature was controlled by an air conditioned machine. Necessary materials were kept at the temperature controlled room into the laboratory before 24 hour of casting. During casting of concrete, room temperature was maintained nearly 20 ^{o}C $\pm$ 2 ^{o}C. After 24 hours later, specimens were demolded and placed in curing chamber that was situated in the same room for 28 days. The room temperature was also maintained at 20 ^{o}C $\pm$ 2 ^{o}C. 28 days later, specimens were taken out from curing chamber. Some of the specimens were connected in corrosion test setup and the rest specimens were stored to carry out bond test.

A 30 ^{o}C temperature specimens were casted and cured at ambient temperature. This time temperature was 30^{o}C $\pm$ 3^{o}C. Also the corrosion test was performed in normal air temperature. A special temperature control chamber was made by arranging bricks and joining some cork sheet for casting and curing at 45 ^{o}C and 60 ^{o}C temperature. Arrangements for 45 ^{o}C and 60 ^{o}C temperature controlled chamber are shown in Figure 3.7.

Figure 3.7: Arrangement of 45 ^{o}C and 60 ^{o}C temperature controlled chamber.

There were two different chambers. One was used as a curing bath. Another was used to carry the temperature controlling instruments like heater and temperature sensor. Heat was produced by an electric heater and it was controlled by a magnetic contactor. Heater was switched on every day at 8.0 am and switched off at 5.0 pm. For 45 ^{o}C and 60 ^{o}C temperature, necessary materials were kept on the temperature controlled chamber before 24 hours of casting. After casting these specimens with mold were kept into this chamber for 24 hours. One day later, demolded specimens were cured into this temperature controlled bath for 28 days. Corrosion test was also performed for 45 ^{o}C and 60 ^{o}C temperate into this chamber.

3.5 Electrochemical Corrosion Test

The objectives of accelerated electrochemical corrosion test is to compare the concrete resistance of different temperature, cement type, aggregate and different coating when steel embedded in concrete. The purpose is to identify which materials provide better protection for reinforcing bar in concrete.

3.5.1 Test setup

To accelerate the corrosion process, current was applied using DC power supply to maintain a constant voltage. 3% salt was mixed with water to prepare electrolyte. Schematic diagram of accelerated electrochemical corrosion test is shown in Figure 3.8.

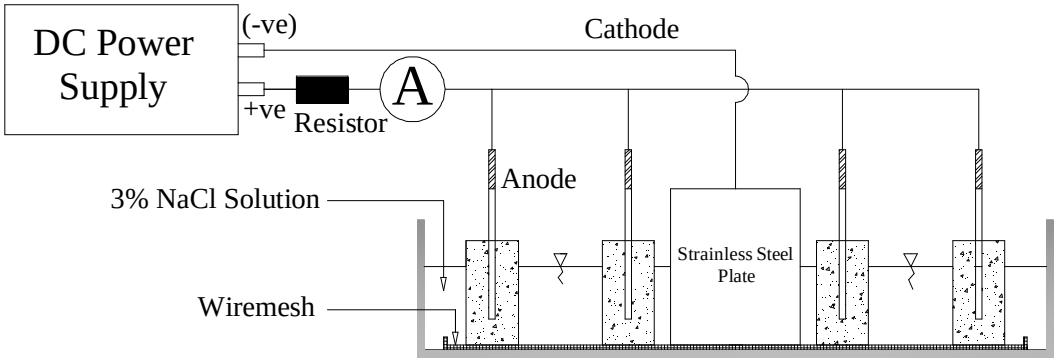

Figure 3.8: Schematic diagram of accelerated electrochemical corrosion test setup

A group of reinforced concrete specimens was set on a wire meshes which placed at the bottom of this electrolyte cell. Specimens were used as an anode and a stainless steel plate and wire mesh acted as a cathode. A digital ammeter was setup in series connection with the specimens. Experimental setup of accelerated electrochemical corrosion test setup is shown in Figure 3.9. After the application of applied voltage, current was measured regularly by digital ammeter for each cell. After few days later when initial cracks were initiated on the surface of concrete body, cracks were measured and noted. The cracks were measured regularly at 24 hours intervals. A specimen was removed from the corrosion cell for pullout test when it was achieved the target crack width like as nearly 1 mm. That time a false specimen was kept in this place as a replacement specimen to maintain the applied voltage as previous.

Figure 3.9: Experimental setup of accelerated electrochemical corrosion test

Digital image analysis method was used to measure the accurate and sophisticated crack width. Accelerated corrosion test was performed at controlled temperature. For each temperature, two different cells were produced to accomplish the corrosion test. Eight specimens were kept in cell. Figure 3.10 shows the accelerated corrosion test for 45 ^{o}C and 60 ^{o}C temperatures.

Figure 3.10: Experimental accelerated corrosion test for 45 ^{o}C and 60 ^{o}C temperatures.

3.5.2 Extent and rate of corrosion

The mass of rust produced per unit surface area of the bar due to applied current over a given time can be determined theoretically using the following expression based on the Faraday's law (Ijsseling, 1986):

$$M_{th} = \frac{WxTxIapp}{F}$$

Where, M_{th} = theoretical mass of rust per unit surface area of the bar (g/cm^2); W=equivalent weight of steel which is taken as the ratio of atomic weight of iron to the valence of iron (27.925g); I_{app}=applied current density (Amp/cm^2); T=duration of induced corrosion (sec), F=Faraday's constant (96487Amp-sec).

The actual mass loss of rust per unit surface area may be determined by gravimetric test in accordance with ASTM G1.

$$M_{ac} = \frac{(Wi - Wf)}{\pi dL}$$

Where, M_{ac} = actual mass of rust per unit area of the bar (g/cm^2); W_i =initial weight of the bar before corrosion (g); W_f = final weight of the bar after corrosion; d is the diameter of the rebar (cm); and L=Length of the rebar sample (cm).

The degree of induced corrosion also expressed in terms of the percentage weight loss (ρ) or corrosion level or Extent of corrosion is calculated as (Ahmad, 2009):

$$\rho = \frac{(Wi - Wf)}{Wi} \text{ x } 100\ \%$$

The penetration rate is calculated using the following equation given in ASTM G1 (Beaudoin et al. 2001):

$$\text{Penetration rate (mm / year)} = \frac{(KxW)}{AxTxd}$$

Where K = a constant equal to 8.7 6×10^4, W =Mass loss (g), A = actual corroded area of steel bar (cm^2) after removal from specimen and visually examining, T=time of exposure (hour), d=density of steel =7.85 (g/cm^3).

3.6 Compressive Strength Test

According to the ASTM C39, 100 mm dia. and height of 200 mm cylindrical concrete specimen were tested by Compression Test machine for different age of concrete.

$$\text{Compressive strength, } \sigma = \frac{P}{A}$$

Where, F= compressive force on cylindrical concrete (kN) and A is area of the concrete cylinder (mm^2)

3.7 Bond Strength Test

After the required curing period, the reinforced concrete cylinders were transferred to the pullout testing frame. By using the concept of ASTM C 900-01, Pullout test frame has been designed and constructed. Detail arrangements of bond test program are shown in Figure 3.11 and Figure 3.12.

A circular plate was placed at the top of the concrete cylinder through the free steel. Its center was hollow and had 100 mm diameter as well as 8 mm thickness. For this cause, uniform pressure on the top of the concrete cylinder was applied by circular plate. At preliminary stage, 2 kN tensile load was applied on the steel through the hydraulic jack to lock the specimens with frame. Sufficient LVDT's and load cell were used to record all the necessary information during the testing. The load was applied with the help of a hydraulic jack having a capacity of 50 tons. Remote pump was used to increase the load until complete failure. Formula of the bond stress calculation are given below:

$$\text{Bond stress, } \tau = P_{max} / (\pi d_b L_d)$$

Where, τ= bond stress, P_{max} = maximum pullout load, d_b= diameter of reinforced steel, L_d = embedded length of reinforced steel into concrete.

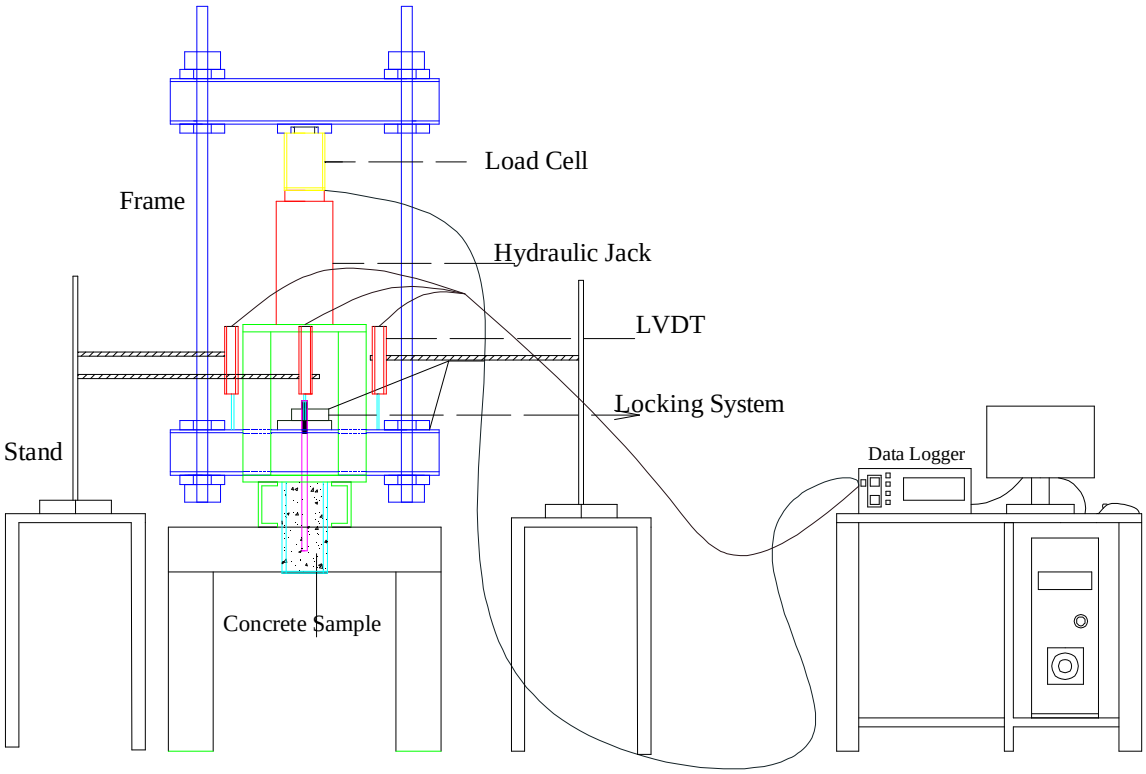

Figure 3.11: Schematic drawing of pullout test setup

Figure 3.12: Experimental setup of pullout test.

3.8 Measurement of Void

Void of concrete is the internal volume of pore spaces in concrete. It directly affects concrete strength and its durability. According to the ASTM C 642-06, volume of voids have been measured by water displacement method. By using the values for mass determined in accordance with the procedures described in ASTM C 642-06, make the following calculations:

Absorption after immersion, (%) = $[(B – A)/A] \times 100$

Absorption after immersion and boiling, % = $[(C – A)/A] \times 100$

Bulk density, dry (g_1) = $[A/(C – D)].\rho$

Bulk density after immersion = $[B/(C – D)].\rho$

Bulk density after immersion and boiling = $[C/(C-D)].\rho$

Apparent density, (g_2) = $[A/ (A – D)].\rho$

Volume of permeable pore space (voids), % = $(g_2 – g_1)/g_2 \times 100$

Where,

A = mass of oven-dried sample in air, g

B = mass of surface-dry sample in air after immersion, g

C = mass of surface-dry sample in air after immersion and boiling, g

D = apparent mass of sample in water after immersion and boiling, g

g_1 = dry bulk density

g_2 = apparent density

ρ = density of water

CHAPTER IV

Results and Discussion

4.1 General

The purpose of this chapter is to discuss the results gathered from the concrete strength, porosity of concrete, bond stress and its failure. Also, the different type of assessment on electrochemical corrosion test are accumulated into this chapter such as measurement of current density, resistance of concrete, time of corrosion, propagation rate and penetration rate, weight loss of corroded steel. Finally, relations between bond stress and corrosion are developed for several parameters. Raw data and parts of similar type of presentation for each section can be found in the Appendix.

4.2 Effect of Temperature

4.2.1 Relation between void and temperature

The relationship between void and temperature for different type of cement and aggregate is shown in Figure 4.1. The figure illustrates that PS-- type specimens give better results than others and PB-- type specimens show nearly low void than OS-- type specimens. OB-- type specimens show higher void and these specimens provide average 15.135% more void than PB-- type specimens. OS-- type specimens offer average 14.455% more void than PS-- type specimens. Finally, OB-- type specimens make 24.36% more porous concrete than PS-- type specimens.

The Figure 4.1 also explains that temperature have a great impact on void on concrete. A 30 ^{o}C temperature induced specimens offer average 7.18% more void than 20 ^{o}C induced specimens that is not a large amount of difference. But a 60 ^{o}C temperature induced specimens show average 43.79% more void than 20 ^{o}C temperature induced specimens. Finally it can be concluded that higher temperature produce more porosity than that of low temperature induced concrete. In this work, water cement ratio was constant for each temperature. At higher temperature, water demand is more than lower temperature that affects the rate of cement hydration (Mather, 1987). High temperature increases initial degree of hydration but it decreases the ultimate degree of hydration (Idorn, 1968). For this reason it rapidly produces

cement gain dense layer. The rapid increment of dense layer thickness hinders further diffusion of water. It ceases the hydration reaction even in the presence of a sufficient amount of water (Soroka, 2004). For this cause 20 ^{o}C temperature induced specimens give better results than 60 ^{o}C.

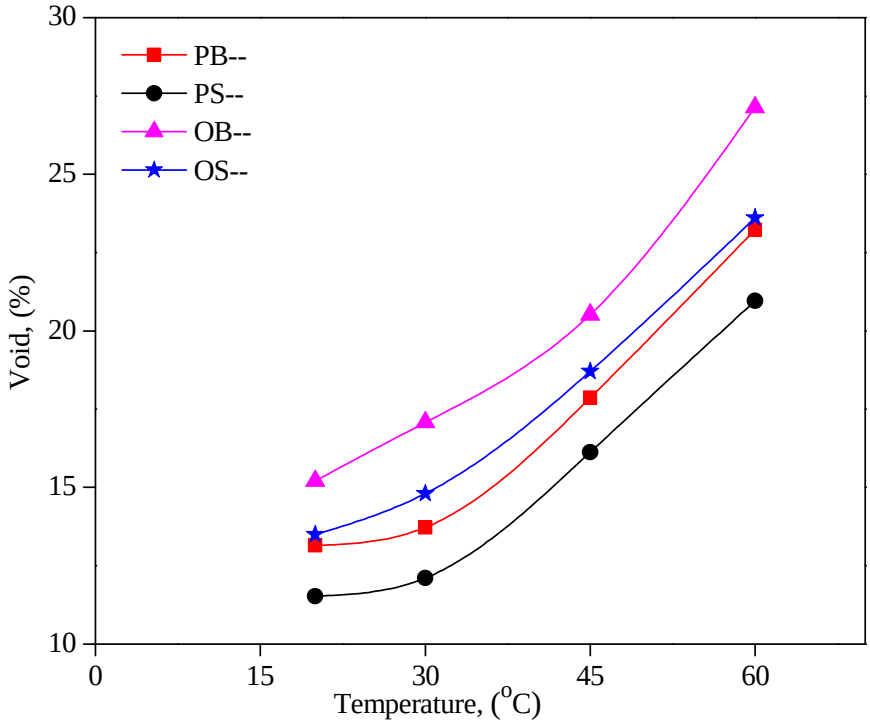

Figure 4.1: Void (%) versus temperature (^{o}C) relationship

Figure 4.1 clarify that ordinary Portland cement induced specimens show more void than Portland composite cement induced specimens. Because of supplementary cementitious material such as slag, fly ash of Portland composite cement increase the ultimate degree of hydration and slowly hydrate the anhydrate cement particles as well as fill the pore spaces of concrete (Siddique and Khan, 2011). According to Table 3.2, crushed stones are 32% more dense than crushed burn brick. Also the water absorption capacity is 1.2 for crushed stone where absorption capacity of crushed burn brick is 8.2. With respect to material property, stone type specimens produced denser concrete than brick type specimens.

4.2.2 Compressive strength

Compressive strength is a vital factor for bond behavior because the force between steel and concrete is transferred mainly by bearing and bond (Orangun, et al., 1977). Bond stress between concrete and steel reinforcement is directly proportional to compressive strength of concrete (Alavi-Fard and Marzouk, 2002). Compressive strength of concrete depends on various factors

such as temperature, cement type, aggregate, water cement ratio, etc. According to ASTM C39, compressive strength test was performed in the laboratory by compressive strength testing machine. Total specimens for compressive strength test were subdivided by four batches (OB, PB, OS, and PS). Each batch was also subdivided into four classes based on temperature regime (20, 30, 45 and 60 degree Celsius). Also, each batch of concrete was matured for 7, 28 and 56 days of curing. Figure 4.2, 4.3, 4.4 and 4.5 show the compressive stress versus curing age relationship.

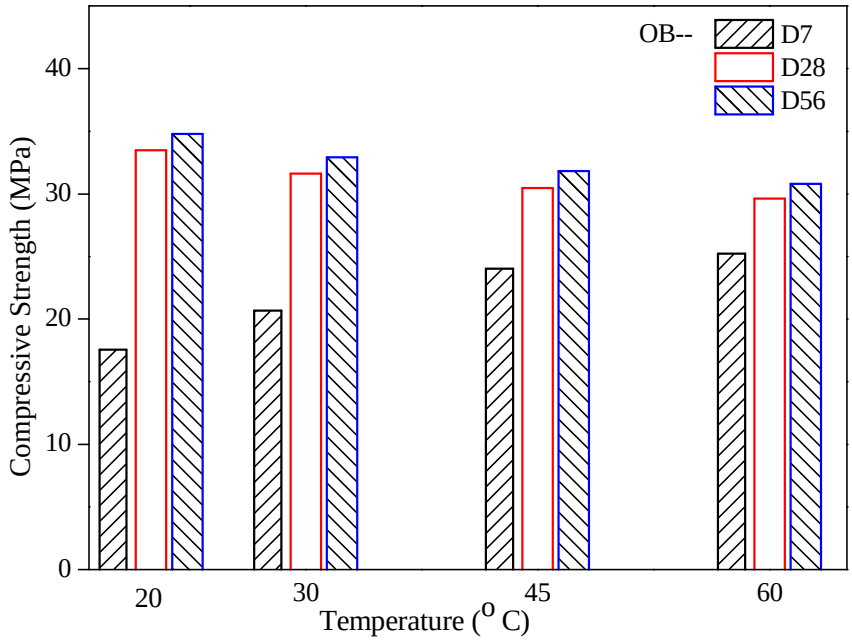

Figure 4.2: Compressive strength (MPa) versus age (days) relationship (C-OPC, CA- Brick)

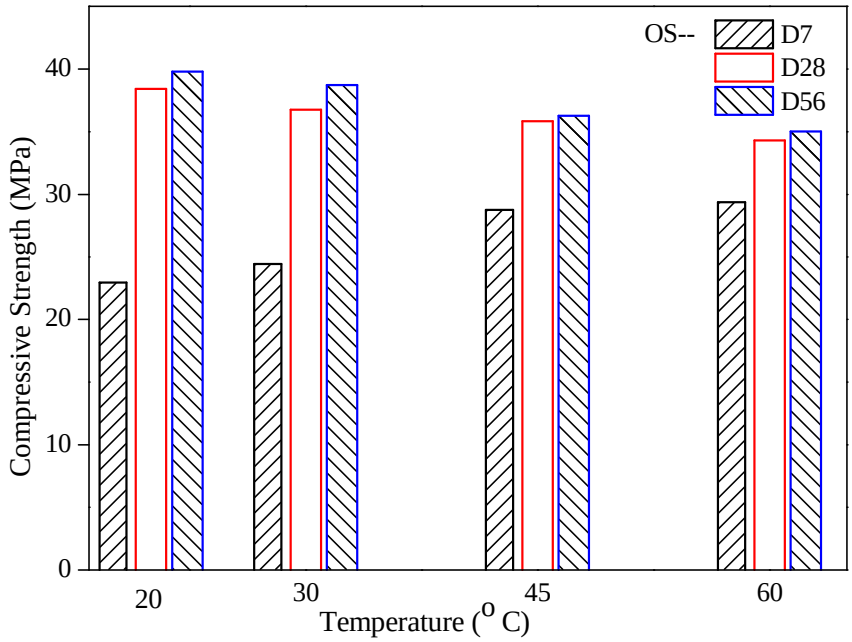

Figure 4.3: Compressive strength (MPa) versus age (days) relationship (C-OPC, CA-Stone)

Those figures illustrate that 60ºC induce specimens give higher early age strength than that of 45 ºC, 30 ºC, and 20 ºC. It also provides high early strength gaining rate but long term strength of this temperature induced specimens are lower than others temperature specimens. According to Elkhadiri, et al. (2009), increasing the casting and curing temperature accelerated the early age hydration reactions, as reflected in the initial increase in mechanical strength. The ultimate strength of concrete cured at low temperature is generally greater than that of concrete cured at a higher temperature. The fast rate of reaction at high temperatures gives relatively high early strengths but the long-term strength and durability are generally reduced (Newman and Choo, 2003).

These results depicted that long term strength of 60 ºC is lower than 45 ºC, 30 ºC, and 20ºC. These results explain that 7 days strength of PCC type specimens offer lower results than OPC type specimens and 28 days strength of OPC type specimens is slightly lower than PCC type specimens. However, 56 days strength of PCC type specimens provide higher strength than OPC type specimens and its initial strength gaining rate is slower than OPC type specimens. The results of compressive strength for PCC and OPC type specimens are shown in similar nature with Raghuprasad, et al., (2005). 150 mm x 150 mm x 150 mm concrete cube specimens were prepared to execute the test of compressive strength. It has been observed that long term strength of concrete is increased considerably of PCC type specimens compare to that of OPC type specimens

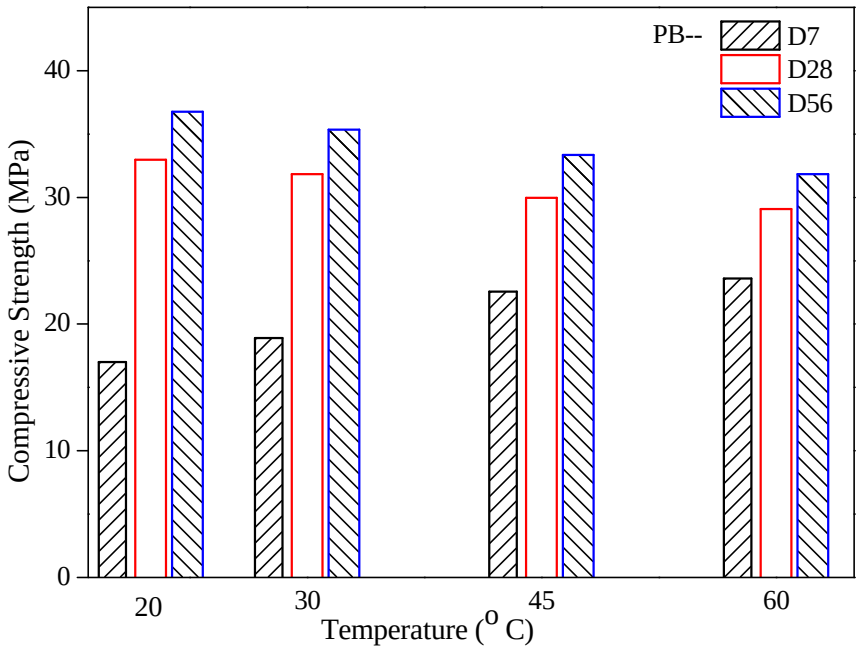

Figure 4.4: Compressive strength (MPa) versus age (days) relationship (C-PCC, CA- Brick)

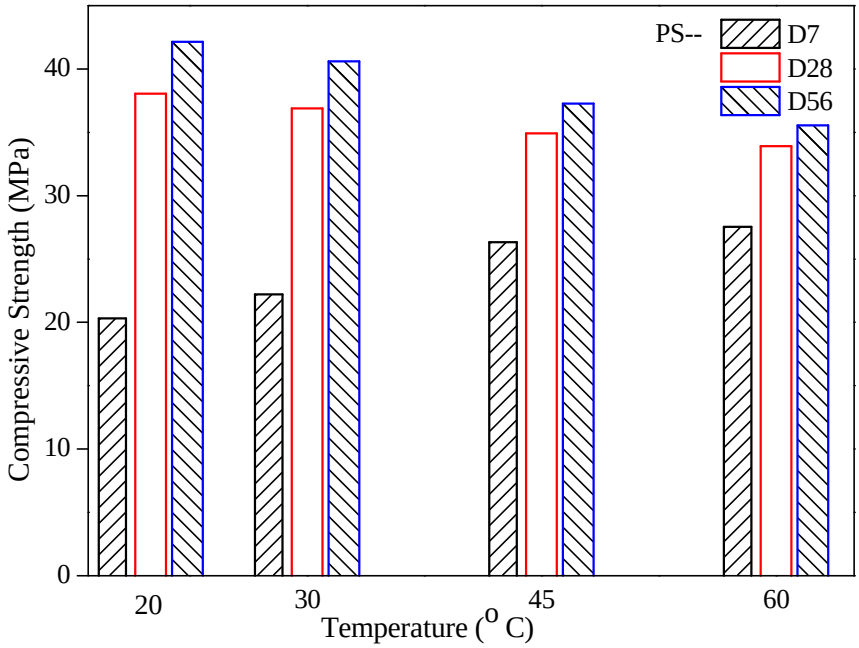

Figure 4.5: Compressive strength (MPa) versus age (days) relationship (C-PCC, CA-Stone)

These behaviors might be due to the presence of some special type of supplementary cementitious materials such as fly ash, slag, etc. in Portland composite cement. These supplementary cementitious materials increase the cement setting time and slowly fill the concrete pore space. For these reason a dense concrete is formed and long term strength is increased than ordinary Portland cement type specimens (Siddique and Khan, 2011). Crushed stone type specimens show same behaviors like crushed burn brick type specimens. Although, these specimens give average 14% to 17% more strength than crushed burn brick type specimens.

The relationship between compressive strength and void for different cement and coarse aggregate is shown in Figure 4.6. Volume of void has a role in the relationship between mechanical properties of concrete, such as the compressive strength and modulus of elasticity relationship (Popovics, 1973).The reduction of void in a cement based material increases its strength (Pantazopoulou and Mills, 1995). This figure explains that higher volume of void shows lower compressive strength. This results clarify that average 28% increments of volume of void decreases about 11% of compressive strength. It also shows that stone type specimens give better results than crushed burned brick type specimens. Also, Portland composite cement induced specimens show little bit better result than ordinary Portland cement.

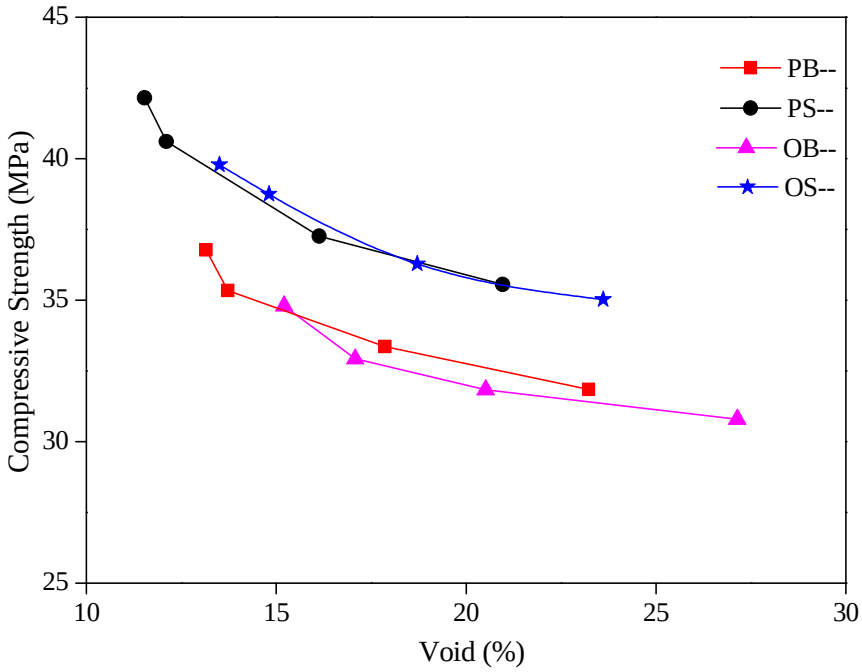

Figure 4.6: Compressive strength versus void (%) relationship

4.3 Bond Strength

Bond strength is the shear strength at the steel-concrete interface which modifies the steel stress by transferring the load between the steel and the surrounding concrete. Bond stress can be calculated as the stress per nominal unit area of the bar surface. Bond strength depends on three basic mechanism such as chemical adhesion, friction and mechanical interlocking. It can be affected by many factors like as concrete and steel strength, bar profile, embedded steel length, concrete cover thickness, temperature, corrosion and coatings.

4.3.1 Relation between bond load and slip

The relationship between bond load and slip for ordinary Portland cement and brick chips specimens for 20 ^{o}C and 60 ^{o}C temperatures are presented in Figure 4.7 and 4.8 respectively. The bond - slip relationship for other temperatures are given in appendix-A. Bond stress is the shear stress at the steel-concrete interface which modifies the steel stress by transferring the load between the steel and the surrounding concrete. Pull out test of all selected specimens were performed by designed pullout test setup according to Figure 3.11.

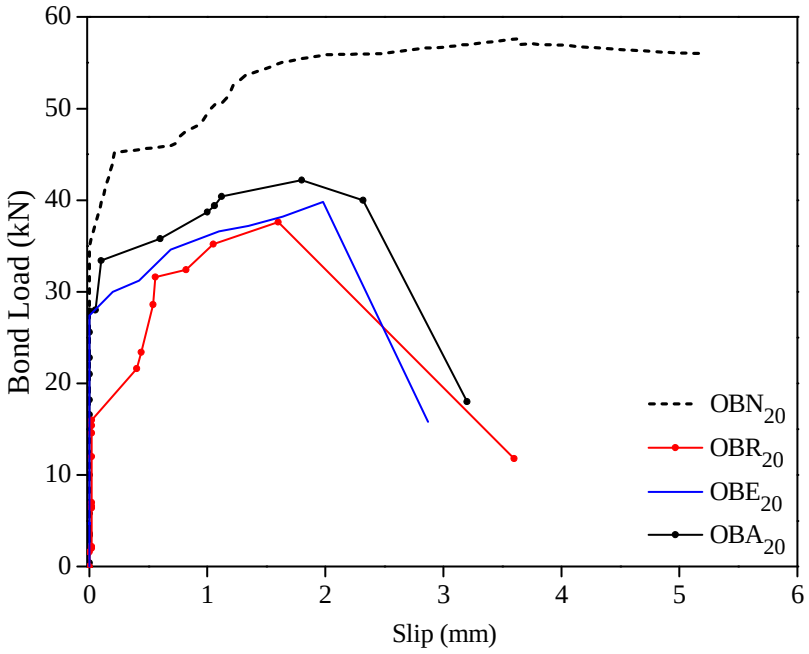

Figure 4.7: Variation of bond load (kN) against slip (mm) due to ordinary Portland cement and brick for 20°C temperature

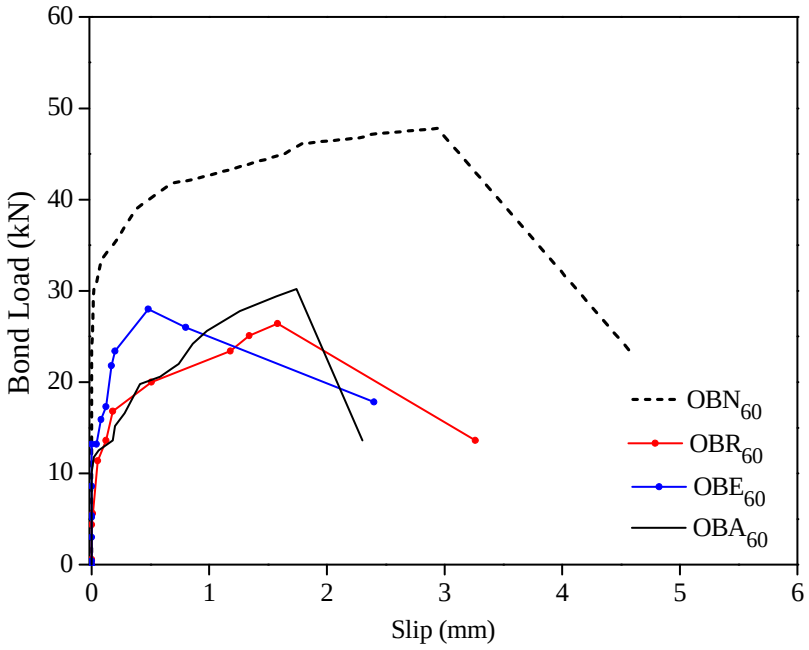

Figure 4.8: Variation of bond load (kN) against slip (mm) due to ordinary Portland cement and brick for 60°C temperature

Initial bond load- slip response of non-coated specimens is quit linear up to 60 % to 65% of bond load. Without OBN_{45}, OBN_{60} and OSN_{60} specimens, reinforced steel of another non-coated specimens had been tired in the range of 56 to 58.5 kN load. According to the laboratory test of steel, the ultimate load of 12 mm diameter bar was 74.3 kN. The necking of steel was created on the threaded portion of steel and this thread was responsible for locking arrangement

of pullout test. For cutting thread, diameter of threaded portion was reduced nearly 3 mm. For this reason, tiring load of steel in bond slip response is reduced nearly of 17%. Those specimens had been failed due to their steel failure. So, the bond load of those specimens will be more according to compressive strength and other parameters. So, without OBN_{45}, OBN_{60} and OSN_{60} specimens, others non-coated specimen's bond-slip failure are actually rebar yielding due to the reduction of rebar cross section at threaded portion. The relationship between bond load and slip for Portland composite cement and stone chips specimens for 20 ^{o}C and 60 ^{o}C temperatures are presented in Figure 4.9 and 4.10. The bond- slip relationship for other temperatures are given in appendix-A.

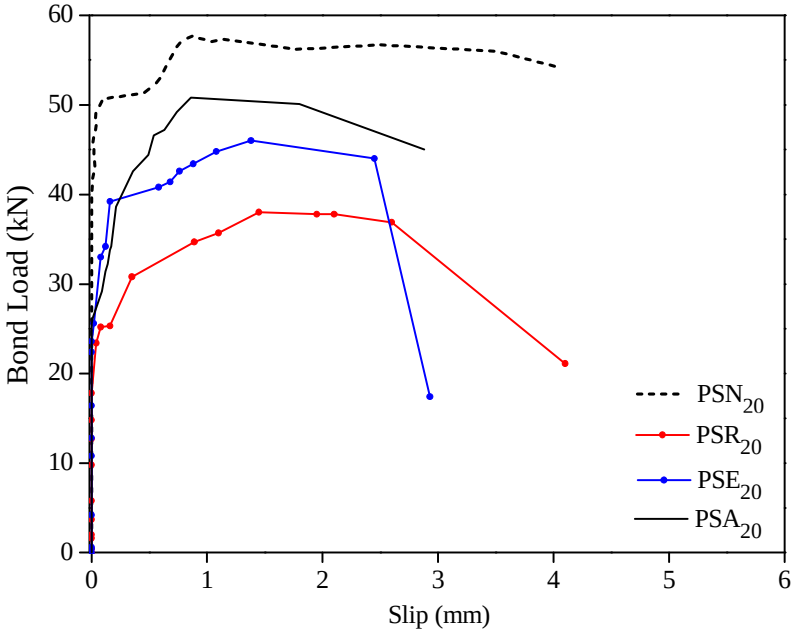

Figure 4.9: Variation of bond load (kN) against slip (mm) due to Portland composite cement and stone for 20^{o}C temperature

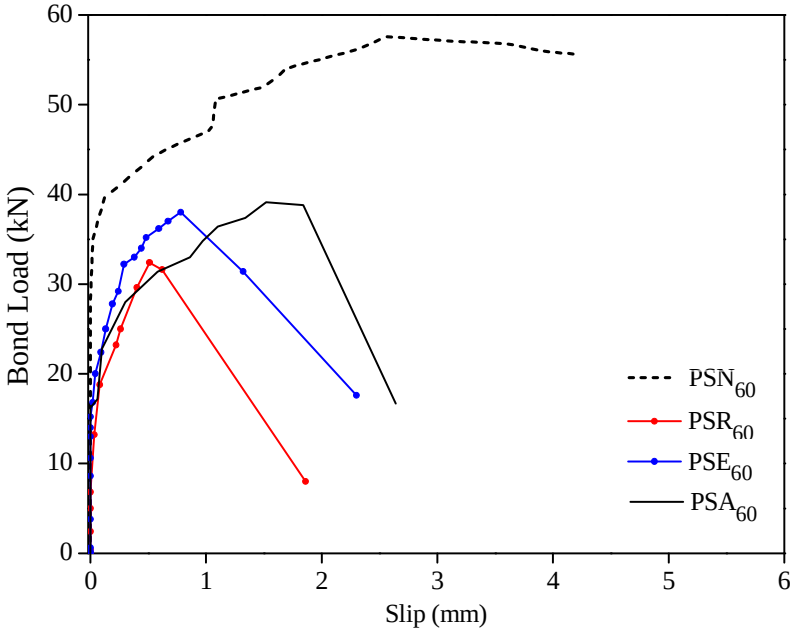

Figure 4.10: Variation of bond load (kN) against slip (mm) due to Portland composite cement and stone for 60 ^{o}C temperature

According to Elkadiri, et al., (2009) and Newman and Choo, (2003), temperature has a significant influence on concrete strength and its durability properties. The bond strength of concrete is a function of compressive strength and is approximately proportional to compressive strength up to about 20 MPa (Gandhimathi, et al., 2012). Northerly, Orangun, et al., (1977), reported that Compressive strength is considered to be a significant parameter in bond behavior because the force between steel and concrete is transferred mainly by bearing and bond. The laboratory results of pullout test show similar nature with previous research for temperature effect. The average ultimate bond stress of 20 ^{o}C specimen is 9.36% more than that of the 30 ^{o}C specimens. But a 45 ^{o}C and 60 ^{o}C induced specimens show average 17.92% and 19.7% lower bond stress than 20 ^{o}C specimens. Similarly, Raghuprasad, et al., (2005), and Siddique and Khan, (2011), reported that supplementary cementitious materials (slag, fly ash) induced cement give more ultimate strength and concrete durability than that of ordinary Portland cement. It is also observed from test results that PCC specimens show better performance on bond strength than that of OPC specimens.

For deformed bar, bond strength defends on two mechanism 1) bearing of the rebar deformation against concrete and 2) adhesion between concrete and rebar. Friction can contribute up to 35% of the ultimate strength governed by the splitting of the concrete cover (Treece and Jirsa, 1989). And adhesion is the chemical bond between the bar and the concrete. When a bar moves with respect to the surrounding concrete due to increase in the loads, the chemical adhesion along the bar surface is lost. For this cause, coating plays an important role to reduce the bond stress of reinforced concrete. It creates a smooth surface and reduces adhesion between rebar and concrete.

Red oxide, synthetic enamel paint and aluminum oxide induced specimen's present 39.45%, 33.17% and 29.4% less average ultimate bond stress from non-coated specimens. Northerly, aluminum oxide induced specimens give 14% and 5.3% superior performance than red oxide and synthetic enamel paint specimens, respectively. According the Miller, et al., 2004, coating thickness of similar type of coating material above 420 µm increases the bond strength than lower coating thickness specimens for No. 8 bars or larger bars but below this range there have no significant effect on bond strength. Bond strength drops significantly with increasing coating thickness for No. 5 and smaller bars (Choi et al., 1990 and Hester et al., 1991).

According to the Table 3.1, thickness of red oxide, synthetic enamel paint and aluminum paint on steel was 61.70 µm, 51.60 µm, and 21.67 µm. In spite of 64.8% lower thickness of aluminum paint, it presents 14 % better performance than red oxide. It has only possible for its adhesion properties. Adhesion between rebar and concrete is shown is Figure 4.11.

(a) (b) (c)

Figure 4.11: Adhesion effect of coatings on bond between steel and concrete a) red oxide, b) synthetic enamel paint and c) aluminum paint.

Bond strength is plotted against temperature in Figure 4.8 with ordinary Portland cement and brick type coarse aggregate.

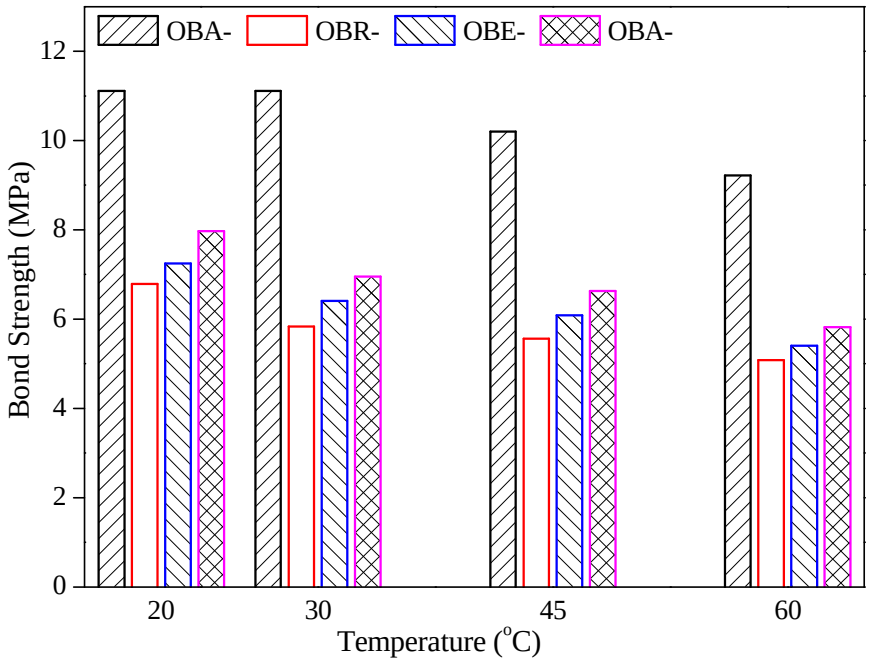

Figure 4.12: Bond strength (MPa) versus temperature (°C) relationship (C-OPC & CA-Brick)

Bond strength is plotted against temperature in Figure 4.8 with ordinary Portland cement and stone type coarse aggregate.

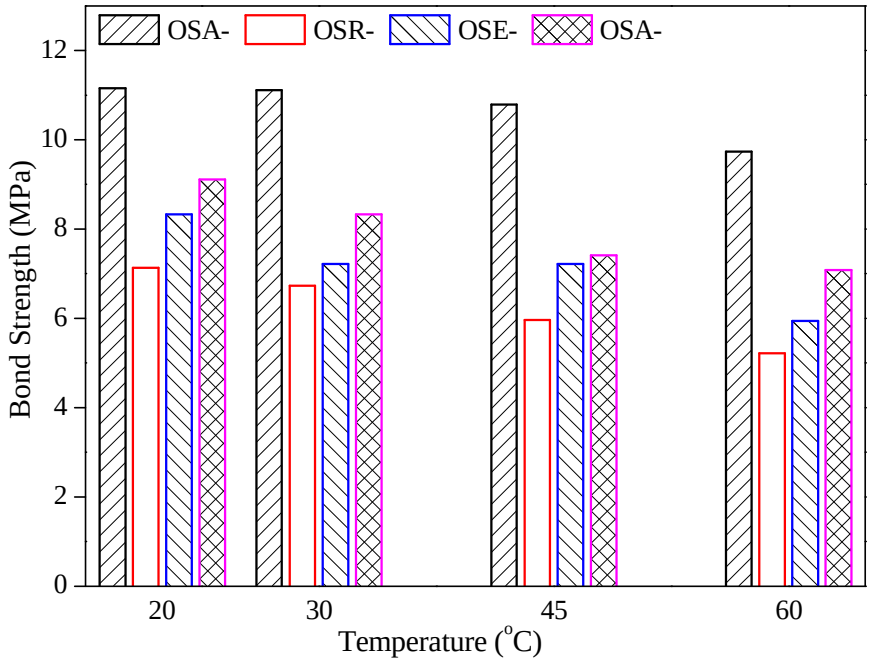

Figure 4.13: Bond strength (MPa) versus temperature (°C) relationship (C-OPC & CA-Brick)

Bond strength is plotted against temperature in Figure 4.8 with Portland composite cement and brick type coarse aggregate.

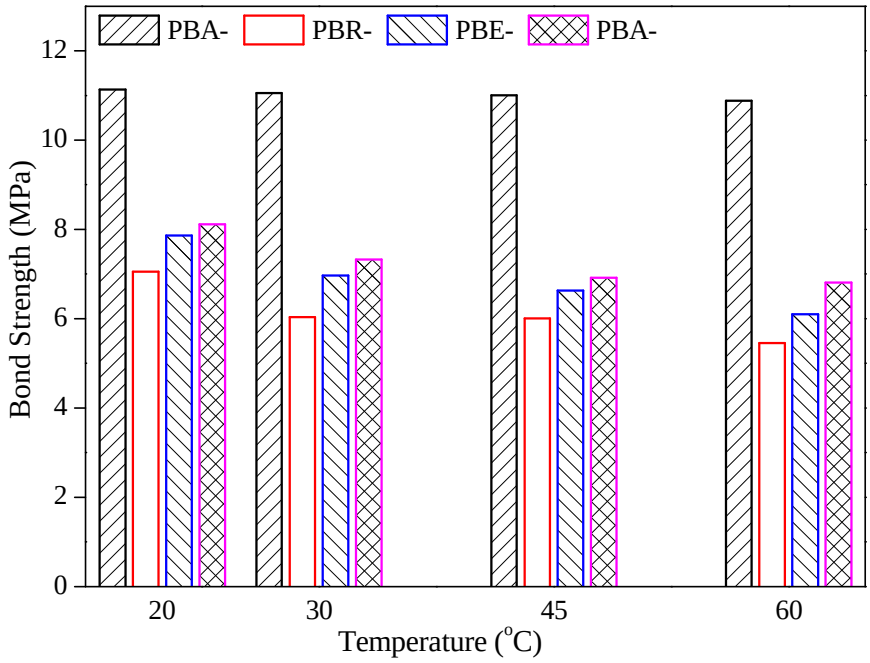

Figure 4.14: Bond strength (MPa) versus temperature (°C) relationship (C-OPC and CA-Brick)

Bond strength is plotted against temperature in Figure 4.8 with Portland composite cement and stone type coarse aggregate.

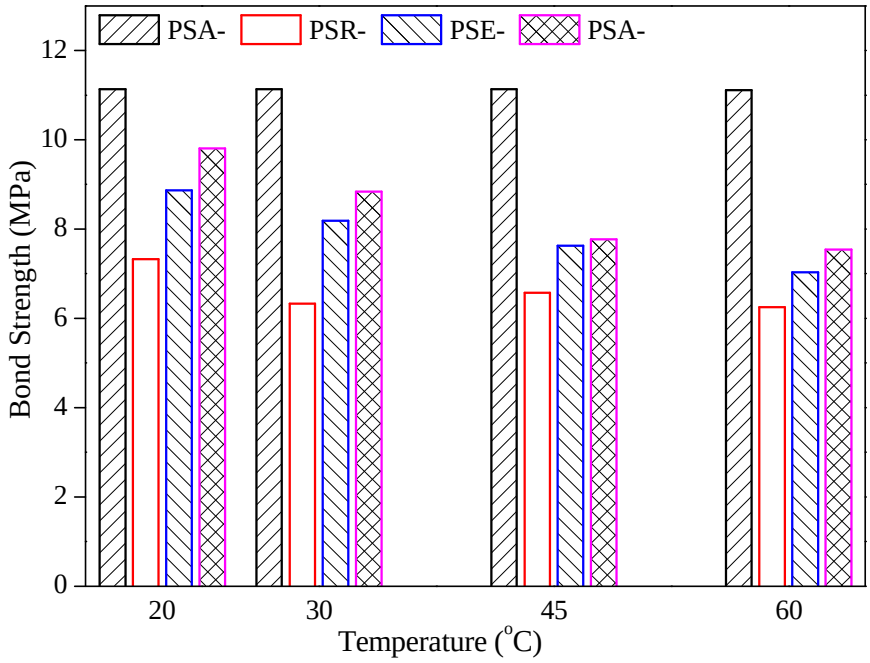

Figure 4.15: Bond strength (MPa) versus temperature (°C) relationship (C-OPC & CA-Brick)

In previous, to protect the reinforcing steel from severe environmental conditions (sulphate attack, chloride attack and carbonations), numerous research has been carried out regarding the bond behavior of epoxy-coated reinforcing bars. It has been focused from this previous work that a) adhesion is prevented because the layer of epoxy acts as a bond breaker between the steel and the hydrating cement b) epoxy coating is liable to reduce the friction. The use of epoxy-coated bars increases the angle of the resultant bond force and causes higher radial splitting force. This indicates that epoxy-coated bars will have less bond capacity because it is the cause of premature splitting failure than are uncoated bars (Kayyali, 1995). Cusens and Yu, 1993, reported that bond forces are not transferred into coated reinforcing bar as efficiently as they are into uncoated reinforcement. According to Treece and Jirsa, (1989), it has been found that maximum bond load for the coated steel decreased by approximately 40%, as compared with the uncoated steel. And this finding is near about similar with laboratory test results of this work.

4.3.2 Failure types of bond

Two failure types were observed in the experimental program. A pullout splitting failure occurs when the bar reaches a higher load and then a crack appeared parallel to the applied force on the face of concrete perimeter as bar pullout. The failure types are shown in Figure 4.16.

(a) (b) (c) (d) (e)

Figure 4.16: Longitudial bond fracture of pullout test specimens a) shear failure, b) shear and cone failure, c) split and cone failure, d) columnar failure and e) bar yielding

Due to the bearing stresses, equal and opposite forces develop between the reinforcing bars and the concrete. These initial forces are caused by the wedging action of the ribs bearing against concrete. They will cause tensile stresses in a cylindrical piece of concrete around the bar. If the tension becomes too high, the concrete cylinder will split. Splitting resistance along the bar depends on quite a few factor, such as concrete cover, coating, and types of aggregate and spacing of bars. Four splitting pullout types failure were found in the experimental program like as shear failure, shear and cone failure, split and cone failure, columnar failure. Another failure is bar yielding, when the bar reaches a load that is sufficient to cause yielding. Because of this, the peak load must be considered separately from splitting or pullout type failures.

4.4 Corrosion Effect

4.4.1 Relation between time of crack initiation and elapsed time

In severe exposure, crack initiation on concrete surface is the first symbol of corrosion starting. First corrosion crack seems like a hair line crack. But the time of crack initiation is the most important measurement that helps to assess the impacts of parameter on corrosion of reinforced concrete. Time of crack initiation is plotted against temperature in Figure 4.17 with ordinary Portland cement and brick type coarse aggregate.

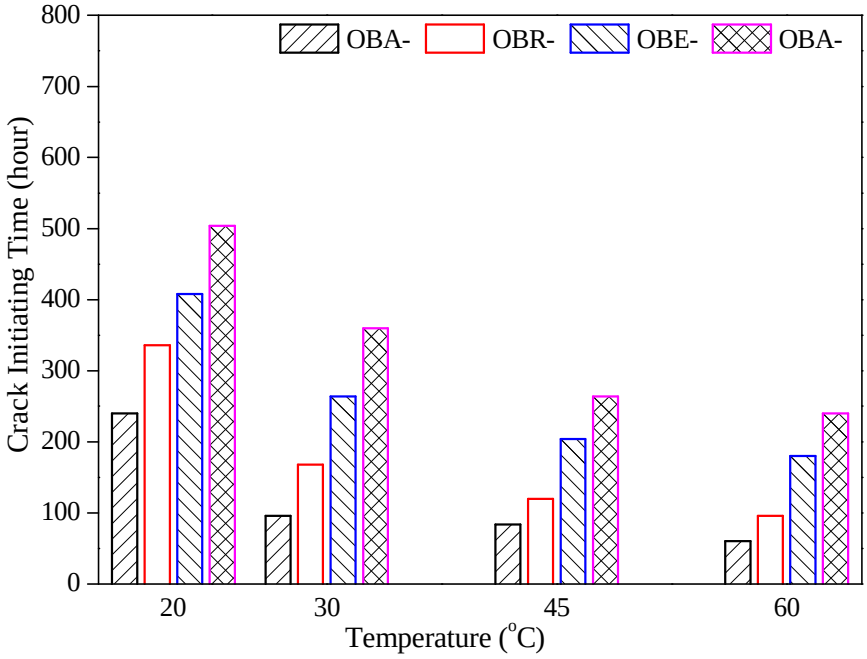

Figure 4.17: Time of crack initiation versus temperature relationship (C-OPC and CA-Brick)

Time of crack initiation is plotted against temperature in Figure 4.16 with ordinary Portland cement and stone type coarse aggregate.

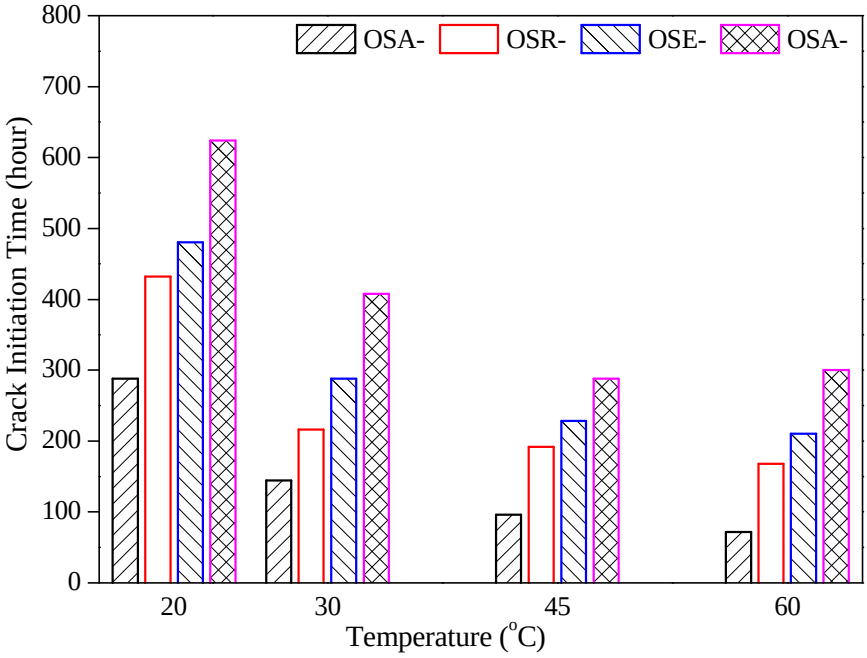

Figure 4.18: Time of crack initiation versus temperature relationship (C-OPC and CA-Stone)

Figure 4.17 and 4.18 show that Portland composite cement consumes 22.1% more time to make a hair line crack than ordinary Portland cement. Because of, Portland composite cement is liable to enlarge the time of crack initiation. Slag and fly ash reduce the pore space of concrete

and raise the resistance of reinforced concrete (Siddique and Khan, 2011). And also the supplementary materials like those are directly responsible to develop the long term strength. According to these figures, coatings also increase the crack initiation time. Red oxide, synthetic enamel paint and aluminum oxide take 30.8%, 43.6%, and 58.4% more time than non-coated specimens to create a hair line crack. Aluminum oxide also offers 39.8% and 26.2% better performance than red oxide and, synthetic enamel paint.

Maaddawy and Soudki, 2003, did an experiment on electrochemical corrosion test of 150 mm x 250 mm x 300 mm reinforced concrete for different current density. It has been seen from the observed results that higher current density induced specimens take less time to initiate first hairline crack compare to lower current density. It also seemed that it accelerates the propagation rate of crack and rapidly fulfill the target crack width than that of low current density.

Time of crack initiation is plotted against temperature in Figure 4.19 with Portland composite cement and brick type coarse aggregate.

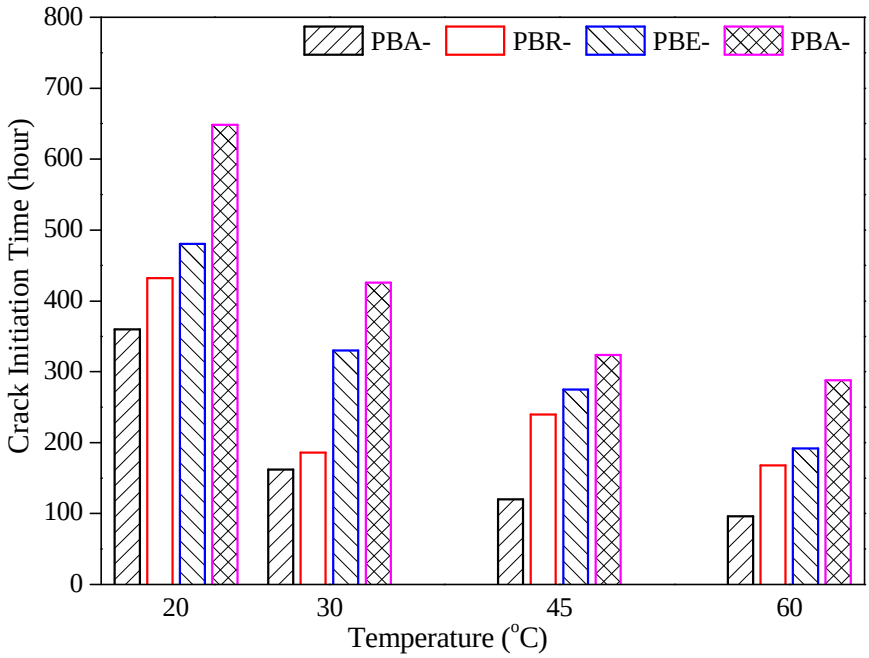

Figure 4.19: Time of crack initiation versus temperature relationship (C-PCC and CA-Brick)

Time of crack initiation is plotted against temperature in Figure 4.20 with Portland composite cement and stone type coarse aggregate.

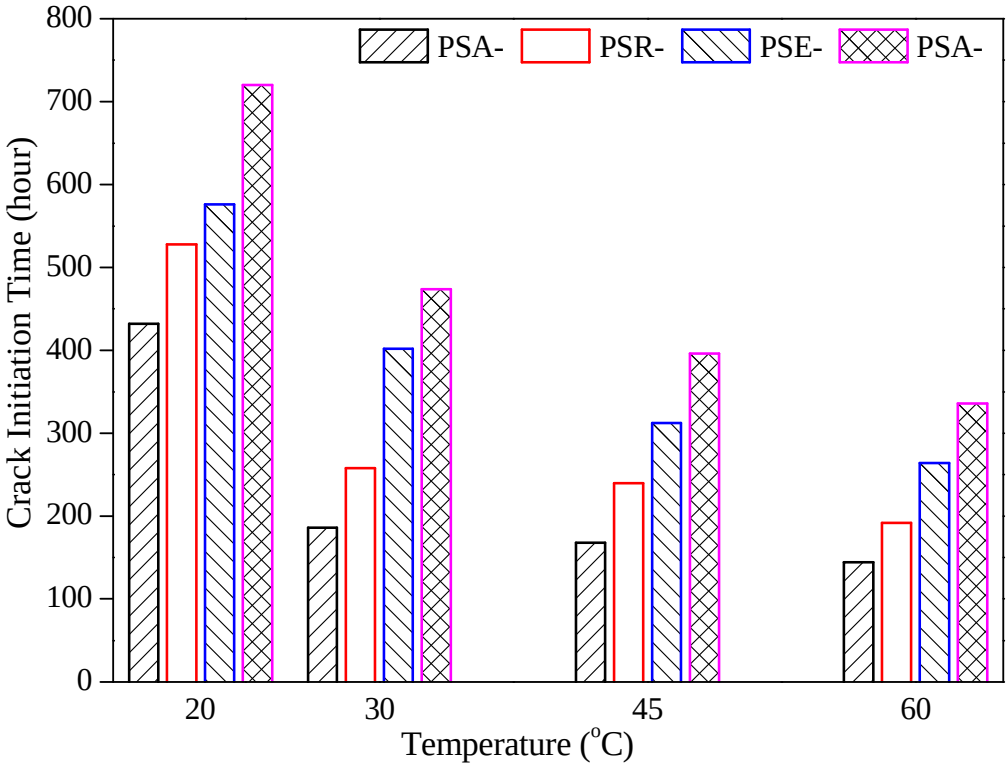

Figure 4.20: Time of crack initiation versus temperature relationship (C-PCC and CA-Stone)

From Figure 4.17, 4.18, 4.19 and 4.20, it is found that 20 ^{o}C induced specimens under corrosion cell take 41.6%, 54.3%, and 61.1% extra time to visualize the first crack on concrete surface than 30 ^{o}C, 45 ^{o}C, and 60 ^{o}C specimens. When corrosion of steel starts into the concrete then the formation of ferric oxide that means rust apply a tensile stress on the transverse site of concrete cylinder. So the tensile stress of concrete is directly proportional to concrete compressive strength (Mansfeld, 1981). Compressive strength of concrete is also comparative to temperature. Temperature also increases the electrochemical reaction rate. For this reason, formation of rust inside the concrete generates rapidly and applies more pressure to make a crack. Other results on corrosion- time relationship are given in Appendix-C.

4.4.2 Influence of temperature on concrete crack propagation

Propagation of crack width measurement is an important observation for corrosion of reinforced concrete. In this subdivision, crack width is plotted against time due to 20 ^{o}C and 60 ^{o}C specimen in Figure 4.21. Target crack width of this corrosion test was 0.60 mm. But some specimen's crack width exceeds the target width because of visual identification. According to the ACI 224R code, allowable crack width for dry air or protective membrane is 0.41 mm, for humidity and moist air is 0.30 mm for sea water and sea water spray is 0.15 mm. This code

provision is also shown in this figure. Where A indicates 0.15 mm crack width, B indicates 0.30 mm crack width and C indicates 0.41 mm crack width.

Figure 4.21 clearly shows that OBN_{20} takes 168 hours more time to generate the first hair line crack on concrete surface due to corrosion than OBN_{60}. Also, after the initiation of first crack, propagation rate of crack width is lower than OBN_{60}. That means, high temperature shows higher propagation rate than lower temperature. Because of, higher temperature decreases the long term strength of concrete. For this reason, ferric oxide (rust) can easily overcomes the barrier of tensile stress of concrete and generates hair line. And also, higher temperature increases the porosity of concrete that helps to the ferric oxide to pass through the concrete and propagate the crack width. This figure also shows that propagation line of crack width is linear below the B line. And most the specimens show non-linear behavior above the B line.

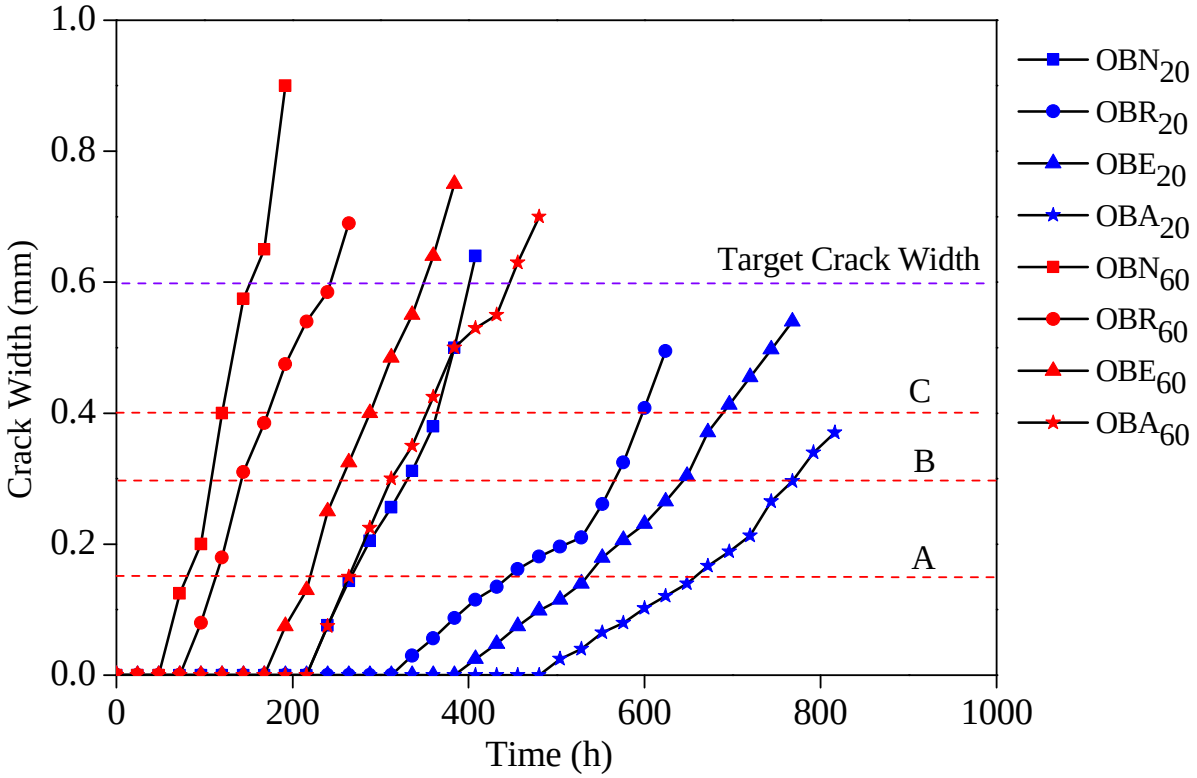

Exposure condition: A= Sea water; B= Humidity, moist air; C= Dry air

Figure 4.21: Propagation of crack width against time due to ordinary Portland cement and crushed burn brick.

Crack width is plotted against time in Figure 4.22 with ordinary Portland cement and crushed stone.

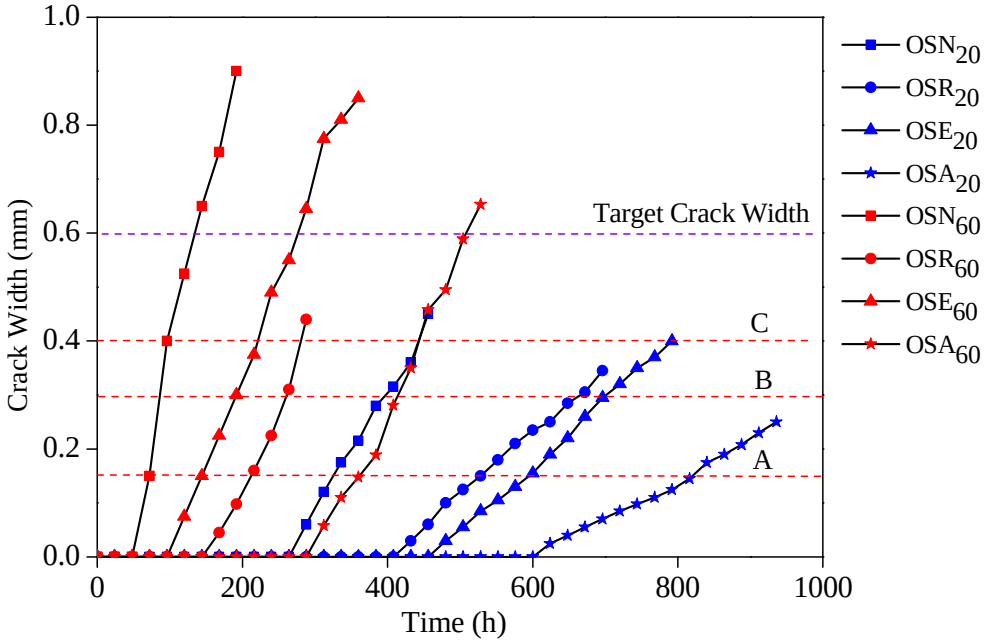

Exposure condition: A= Sea water; B= Humidity, moist air; C= Dry air

Figure 4.22: Propagation of crack width against time due to ordinary Portland cement and crushed stone.

Crack width is plotted against time in Figure 4.23 with Portland composite cement and crushed burn brick.

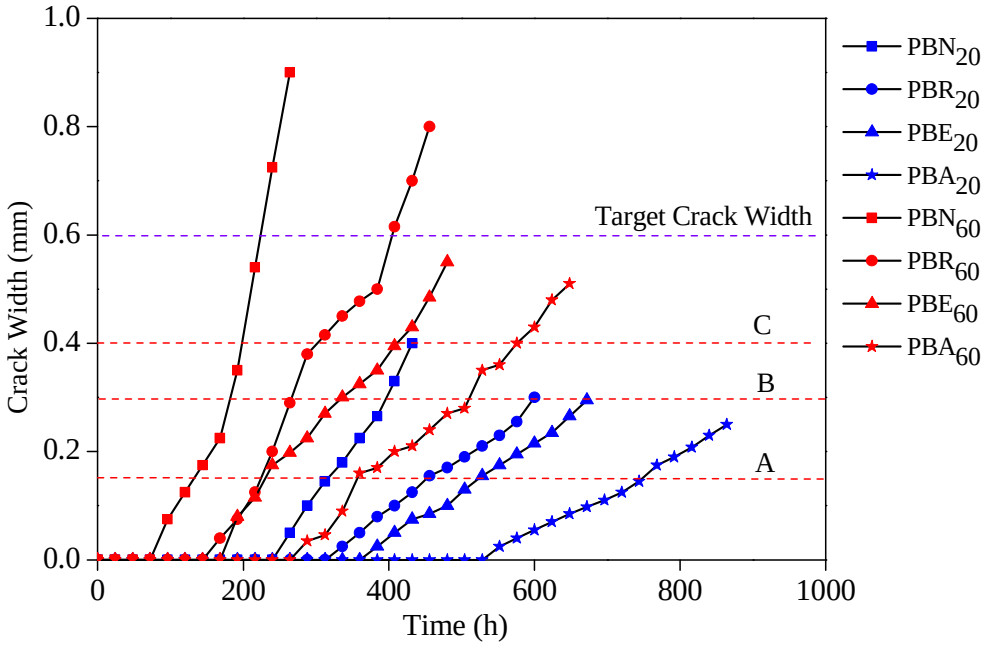

Exposure condition: A= Sea water; B= Humidity, moist air; C= Dry air

Figure 4.23: Propagation of crack width against time due to Portland composite cement and crushed burn brick.

Crack width is plotted against time in Figure 4.24 with Portland composite cement and crushed stone.

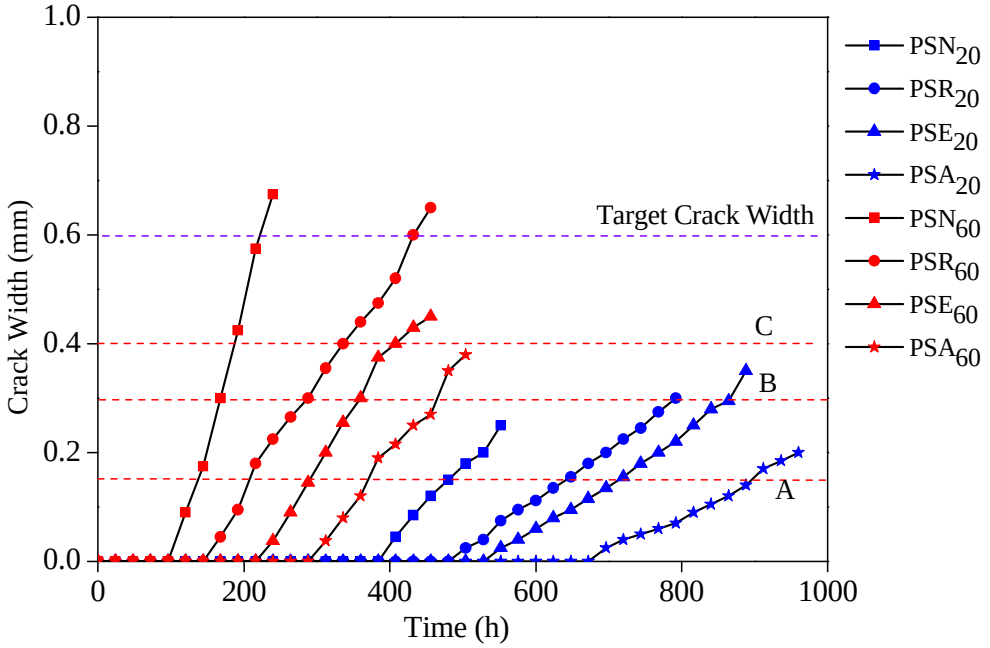

Exposure condition: A= Sea water; B= Humidity, moist air; C= Dry air

Figure 4.24: Propagation of crack width against time due to Portland composite cement and crushed stone.

From the above graph, it can be illustrated that cement also plays an important role on propagation rate of concrete crack. Below the B line, OBN_{60} shows 62% more slope of tangent line for the plot of crack width vs. time than PBN_{60}. So, Portland composite cement type specimens confirm lower propagation rate than ordinary Portland cement type specimens. These figures also show that brick induced specimen takes more time to generate hair line crack than stone induced specimen. And it also gives 12.73% more propagation rate than stone induced specimen.

These figures illustrate that coatings reduce the propagation rate of concrete. Coatings resist the electrons to pass through the concrete. This cause was liable to delay the occurring of crack on the surface of the concrete. From Figure 4.23, it can be observed that below B line, PBN_{20} shows 43.5%, 48.6%, and 60% more slope of tangent line than PBR_{20}, PBE_{20} and PBA_{20} respectively. Northerly, among the coatings, aluminum oxide induced specimens consume more time for formation of target crack. So it shows almost lower propagation rate. Finally, Aluminum oxide type specimens show average 27% and 19% lower propagation rate than red oxide and synthetic enamel type specimens. According to Maaddawy and Soudki, (2003), concrete side strain versus time relationship has been found. It has been observed that higher strain were measured as current density increased. It has been also observed that current density

has significant influence on maximum crack width. Finally, it has been seen from this research work that low current density level requires a longer corrosion period than that required to reach the same percentage of mass loss at a higher current density level. It can be concluded from the above discussion that a greater concentration of the corrosion products around the steel reinforcing bars causes higher expansion and internal stresses, which in turn lead to further deterioration of the concrete around the steel reinforcing bars and larger crack width. Other plots related with crack width vs. time are placed in Appendix-D

4.4.3 Loss of mass due to corrosion

Relation between measured mass loss and predicted mass loss according to Faradays law is discussed in this subdivision. Mass loss is plotted against specimens in Figure 4.25 and 4.26 with ordinary Portland cement and Portland composite cement for 20 ^{o}C temperature. From Figure 4.25 and 4.26, it is initially seemed that there have no linear relationship among measured mass loss and any parameter. Because of mass loss is depended on current density and elapsed time of corrosion. Each specimen was picked up from the corrosion cell when the target crack had been generated. For this reason, elapsed time of corrosion for every specimen is not same. These figure also demonstrate that predicted mass loss shows 59.64% more result than measured mass loss. Because of, it is measured according to Faraday's law and it is also a theoretical law. In this law's assumption, there have no protected layer surrounding the steel.

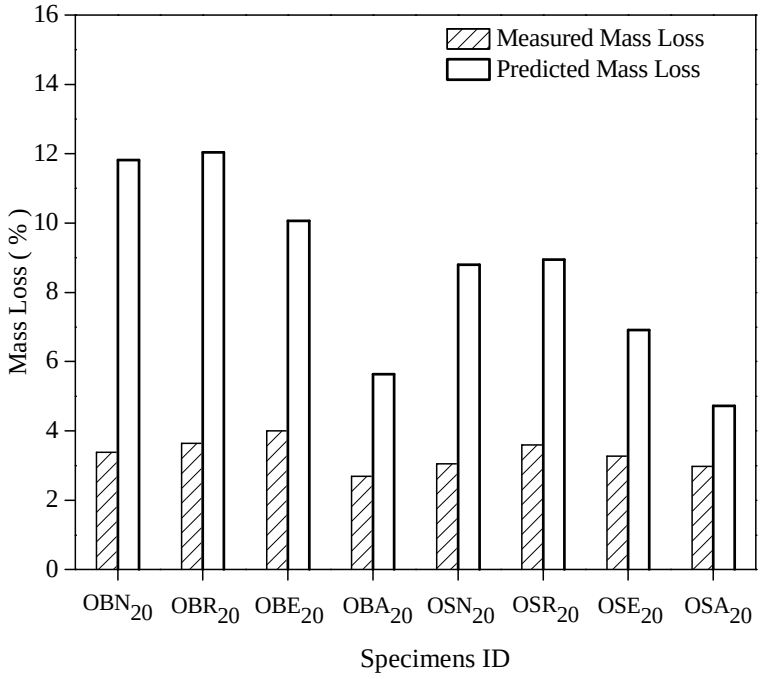

Figure 4.25: Variation of mass loss (%) due to ordinary Portland cement for 20 ^{o}C temperature

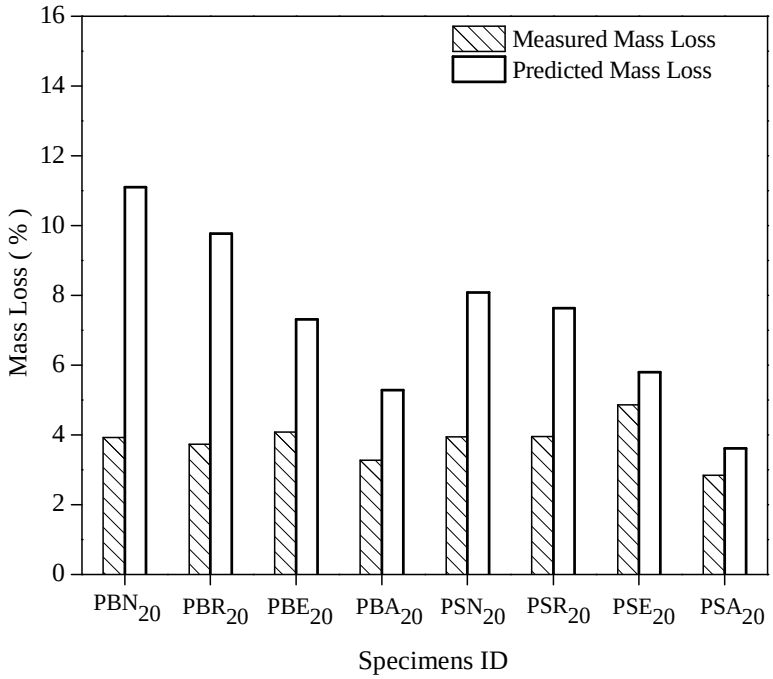

Figure 4.26: Variation of mass loss (%) due to Portland composite cement for 20^{o}C temperature

But in this research work, steel was bounded by 44mm thick harden concrete layer and concrete is a high resistance material. For this cause, measured mass loss gives lesser result than predicted mass loss. Predicted mass loss of ordinary Portland cement offers 7.12% more mass loss than Portland composite cement. Because of predicted mass loss is directly depended on current density. And ordinary Portland cement induced specimens consume more current density to decay the steel. Northerly, measured mass loss of ordinary Portland cement shows 9.7% better performance than Portland composite cement. But this performance is not actual performance. Measured mass loss is a function of current density and elapsed time of corrosion. Portland composite cement induced specimens need minor current density and more elapsed time to generate the target crack on concrete surface. For this basis, decomposition of steel on the outer contract point of steel and concrete was more than ordinary Portland cement induced specimens. Actually, this is the main cause to enlarge the mass loss of Portland composite cement induced specimens.

Figure 4.27: Corroded reinforcing steel

4.4.4 Penetration rate and elapsed time

Penetration rate and elapsed time response of 20^{o}C induced specimens is plotted in Figure 4.28. Other results are given in Appendix- F. The penetration rate is calculated using the following equation given in ASTM G1 (Beaudoin, et al., 2001):-

$$\text{Penetration rate (mm / year)} = \frac{(KxW\ )}{AxTxd} \quad \text{..... (Eq. 4.1)}$$

Where K = a constant equal to 8.7 6×10^{4}, W = Mass loss in grams, A = actual corroded area of steel bar in cm^{2} after removal from specimen and visually examining, T= time of exposure in hours, d = density of steel 7.85 (g/cm^{3}). According to this equation, penetration rate is mainly depended on weight loss and elapsed time of corrosion. Penetration rate is plotted against temperature in Figure 4.28 with ordinary Portland cement and brick type coarse aggregate. From mass loss versus specimen's relationship, it is clear that there have no linear relationship of measured mass loss. But this figure shows penetration rate presents a good relationship with respect to elapsed time for every specific parameter. But coating has a great impact on penetration rate of corroded steel. Coating cases the passing of current density through reinforced concrete. Also it enlarges the elapsed time of corrosion. For this reason, OBN_{20} offers 26.3%, 36.9%, and 53.4% further penetration rate than OBR_{20}, OBE_{20} and OBA_{20}. Northerly, this figure explains that OBA_{20} shows 37.37% and 26.8% better performance than OBR_{20} and OBE_{20}. It is also seemed that OSN_{20} shows 13.32% more penetration rate than OBN_{20}.

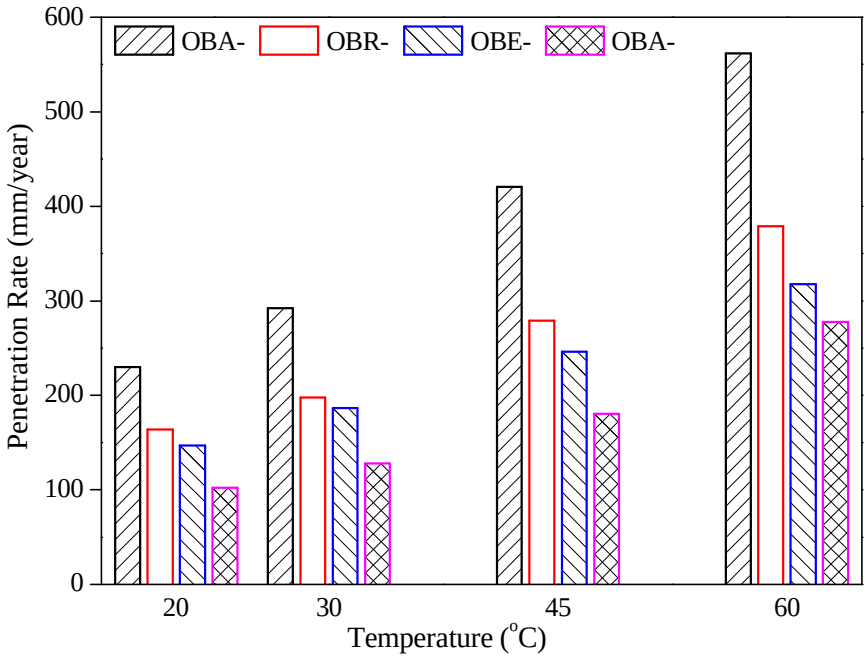

Figure 4.28: Penetration rate versus temperature relationship (C-OPC and CA-Brick)

Penetration rate is plotted against temperature in Figure 4.29 with ordinary Portland cement and stone type coarse aggregate.

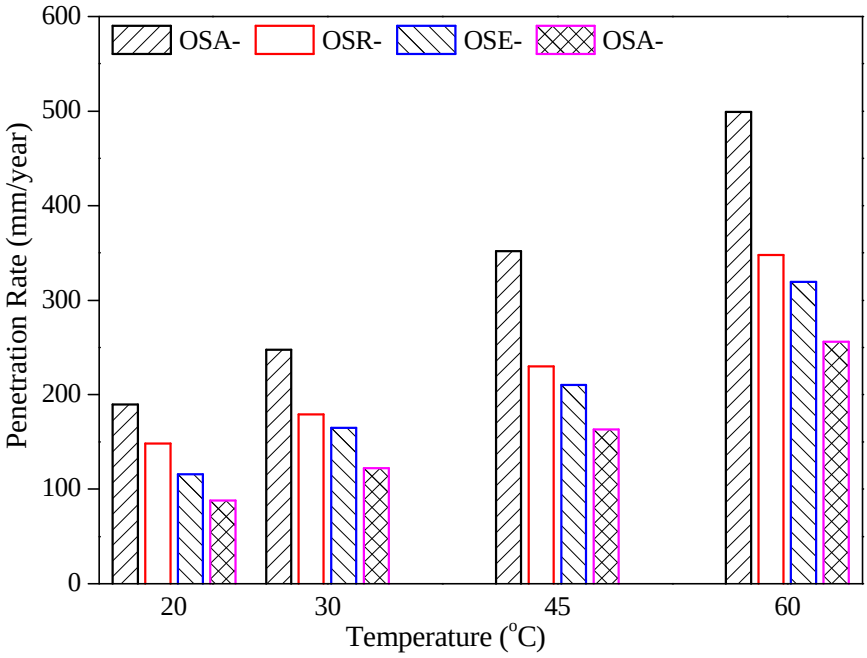

Figure 4.29: Penetration rate versus temperature relationship (C-OPC and CA-Stone)

Penetration rate is plotted against temperature in Figure 4.30 with Portland composite cement and brick type coarse aggregate.

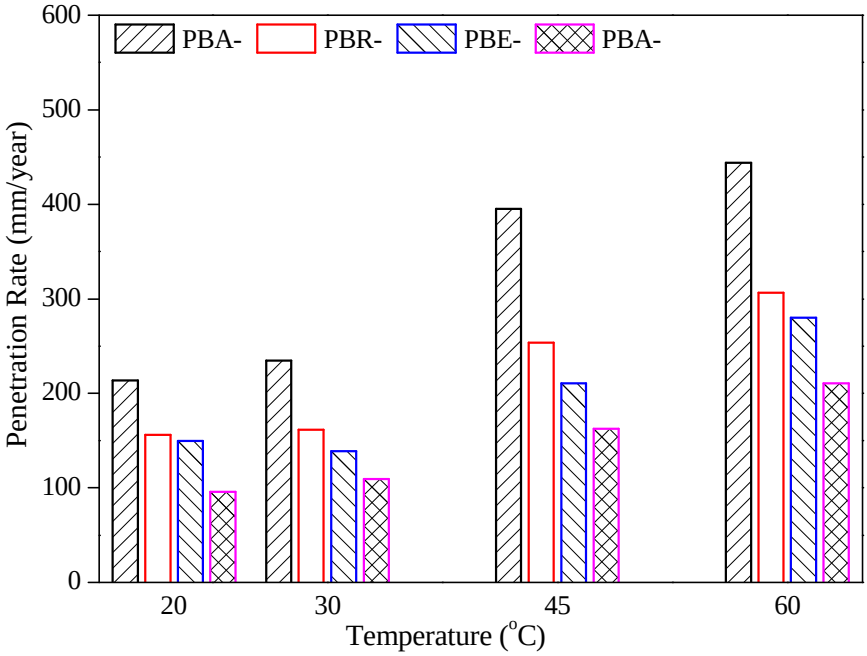

Figure 4.30: Penetration rate versus temperature relationship (C-PCC and CA-Brick)

Penetration rate is plotted against temperature in Figure 4.31 with Portland composite cement and stone type coarse aggregate.

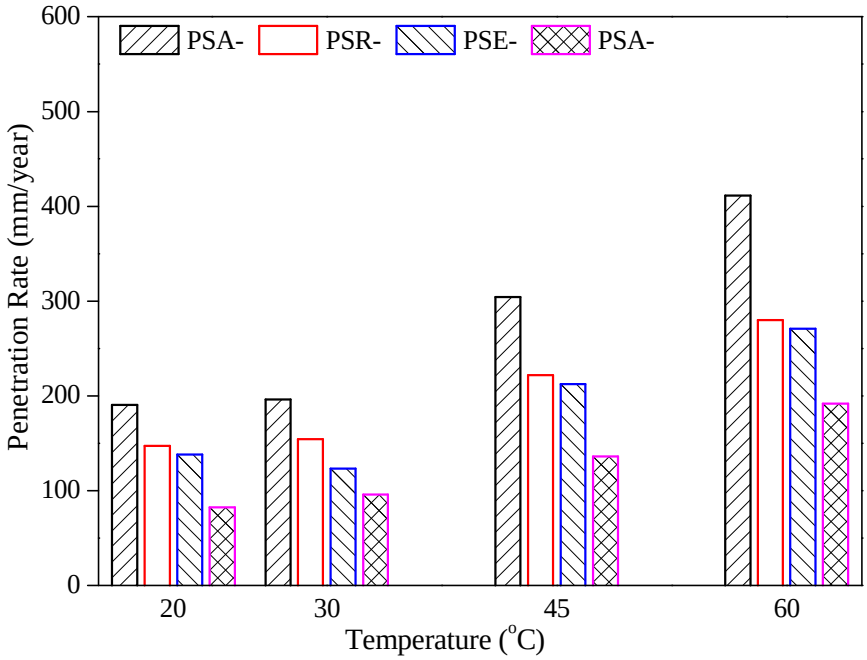

Figure 4.31: Penetration rate versus temperature relationship (C-PCC and CA-Stone)

From the comparison of Figure 4.28, 4.29, 4.30 and 4.31, it can be seen that temperature has major impact on penetration rate. The 20 ^{o}C specimens consume more time to generate the target crack. And 20 ^{o}C specimens give 7.3%, 40.9%, and 56% better performance on

penetration rate than 30 ^{o}C, 45 ^{o}C, and 60 ^{o}C temperature. Northerly, Portland composite cement gives average 16.2% better performance than ordinary Portland cement.

This results of penetration rate show similar nature with Hussain and Ishida, (2011). "Electrochemical corrosion for reinforced concrete under different temperature" had been performed in that research work. It has been clearly found from the penetration rate versus temperature relationship that penetration rate is increased with the raise in temperature. It can be found a clear observation from Siddique and Khan, 2011, about the effect of fly ash on corrosion of reinforced concrete. It has been clarified in Table 1.23 (Siddique and Khan, 2011) that for As-received Fly Ash (AFA), pure OPC induced specimens take 29% more corrosion current than that of 20% to 30% replacement of fly ash with OPC. So it is very significant issue for the observation of penetration rate because of penetration rate is directly proportional to corrosion current density.

4.5. Bond Stress and Corrosion Relationship

Bond strength and penetration rate are plotted against temperature in Figure 4.32 below with Portland composite cement and brick type coarse aggregate. This relationship explains that OBN_{20} gives 13.32% more penetration rate than OSN_{20}. But for the measurement of bond stress, this reversible. Stone type specimens show average 9.61% more bond stress than brick type specimens. Northerly, for penetration rate measurement, OBN_{20} shows 16.5% more penetration rate than PBN_{20}. Also Portland composite cement type specimens give average 6.7% more bond stress than ordinary Portland composite cement type specimens. This result is also reversible from the point of view. Again, OBN_{20} show 26.29%, 36.9% and 53.83% more penetration rate than OBR_{20}, OBE_{20} and OBA_{20}. And also OBN_{20} offers 39.45%, 33.167% and 29.43% more bond stress than OBR_{20}, OBE_{20} and OBA_{20}.

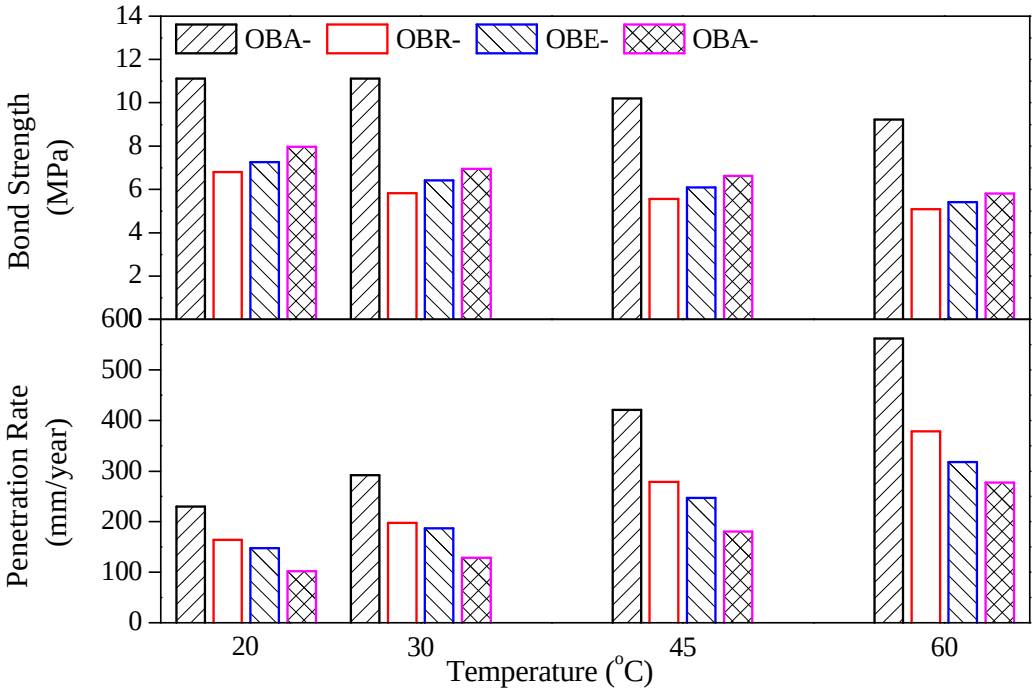

Figure 4.32: Bond strength and penetration rate versus temperature relationship (C-OPC and CA-Brick).

Bond strength and penetration rate are plotted against temperature in Figure 4.33 below with Portland composite cement and brick type coarse aggregate.

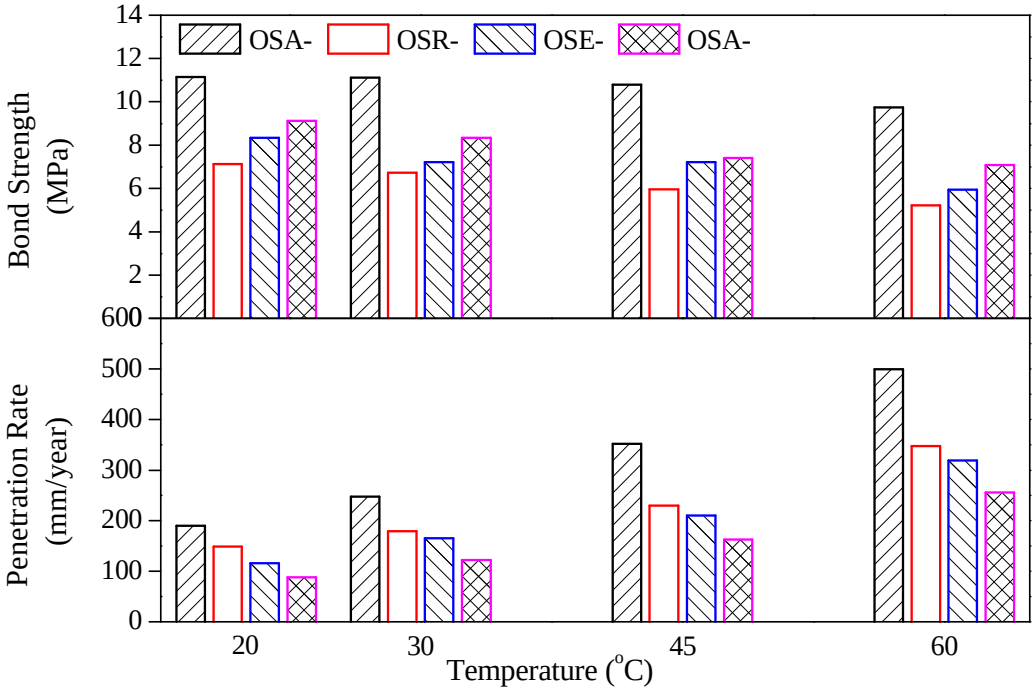

Figure 4.33: Bond strength and penetration rate versus temperature relationship (C-OPC and CA-Stone).

Bond strength and penetration rate are plotted against temperature in Figure 4.34 below with Portland composite cement and brick type coarse aggregate.

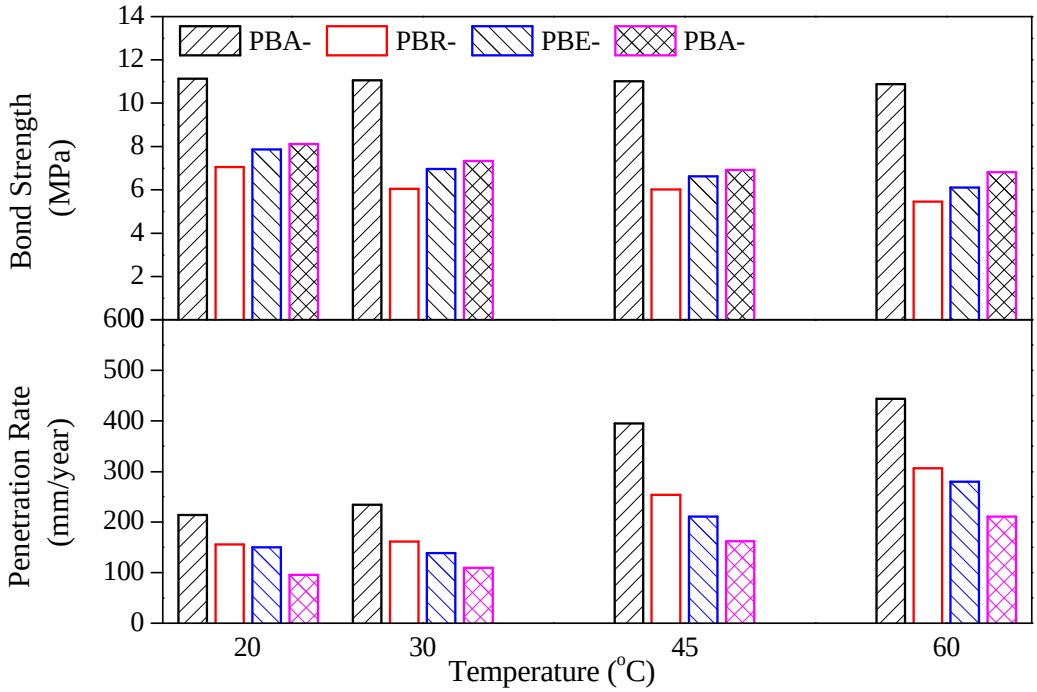

Figure 4.34: Bond strength and penetration rate versus temperature relationship (C-PCC and CA-Brick).

Bond strength and penetration rate are plotted against temperature in Figure 4.35 below with Portland composite cement and brick type coarse aggregate.

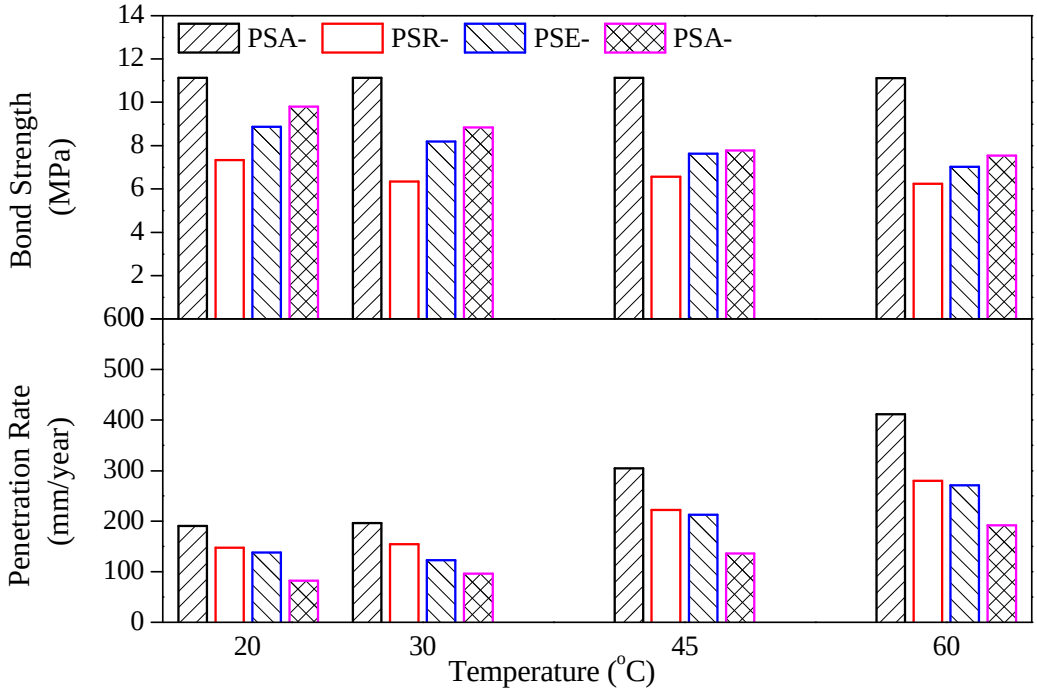

Figure 4.35: Bond strength and penetration rate versus temperature relationship (C-PCC and CA-Stone).

From the comparison of Figure 4.32, 4.33, 4.34 and 4.35, it can be seemed that 30 ^{o}C, 45 ^{o}C, and 60 ^{o}C induced specimens show average 7.27%, 40.98% and 55.96% more penetration rate than 20 ^{o}C induced specimens. And 20 ^{o}C induced specimens give 9.36%, 17.92%, and 19.78% more bond stress than 30 ^{o}C, 45 ^{o}C, and 60 ^{o}C induced specimens respectively. From the analysis of those results, it is cleared that similar type of parameter show reversible response between penetration rate and bond stress. But the increment of bond stress is a positive sign and the increment of penetration rate is a negative sign. So, it can be concluded that increment of temperature decreases the bond stress and increases the penetration rate.

Those figures also demonstrate that coatings reduce the bond stress but also reduce the penetration rate. So it is finally cleared that coatings give average 39.01% better result for penetration rate but those coatings also show average 34.02% lower bond stress than non-coated rebar induced specimens.

CHAPTER V

Conclusions and Recommendations

5.1 Conclusions

Based on the results of laboratory test program, the following main conclusions can be drawn with respect to different temperature, coatings and materials.

1. Porosity of concrete is increased to a great extent due to elevated casting and curing temperature.
2. Long term compressive strength is decreased with the increase of casting and curing temperature.
3. Bond stress of 20 ^{o}C temperature induced specimen's gives 20% better performance compared to 60 ^{o}C temperature.
4. Coatings offer lower bond stress of reinforced concrete than non-coated rebar. Aluminum oxide shows better bond stress compared to red oxide, synthetic enamel paint.
5. Corrosion crack visualization of 20 ^{o}C temperature is prolonged by 1.6 times more than 60 ^{o}C temperature. And corrosion rate is reduced about 56% by lower temperature.
6. Coatings protect the concrete by increasing electrical resistance, enhancing the crack initiating time and reducing corrosion rate. Aluminum oxide increases average 36% more crack initiating time and reduces average 31% corrosion rate than others.
7. Portland composite cement shows good results for porosity, bond stress and corrosion compared to ordinary Portland cement. Crushed stone also offers better agreements than crushed burn brick.

Finally, it can be concluded that long term concrete strength and bond stress of reinforced concrete is increased by lower casting and curing temperature. It also provides better protection for corrosion compared to elevated temperature. Coatings give average 39% better result for corrosion but those coatings also show average 34% lower bond stress than non-coated rebar.

5.2 Recommendations for Future Study

Here coating thickness was same for specific coatings. So, effect of coating thickness on bond stress and corrosion can be observed for each coating.

Coating reduces the bond stress and performs better against corrosion. For this reason, variation of development length can be found to get the similar bond stress of non-coated rebar for constant coating thickness.

REFERENCES

ACI 306R-88., (1994). Cold Weather Concreting, ACI Manual of Concrete Practice, Part 2-1992; Construction Practices and Inspection Pavements, pp.23.

ACI Committee 408 (1992). “Bond under Cyclic Loads”, Journal of the American concrete Institute.

ACI Committee 408. (1966). "Bond Stress - The State of the Art", Journal of the American Concrete Institute, Vol. 63, No. II, pp. 1161-1188

Al-Amoudi, O.S.B., Rasheeduzzafar & Maslehuddin, M., (1991). Carbonation and corrosion of rebars in salt contaminated OPC/PFA concretes. Cement Concrete Res., 21(1), 38–50.

Alavi-Fard, M., and Marzouk, H., (2002). “Bond Behavior of High Strength Concrete Under Reversed Pull-out Cyclic Loading”, Canadian Journal of Civil Engineering, Vol. 29, No. 2, pp.191-200.

Alavi-Fard, M., and Marzouk, H., (2002). “Bond Behavior of High Strength Concrete Under Reversed Pull-out Cyclic Loading”, Canadian Journal of Civil Engineering, Vol. 29, No. 2, pp.191-200.

Ali, A. M., and Ameen, A. H. A., (2011). “The effect of Zinc, Tin, and Lead coating on corrosion protective effectiveness of steel reinforcement in concrete”. American Journal of Scientific and Industrial Research, 2(1): 89-98

Andrade, C., and Alonso, C., (2001). "On-site Measurements of Corrosion Rate of Reinforcements." Journal of Construction and Building Materials, Vol.15, pp.141-145.

Andrade, C., and Alonso, C., (2001). "On-site Measurements of Corrosion Rate of Reinforcements." Construction and Building Materials, 15, 141-145.

Berkely, K. G. C., and Pathmanaban, S., (1990). Cathodic Protection of Reinforcement Steel in Concrete, Butterworths - Heinemann, London.

Cairns, J., and Abdullah, R. B., (1996). “Bond Strength of Black and Epoxy-Coated Reinforcement- a Theoretical Approach”, ACI Materials Journal, Vol. 93, No. 4, pp.362-370.

Choi, O. C., Hadje Ghaffari, H., Darwin, D., and McCabe, S. L., (1991). “Bond of Epoxy-Coated Reinforcement to Concrete: Bar Parameters,” ACI Materials Journal, V. 88, No. 2.

Courtault, B., & Longuet, P., (1982). "Flux adaptable calorimeter for studying heterogeneous solid-liquid reactions—Application to cement chemistry." IVe Journals Nationales de Calorimetrier, pp. 2/41–2/48.

Cusens, A. R., & Yu, Z., (1993). "Bond strength and flexural behavior of reinforced concrete beams with epoxy-coated reinforcing bars." The Structural Engineer, 71, 117–124.

Elkhadiri, I., Palacios, M., Puertas, F., (2009). “Effect Of Curing Temperature On Cement Hydration”. Ceramics , Silikáty 53 (2) 65-75.

Fernández Bertos, M., Simons, S. J. R., Hills, C. D. and Carey, P. J., (2004). "A review of accelerated carbonation technology in the treatment of cement-based materials and sequestration of CO2." Journal of Hazardous Materials, B112: 193-205.

Gandhimathi, A., Haganesh, B., and Meenambal, T., (2012). "An Experimental Study on Fly Ash Blended Cement Concrete Structures with Organic (Corrosion) Inhibitor". International Journal of Engineering Research & Technology (IJERT), ISSN: 2278-0181, Vol. 1 Issue 6.

Goñi, S. and Guerrero, A., (2003). "Accelerated carbonation of Friedel's salt in calcium aluminate cement paste." Cement and Concrete Research, 33: 21-26.

Hansen, P.P. & Pedersen, E.J., (1984). Curing of Concrete Structure. Report prepared for CEB—General Task Group No. 20, Danish Concrete and Structural Research Institute.

Hester, C. J., Salamizavaregh, S., Darwin, D., and McCabe, S. L., (1993). "Bond of Epoxy Coated Reinforcement: Splices," ACI Structural Journal, V. 90, No. 1, pp. 89-102.

Hussain, R. R., and Ishida, T., (2011). "Enhanced Electrochemical Corrosion Model for Reinforced Concrete under Severe Coupled Action of Chloride and Temperature". Construction and Building Materials, 25, 1305–1315.

Idorn, G.M., (1968). "Hydration of Portland cement paste at high temperatures under atmospheric pressure." In *Proc. Sump. Chem. Cement*, Tokyo, The Cement Association of Japan, Tokyo, pp. 411–35.

Kayyali, O. A., & Yeomans, S. R., (1995). "Bond and slip of coated reinforcement in concrete." Construction & Building Materials, 9, 219–226.

Kianousha, M.R., Acarcanb, M., Ziaria, A., (2008). "Behavior of base restrained reinforced concrete walls under volumetric change." Journal of Engineering Structures, Vol.30, pp.1526–1534.

Kim, Soo G., (2010). "Efect of heat generation from cement hydration on mass concrete placement", Graduate Thesis and Dissertations, Iowa State University, Paper 11675.

Kivell, A., Palermo, A. and Scott, A., (2011). "Effects of Bond Deterioration due to Corrosion in Reinforced Concrete", Pacific Conference on Earthquake Engineering, New Zealand, pp.14-16.

Klieger, P., (1958). "Effect of mixing and curing temperature on concrete strength" ACI journal, Vol.54, No.12, pp.1063–81.

Lange, L. C., Hills, C. D. and Poole, A. B., (1996). "The effect of accelerated carbonation on the properties of cement-solidified waste forms." Waste Management, 16(8): 757-763.

Liu, L., Ha, J., Hashida, T. and Teramura, S., (2001). "Development of a CO_2 solidification method for recycling autoclaved lightweight concrete waste." Journal of materials science letters, 20: 1791-1794.

Lundgren, K., (2005). "Bond Between Ribbed Bar and Concrete. Part 1: Modified Model", Magazine of Concrete Research, Vol. 57, No. 7, pp.371-382

Maaddawy, T. A. E., and Soudki, K.A., (2003). “Effectiveness of Impressed Current Technique to Simulate Corrosion of Steel Reinforcement in Concrete”. Journal of Materials In Civil Engineering, 15:41-47.

Mahter, B., (1987). "The warmer the concrete the faster the cement hydrates." *Concrete Int.*, **9**(8), 29–33.

Mansfeld, F., (1981). "Recording and Analysis of AC Impedance Data for Corrosion Studies." Corrosion, 37(5), 301-307.

Martin, H., (1982). “Bond Performance of Ribbed Bars (Pull-Out-Tests) - Influence of Concrete Composition and Consistency “, International Conference – Bond in Concrete, Paisley, Scotland, pp. 289–299.

Miller, G. G., Jennifer L. Kepler, J. L., and David Darwin, D., (2004). “Effect of Epoxy Coating Thickness on Bond Strength of Reinforcing Bars”, ACI Structural Journal, Title no. 100-S34.

Neville, A.M., (4th Edition) (2006). *Properties of Concrete*, Pearson Education, Inc. One Lake Street, Upper Saddle River, NJ 07458 USA.

Newman, J. & Choo, B.N., (2003). *Advanced Concrete Technology* (Concrete Properties), Replika Press Pvt Ltd, India, pp. 3/09.

Newman, J. and Choo. B.S., (First edition) (2003). “Advanced Concrete Technology (Concrete Properties)”Linacre House, Jordan Hill, Oxford OX2 8DP 200 Wheeler Road, Burlington MA 01803.

Orangun, C. O., Jirsa, J. O., and Breen, J. E., (1977). “Reevaluation of Test Data on Development Length and Splices”, ACI Journal, Proceedings Vol. 74, No. 3, pp. 114-122.

Orangun, C.O., Jirsa, J.O., and Breen, J. E., (1977). “Reevaluation of Test Data on Development Length and Splices”, ACI Journal, Proceedings Vol. 74, No. 3, pp. 114-122.

Page, C.L., Short, N.R. & El Tarras, A., (1981). "Diffusion of chloride ions in hardened cement pastes." Cement Concrete Res., 11(3), 395–406.

Pantazopoulou SJ, Mills RH (1995). “Microstructural aspects of the mechanical response of plain concrete”, ACI Mater J; 92(6):605–16.

Park, R., and Paulay, T., (1975). "Reinforced Concrete Structures," John Wiley & Sons, Inc. New York, USA.

Pfeifer, D. W. (2000), "High Performance Concrete and Reinforcing Steel with 100-Year Service Life." PCI Journal, Vol.45, No.3, pp.46-54.

Pfeifer, D. W., (2000). "High Performance Concrete and Reinforcing Steel with 100-Year Service Life." PCI Journal, 45(3), 46-54.

Popovics S (1973). “Method for developing relationships between mechanical properties of hardened concrete”, J Am Concr Inst; 70:795–8.

Poursaee, A. and Hansson, C.M., (2008). “The influence of longitudinal cracks on the corrosion protection afforded reinforcing steel in high performance concrete”. Cement and Concrete Research 38, 1098–1105.

Powers, T.C., (1962). Physical properties of cement paste. In *Proc. Symp. Chem.Cement*, Washington, National Bureau of Standards Monograph No. 43, Washington, pp. 577–613.

Raghuprasad, P.S., Kumar A.V. P., Rao, K.B., and Muthanna, K.M., (2005). "Experimental Investigation on Long Term Strength of Blended and O.P.C. Concretes- a Comparison". Proceedings offirst national conference on Recent Developments in Structural Engineering (RDSE-2005) Manipal Institute of Technology, Manipal – 576 104.

Raphael, M. & Shalon, R., (1971). "A study of the influence of climate on corrosion of reinforcement." In Proc. RILEM 2nd Int. Symp. On Concrete and Reinforced Concrete in Hot Countries, Haifa, Vol. I, Building Research Station, Technion—Israel Institute of Technology, Haifa, pp. 77–96.

Raphael, M. & Shalon, R., (1971). "A study of the influence of climate on corrosion of reinforcement." In Proc. RILEM 2nd Int. Symp. On Concrete and Reinforced Concrete in Hot Countries, Haifa, Vol. I, Building Research Station, Technion—Israel Institute of Technology, Haifa, pp. 77–96.

Ruetz, W., (1968). "A hypothesis for creep of hardened cement paste and the influence of simultaneous shrinkage." In *Proc. Conf. Structure of Concrete and Its Behavior Under Load*, Cement and Concrete Association, London, UK, pp. 365–403.

Shalon, R. & Ravina, D., (1970). "The effect of elevated temperature on strength of portland cements." In *Temperature and Concrete* (ACI Spec. Publ. SP25), ACI, Detroit, MI, USA, pp. 275–89.

Shetty, A., Gogoi,I. & Venkataramana, K., (2011). "Effect of Loss of Bond Strength Due to Corrosion in Reinforced Concrete Members." International Journal of Earth Sciences and Engineering, Volume 04, No 06 SPL, pp. 879-884

Siddique, R., and Khan, M. I., (2011). "Supplementary Cementing Material", Springer, Verlag,

Berlin, Heidelberg.

Smith, Roger W., (2007). "The effects of Corrosion on the Performance of reinforced Concrete Beam". Thesis and Dissertations. Paper-149.

Song H., Kwon, S., Byun, K. and Park, C., (2006). "Predicting carbonation in early-aged cracked concrete." Cement and Concrete Research, 36: 979-989

Soroka, I., (1979). *Portland Cement Paste and Concrete.* The Macmillan Press Ltd, London, UK, p. 28.

Soroka, I., (2004). *Concrete in Hot Environment*. Chapman & Hall, 2–6 Boundary Row, London, UK, pp.169

Soroka, I., (First edition) (2004). "Concrete in hot environments", Chapman & Hall Inc., 29 West 35th Street, New York NY10001, USA.

Tepfers, R. A., (1979). "Cracking of Concrete Cover along Anchored Deformed Reinforcing Bars", Magazine of Concrete Research, Vol. 31, No. 106, pp. 3-12

Torres-Acosta, A. A., and Sagues, A. A., (2004). "Concrete Cracking by Localized Steel Corrosion - Geometric Effects." ACI Materials Journal, 101(6), 501-507.

Treece, R. A., & Jirsa, J. O., (1989). "Bond strength of epoxy-coated reinforcing bars." ACI Materials Journal, 86, 167–174

Treece, R. A., and Jirsa, J. O., (1989). “Bond Strength of Epoxy-Coated Reinforcing Bars”, ACI Materials Journal, Vol. 86, No. 2, pp. 167-174

Tuthill, L.H. & Cordon, W.A., (1955). "Properties and uses of initially retarded concrete." *Proc. ACI,* **52**(3), 273–86.

Van Balen, K. and Van Gemert, D., (1994). "Modelling lime mortar carbonation." Material and Structures, 27: 393-398.

Verbeck, G., (1958). "Carbonation of hydrated Portland cement." Research Department Bulletin RX087, Portland cement Association.

Verbeck, G.J. & Helmuth, R.A., (1968). "Structure and physical properties of cement paste." In *Proc. Symp. Chem. of Cement,* Tokyo, Vol. 3, The Cement Association of Japan, Tokyo, pp. 1–37.

Wierig, H.J. (1984). "Longtime studies on the carbonation of concrete under normal outdoor exposure." In *Proc. RILEM Seminar on Durability of Concrete Structures under Normal Exposure*, pp. 239–53.

Yamamoto, Y. & Kobayashi, S.(1986). "Effect of temperature on the properties of super plasticized concrete". *Proc. ACI,* **83**(1), 80–6.

Yousuf, M., Mollah, A., Hess, T. R., Tsai, Y.-N. and Cocke D.L. (1993). "An FTIR and XPS investigations of the effects of carbonation on the solidification/stabilization of cement based systems-Portland type V with Zn." Cement and Concrete Research, 23: 773-784.

Zuo, J., and Darwin, D., (1998). “Bond Strength of High Relative Rib Area Reinforcing Bars”, SM Report No. 46, University of Kansas Center for Research, Lawrence, Kansas, USA, and 350 pp.

Appendix

Appendix A: Experimental Results- Bond Load (kN) and Slip (mm)

Appendix B: Experimental Results- Bond Stress (MPa)

Appendix C: Experimental Results- Propagation of Corrosion Crack

Appendix D: Experimental Results- Measured and Predicted Mass Loss

Appendix E: Experimental Results- Corrosion Level & Penetration Rate

Appendix A: Experimental Results- Bond Load (kN) and Slip (mm)

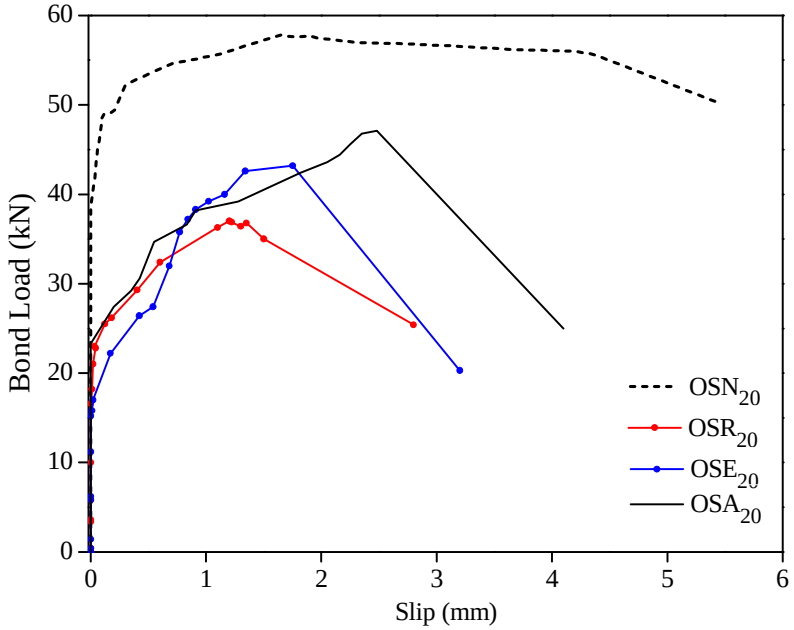

Figure A-01: Bond load (kN) versus slip (mm) relationship (T-20ºC & C-OPC)

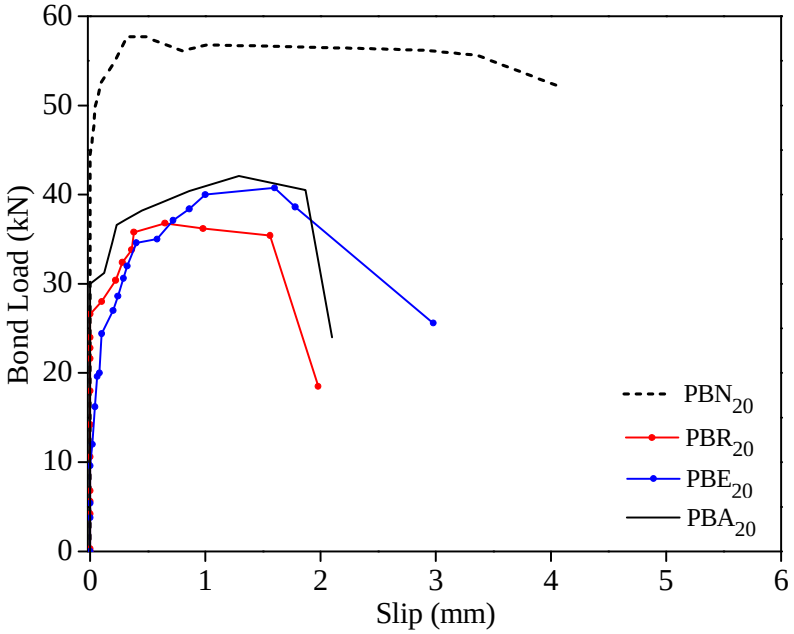

Figure A-02: Bond load (kN) versus slip (mm) relationship (T-20ºC & C-PCC)

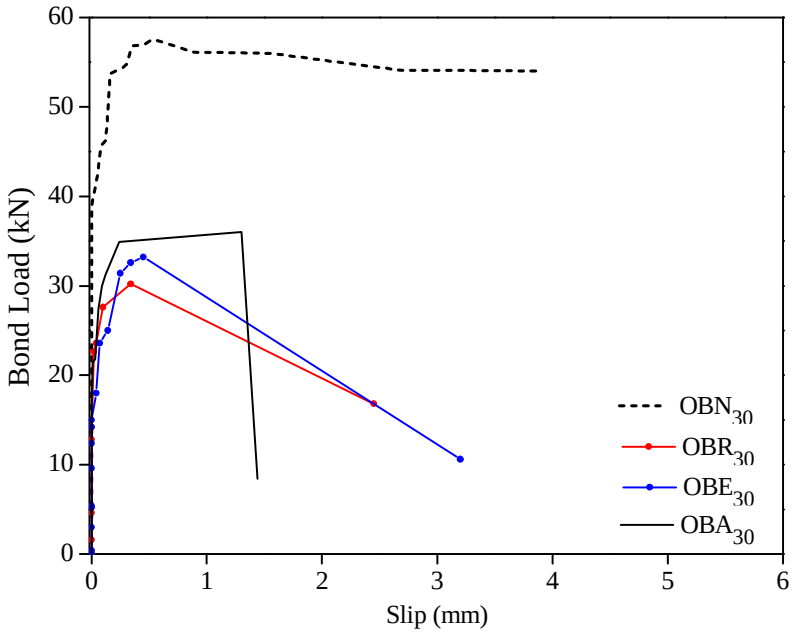

Figure A-03: Bond load (kN) versus slip (mm) relationship (T-30ºC & C-OPC)

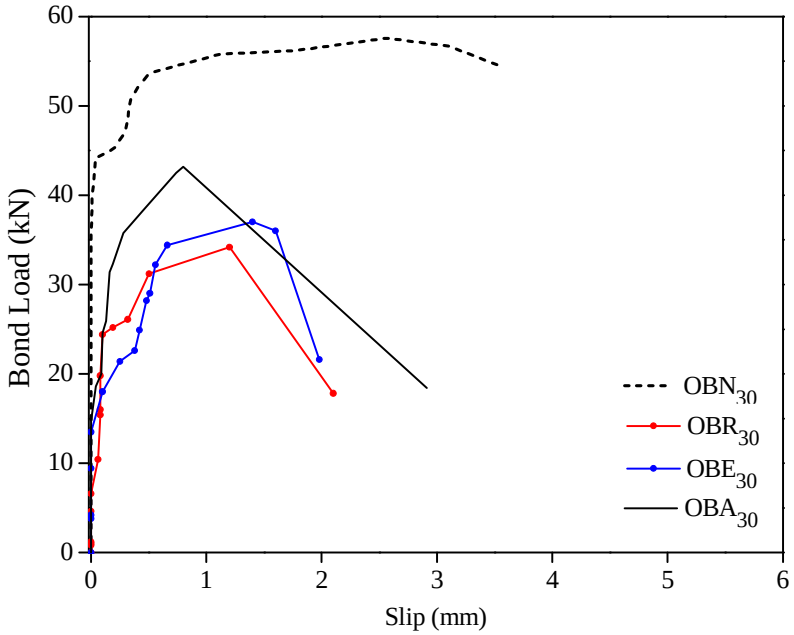

Figure A-04: Bond load (kN) versus slip (mm) relationship (T-30ºC & C-OPC)

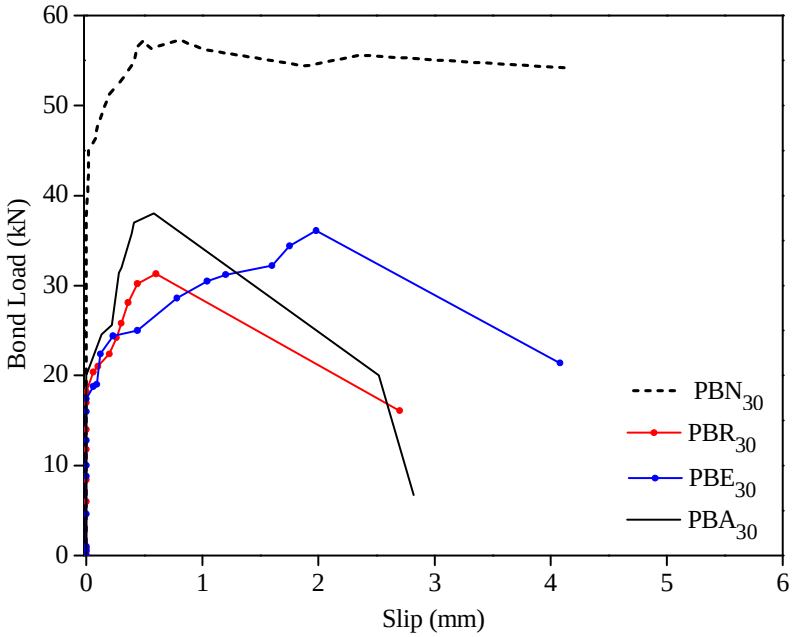

Figure A-05: Bond load (kN) versus slip (mm) relationship (T-30ºC & C-PCC)

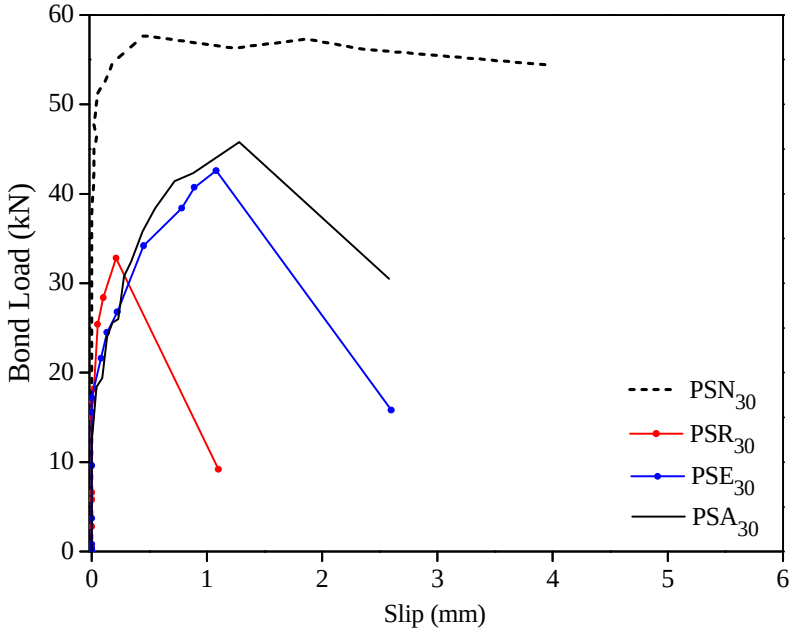

Figure A-06: Bond load (kN) versus slip (mm) relationship (T-30ºC & C-PCC)

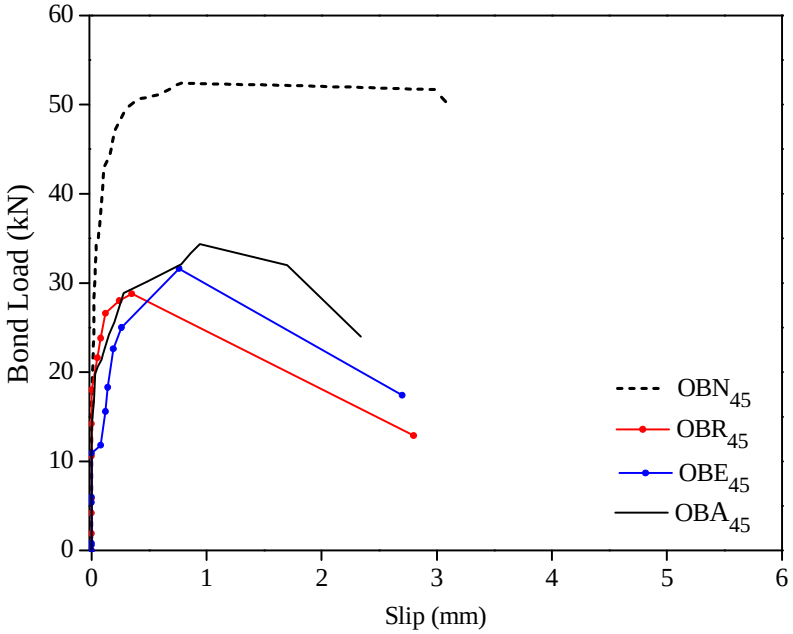

Figure A-07: Bond load (kN) versus slip (mm) relationship (T-45ºC & C-OPC)

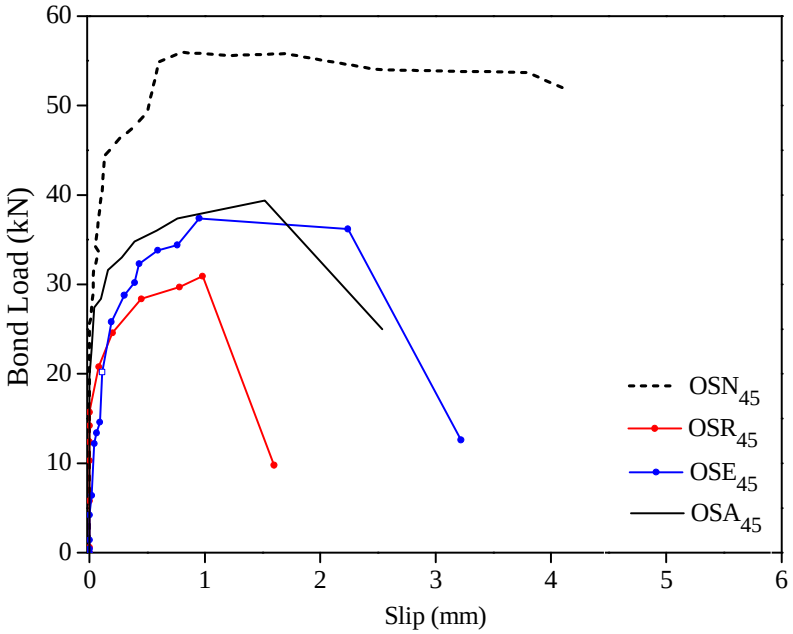

Figure A-08: Bond load (kN) versus slip (mm) relationship (T-45ºC & C-OPC)

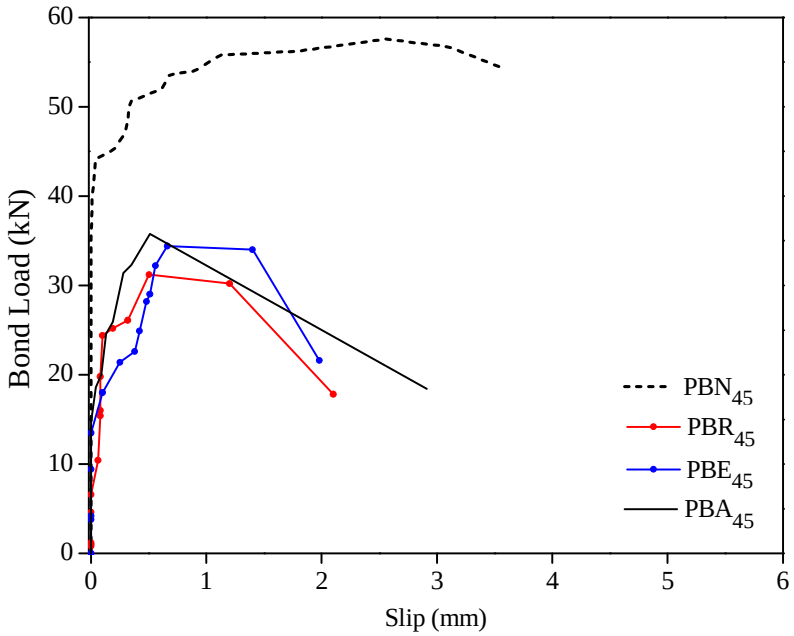

Figure A-09: Bond load (kN) versus slip (mm) relationship (T-45ºC & C-PCC)

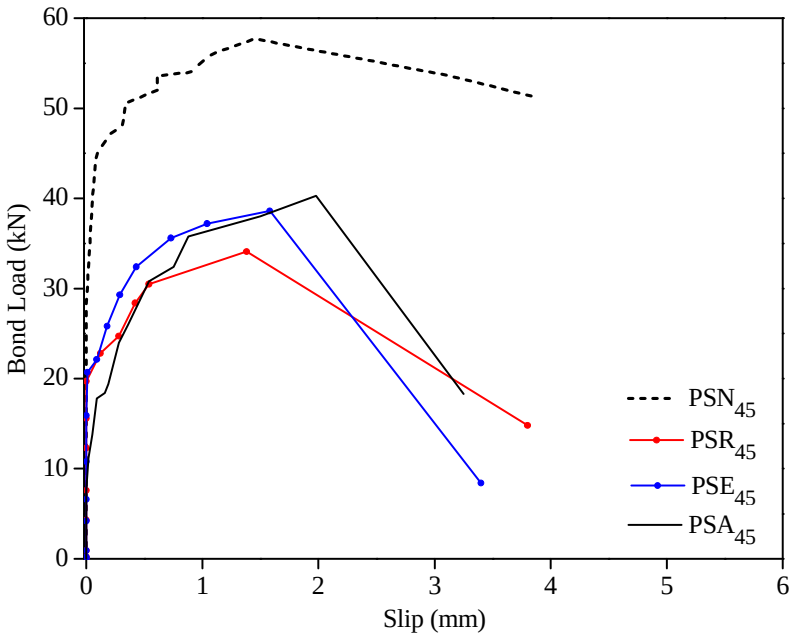

Figure A-10: Bond load (kN) versus slip (mm) relationship (T-45ºC & C-PCC)

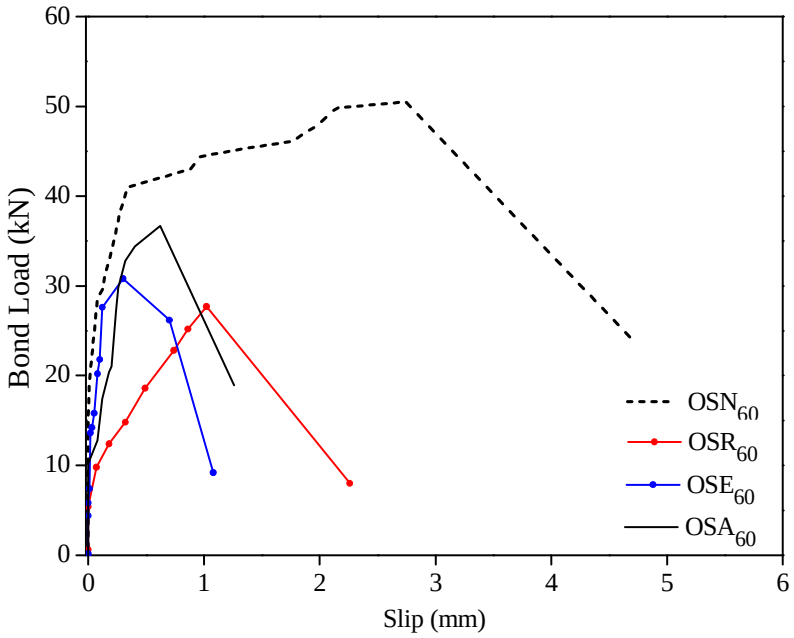

Figure A-11: Bond load (kN) versus slip (mm) relationship (T-60ºC & C-OPC)

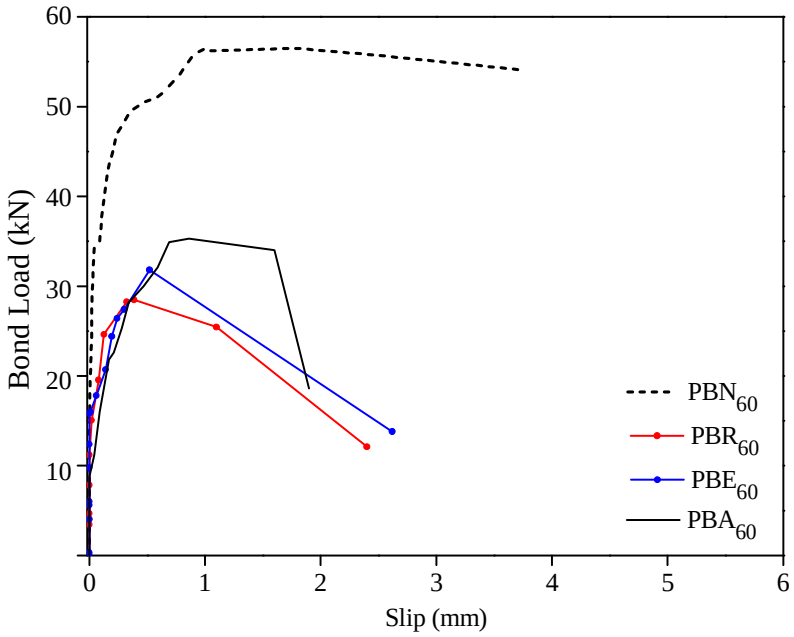

Figure A-12: Bond load (kN) versus slip (mm) relationship (T-60ºC & C-PCC)

Appendix B: Experimental Results- Bond Stress (MPa)

Observed bond load from laboratory tests and calculated bond stress is given in Table 4.1.

Table 4.1: Results of bond load (kN) and bond stress (MPa)

	OBN_{20}	OBR_{20}	OBE_{20}	OBA_{20}	OSN_{20}	OSR_{20}	OSE_{20}	OSA_{20}
Bond Load (kN)	57.6	35.20	37.6	41.32	57.8	37	43.2	47.2
Bond Stress (MPa)	11.11	6.79	7.25	7.97	11.15	7.13	8.33	9.11

	PBN_{20}	PBR_{20}	PBE_{20}	PBA_{20}	PSN_{20}	PSR_{20}	PSE_{20}	PSA_{20}
Bond Load (kN)	57.7	36.55	40.75	42.10	57.7	38	46	50.8
Bond Stress (MPa)	11.13	7.05	7.86	8.12	11.13	7.33	8.87	9.80

	OBN_{30}	OBR_{30}	OBE_{30}	OBA_{30}	OSN_{30}	OSR_{30}	OSE_{30}	OSA_{30}
Bond Load (kN)	57.6	30.2	33.23	36.04	57.6	34.9	37.4	43.2
Bond Stress (MPa)	11.11	5.82	6.41	6.95	11.11	6.73	7.21	8.33

	PBN_{30}	PBR_{30}	PBE_{30}	PBA_{30}	PSN_{30}	PSR_{30}	PSE_{30}	PSA_{30}
Bond Load (kN)	57.3	31.3	36.1	38	57.7	32.8	42.6	45.8
Bond Stress (MPa)	11.05	6.03	6.96	7.33	11.13	6.32	8.18	8.83

	OBN_{45}	OBR_{45}	OBE_{45}	OBA_{45}	OSN_{45}	OSR_{45}	OSE_{45}	OSA_{45}
Bond Load (kN)	52.88	28.77	31.6	34.37	55.95	30.91	37.4	38.4
Bond Stress (MPa)	10.20	5.55	6.09	6.63	10.79	5.96	7.21	7.40

	PBN_{45}	PBR_{45}	PBE_{45}	PBA_{45}	PSN_{45}	PSR_{45}	PSE_{45}	PSA_{45}
Bond Load (kN)	57.1	31.2	34.4	35.88	57.7	34.1	39.6	40.3
Bond Stress (MPa)	11.01	6.01	6.63	6.92	11.13	6.57	7.63	7.77

	OBN_{60}	OBR_{60}	OBE_{60}	OBA_{60}	OSN_{60}	OSR_{60}	OSE_{60}	OSA_{60}
Bond Load (kN)	47.8	26.4	28	30.2	50.5	27.06	30.8	36.7
Bond Stress (MPa)	9.22	5.08	5.40	5.82	9.74	5.22	5.94	7.08

	PBN_{60}	PBR_{60}	PBE_{60}	PBA_{60}	PSN_{60}	PSR_{60}	PSE_{60}	PSA_{60}
Bond Load (kN)	56.4	28.30	31.6	35.3	57.6	32.4	36.5	39.1
Bond Stress (MPa)	10.88	5.45	6.10	6.81	11.11	6.25	7.03	7.54

Appendix C: Experimental Results- Propagation of Corrosion Crack

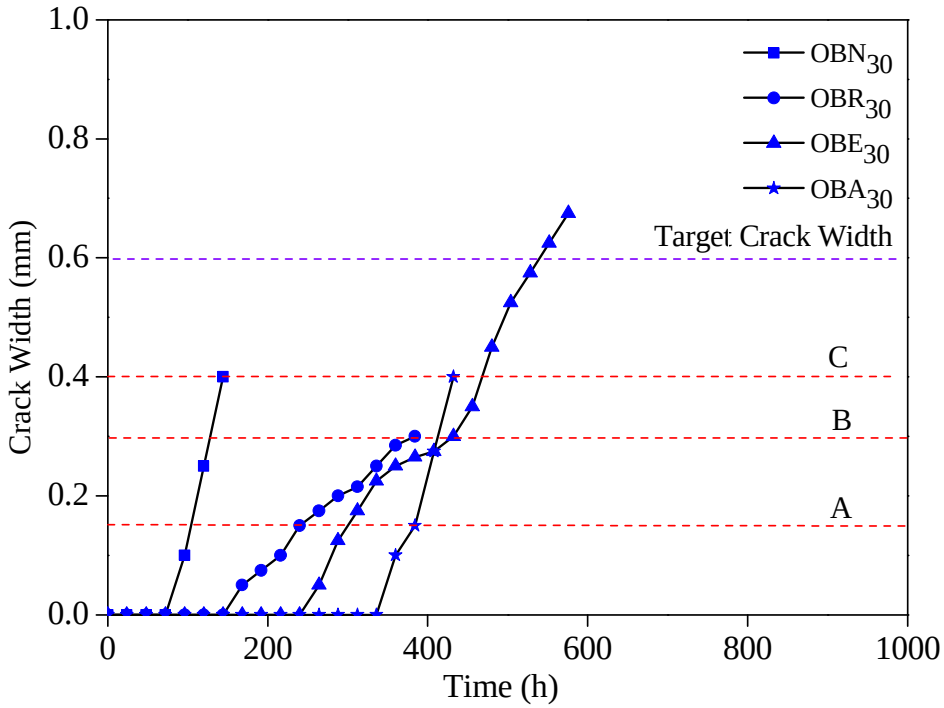

Exposure condition: A= Sea water; B= Humidity, moist air; C= Dry air

Figure C-01: Average crack width (mm) versus time relationship (T-30°C & C-OPC)

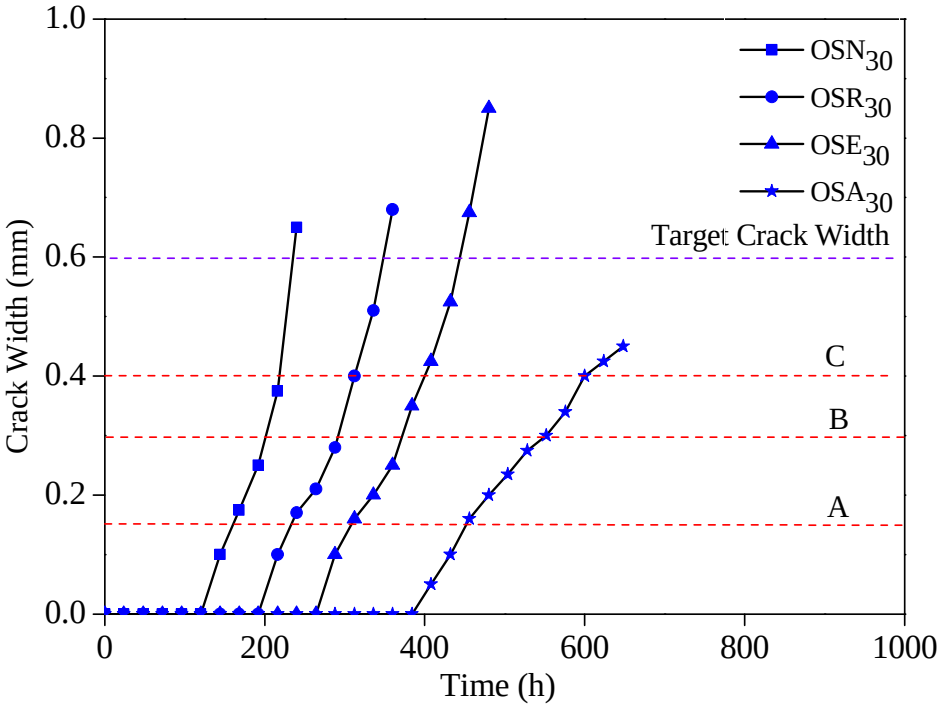

Exposure condition: A= Sea water; B= Humidity, moist air; C= Dry air

Figure C-02: Average crack width (mm) versus time relationship (T-30°C & C-OPC)

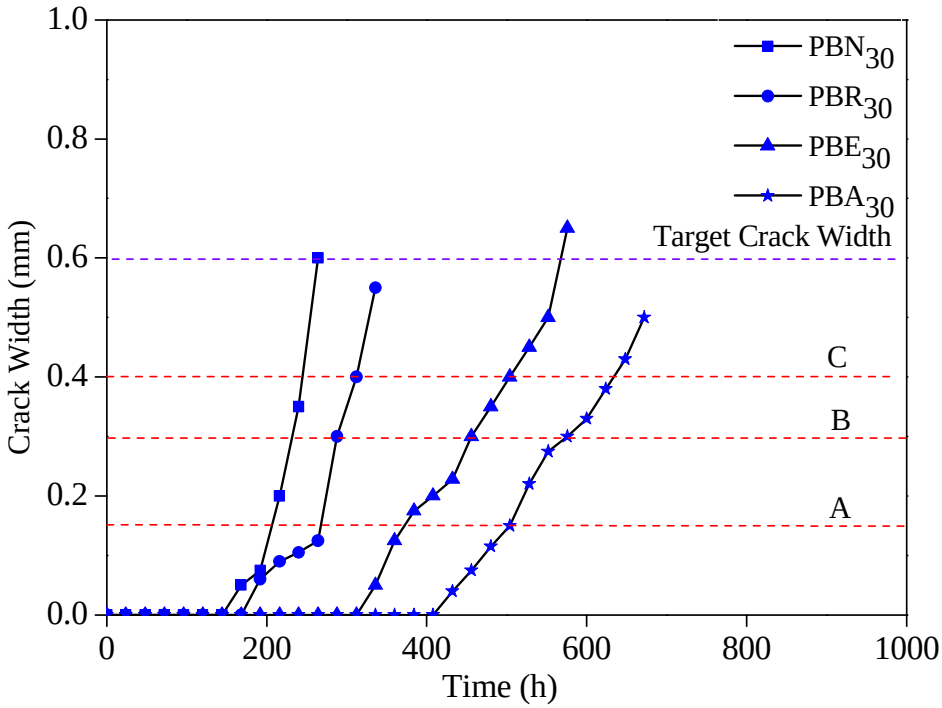

Exposure condition: A= Sea water; B= Humidity, moist air; C= Dry air

Figure C-03: Average crack width (mm) versus time relationship (T-30^{o}C & C-PCC)

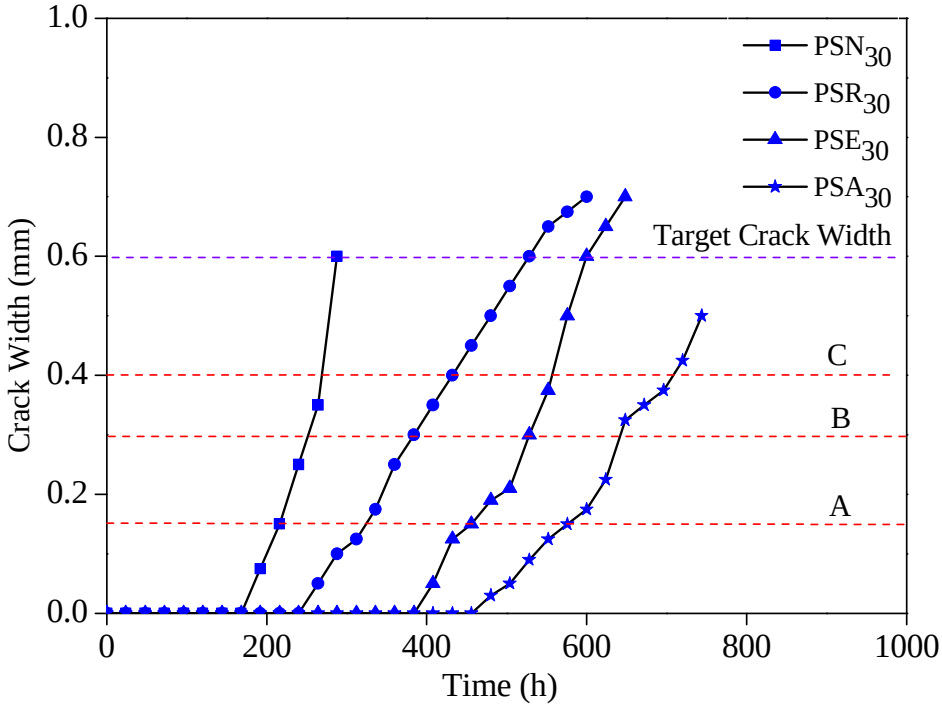

Exposure condition: A= Sea water; B= Humidity, moist air; C= Dry air

Figure C-04: Average crack width (mm) versus time relationship (T-30^{o}C & C-PCC)

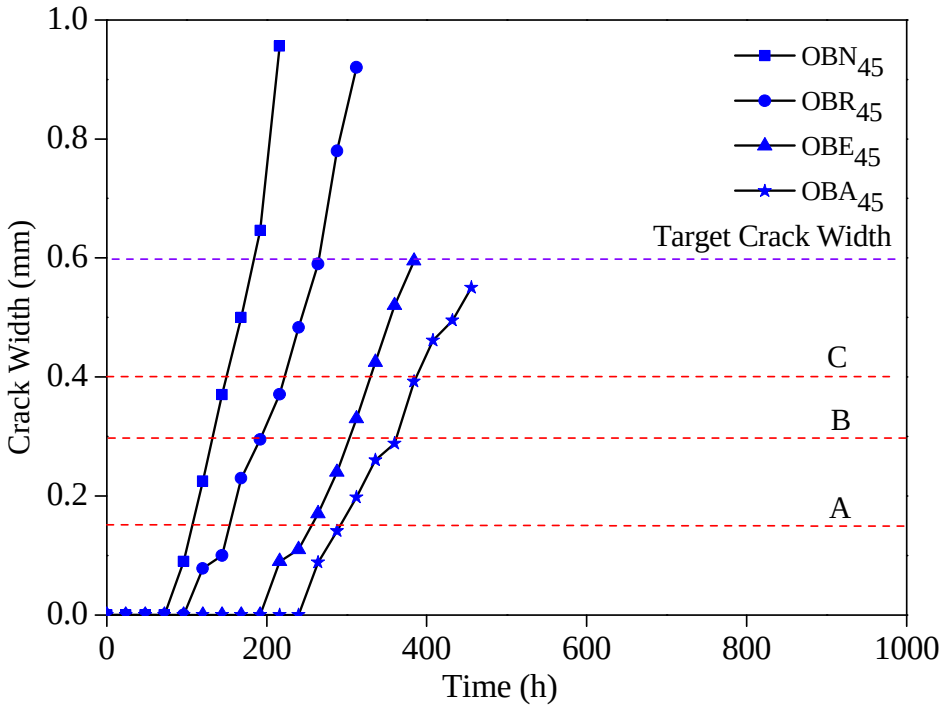

Exposure condition: A= Sea water; B= Humidity, moist air; C= Dry air

Figure C-05: Average crack width (mm) versus time relationship (T-45^{o}C & C-OPC)

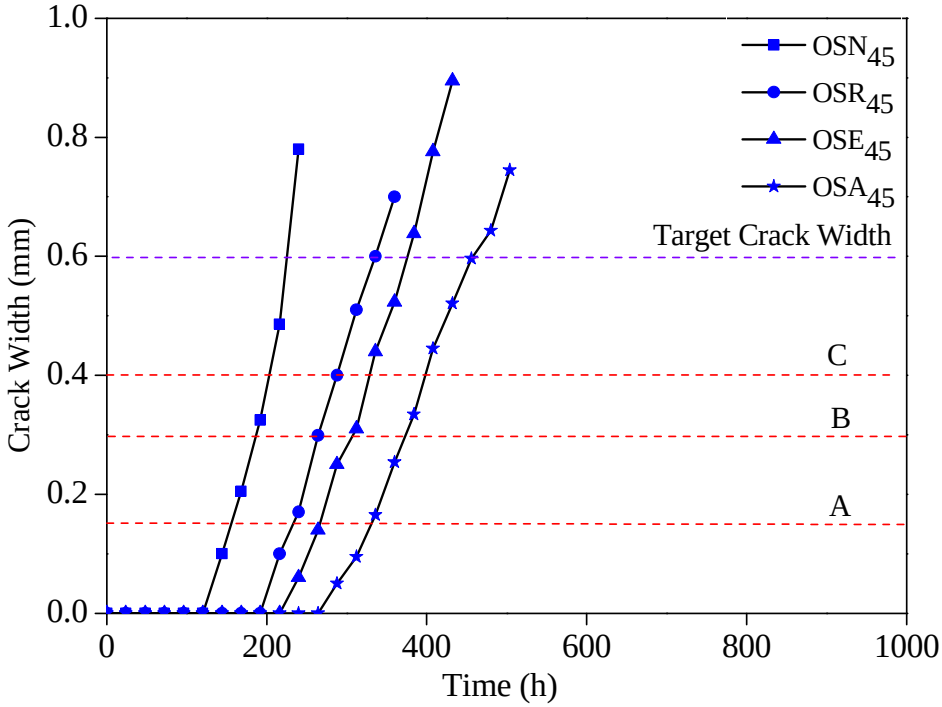

Exposure condition: A= Sea water; B= Humidity, moist air; C= Dry air

Figure C-06: Average crack width (mm) versus time relationship (T-45^{o}C & C-OPC)

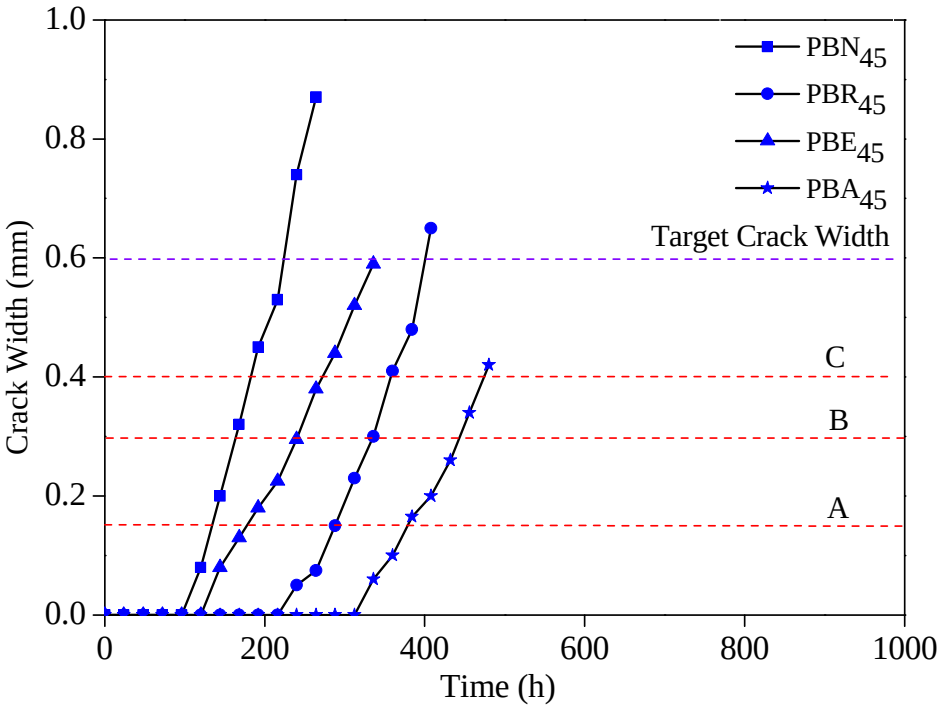

Exposure condition: A= Sea water; B= Humidity, moist air; C= Dry air

Figure C-07: Average crack width (mm) versus time relationship (T-45^{o}C & C-PCC)

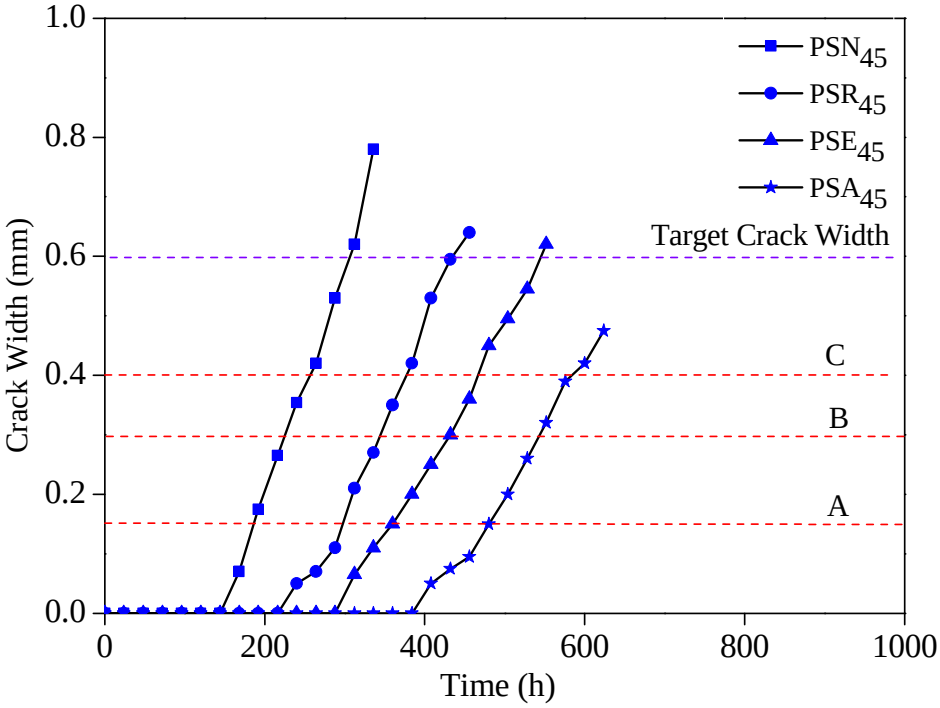

Exposure condition: A= Sea water; B= Humidity, moist air; C= Dry air

Figure C-08: Average crack width (mm) versus time relationship (T-45^{o}C & C-PCC)

Results of corrosion crack width (mm) and elapsed time of corrosion.

	OBN_{20}	OBR_{20}	OBE_{20}	OBA_{20}	OSN_{20}	OSR_{20}	OSE_{20}	OSA_{20}
Elapsed Time (h)	408	624	768	830	456	696	792	936
Crack width (mm)	0.64	0.495	0.54	0.37	0.45	0.345	0.40	0.25

	PBN_{20}	PBR_{20}	PBE_{20}	PBA_{20}	PSN_{20}	PSR_{20}	PSE_{20}	PSA_{20}
Elapsed Time (h)	528	696	768	960	576	816	912	984
Crack width (mm)	0.40	0.30	0.295	0.25	0.25	0.30	0.35	0.20

	OBN_{30}	OBR_{30}	OBE_{30}	OBA_{30}	OSN_{30}	OSR_{30}	OSE_{30}	OSA_{30}
Elapsed Time (h)	144	384	576	432	240	360	480	648
Crack width (mm)	0.40	0.30	0.675	0.4	0.55	0.68	0.85	0.45

	PBN_{30}	PBR_{30}	PBE_{30}	PBA_{30}	PSN_{30}	PSR_{30}	PSE_{30}	PSA_{30}
Elapsed Time (h)	258	330	570	666	282	594	642	738
Crack width (mm)	0.60	0.55	0.65	0.50	0.65	0.70	0.70	0.50

	OBN_{45}	OBR_{45}	OBE_{45}	OBA_{45}	OSN_{45}	OSR_{45}	OSE_{45}	OSA_{45}
Elapsed Time (h)	228	336	372	432	216	336	468	504
Crack width (mm)	1.1	1.05	0.595	0.55	0.95	0.70	1.15	0.745

	PBN_{45}	PBR_{45}	PBE_{45}	PBA_{45}	PSN_{45}	PSR_{45}	PSE_{45}	PSA_{45}
Elapsed Time (h)	264	432	336	468	336	456	552	612
Crack width (mm)	0.87	0.80	0.59	0.42	0.78	0.64	0.62	0.475

	OBN_{60}	OBR_{60}	OBE_{60}	OBA_{60}	OSN_{60}	OSR_{60}	OSE_{60}	OSA_{60}
Elapsed Time (h)	180	264	372	480	192	288	360	516
Crack width (mm)	0.90	0.69	0.75	0.70	0.90	0.44	0.85	0.653

	PBN_{60}	PBR_{60}	PBE_{60}	PBA_{60}	PSN_{60}	PSR_{60}	PSE_{60}	PSA_{60}
Elapsed Time (h)	288	456	480	648	264	480	480	528
Crack width (mm)	1.05	0.80	0.55	0.51	0.675	0.65	0.45	0.38

Appendix D: Experimental Results- Measured and Predicted Mass Loss

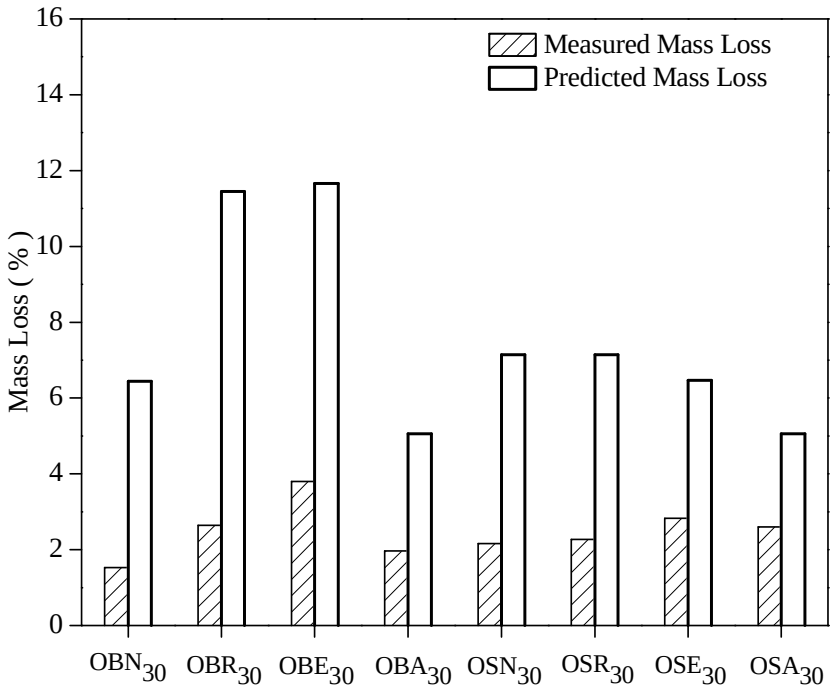

Figure D-01: Relation between measured and predicted mass loss (T-30ºC & C-OPC)

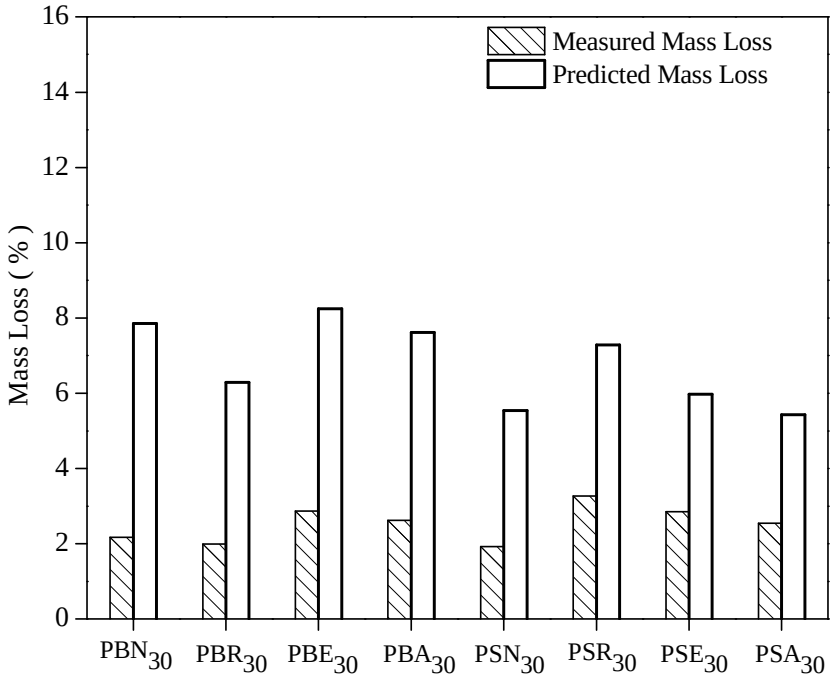

Figure D-02: Relation between measured and predicted mass loss (T-30ºC & C-PCC)

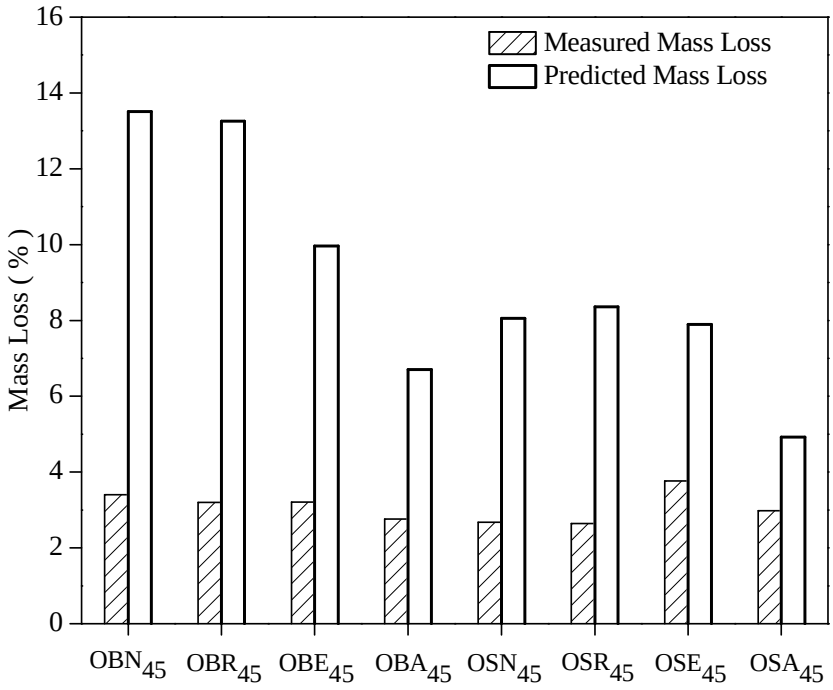

Figure D-03: Relation between measured and predicted mass loss (T-45ºC & C-OPC)

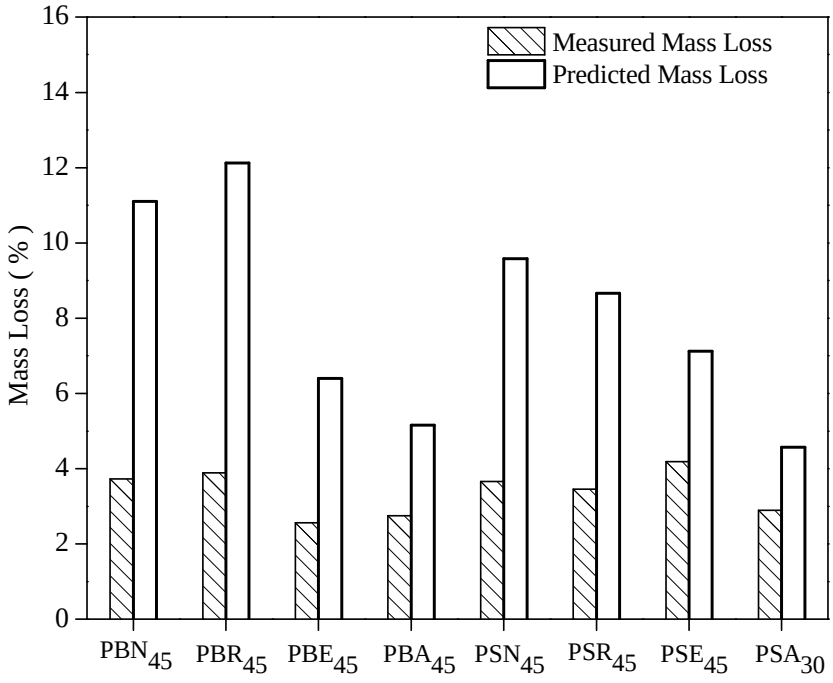

Figure D-04: Relation between measured and predicted mass loss (T-45ºC & C-PCC)

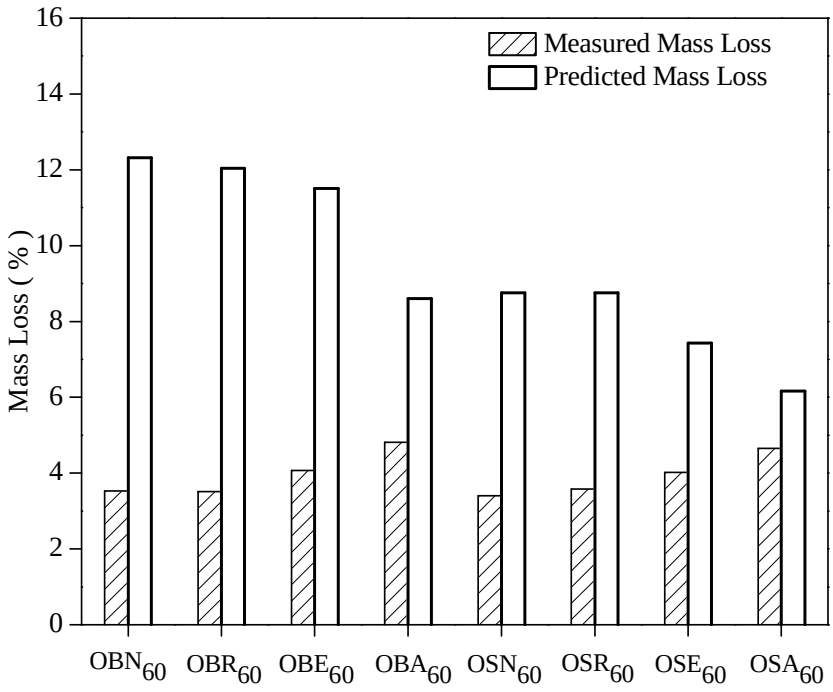

Figure D-05: Relation between measured and predicted mass loss (T-60ºC & C-OPC)

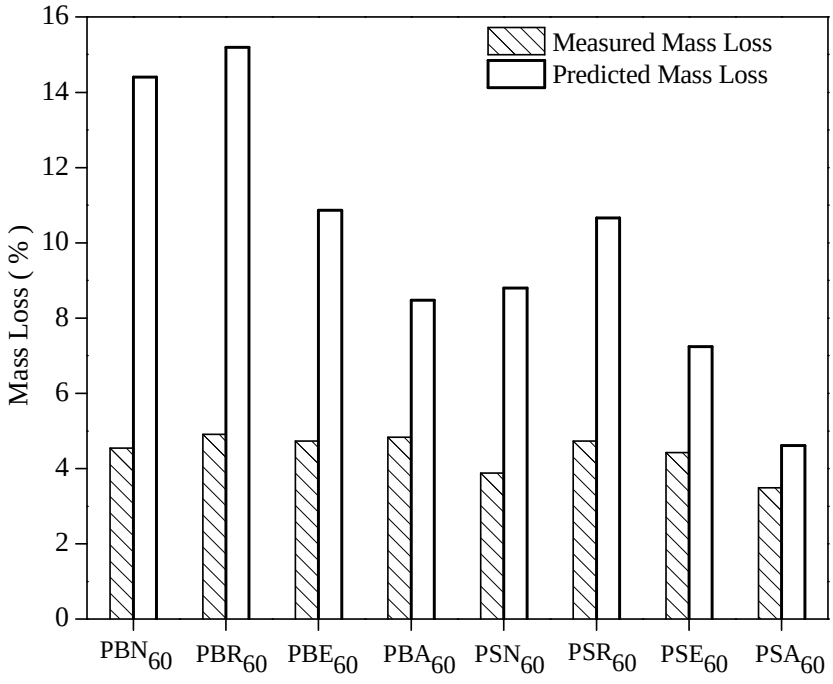

Figure D-06: Relation between measured and predicted mass loss (T-60ºC & C-PCC)

Appendix E: Experimental Results- Corrosion Level & Penetration Rate

Table E-01: Measurement of Corrosion Level (%) & Penetration Rate (mm/year) 20 Degree Specimens

Sample Name	Initial Wt. (W_i) (g)	Final Wt. (W_f) (g)	Elapsed Time , T (hour)	Corrosion Current, I (µA)	Weight loss, W= (W_i- W_f) (g)	Measured Mass Loss (W_i-W_f)* 100/W_i (%)	Predicted Mass Loss (WIT/nF)100 (%)	Actual Steel Area A_{st}, (cm^2)	Steel Density,(D) (g/cm^2)	Corroded Steel Area A= A_{st}- W/(D*L) (cm^2)	Penetration Rate $R=8.76x10^4$ W/(A T D) (mm/ year)
OBN_{20}	272	262.8	408	277.2	9.2	3.382	11.814	1.131	7.85	1.095	229.82
OBR_{20}	275	265.0	624	184.8	10.0	3.636	12.045	1.131	7.85	1.092	163.80
OBE_{20}	275	264.0	768	125.4	11.0	4.000	10.060	1.131	7.85	1.088	146.92
OBA_{20}	278	270.5	744	72.6	7.5	2.698	5.642	1.131	7.85	1.102	102.12
OSN_{20}	278	269.5	456	184.8	8.5	3.058	8.802	1.131	7.85	1.098	189.51
OSR_{20}	280	269.9	696	123.2	10.1	3.607	8.957	1.131	7.85	1.091	148.38
OSE_{20}	274	265.0	792	83.6	9.0	3.285	6.916	1.131	7.85	1.096	115.73
OSA_{20}	271	262.9	936	48.4	8.1	2.989	4.732	1.131	7.85	1.099	87.85
PBN_{20}	280	269.0	528	201.6	11.0	3.929	11.119	1.131	7.85	1.088	213.71
PBR_{20}	284	273.4	696	134.4	10.6	3.732	9.771	1.131	7.85	1.089	156.00
PBE_{20}	274	262.8	768	91.2	11.2	4.088	7.316	1.131	7.85	1.087	149.70
PBA_{20}	274	265.0	960	52.8	9.0	3.285	5.295	1.131	7.85	1.096	95.48
PSN_{20}	271	260.3	576	134.4	10.7	3.948	8.086	1.131	7.85	1.089	190.35
PSR_{20}	278	267.0	816	89.6	11.0	3.957	7.637	1.131	7.85	1.088	138.28
PSE_{20}	267	254.0	912	60.8	13.0	4.869	5.792	1.131	7.85	1.080	147.28
OSA_{20}	281	273.0	984	35.2	8.0	2.847	3.618	1.131	7.85	1.100	82.51

Table E-02: Measurement of Corrosion Level (%) & Penetration Rate (mm/year) 30 Degree Specimens

Sample Name	Initial Wt. (W_i) (g)	Final Wt. (W_f) (g)	Elapsed Time , T (hour)	Corrosion Current, I (μA)	Weight loss, W= (W_i- W_f) (g)	Measured Mass Loss (W_i-W_f)* 100/W_i (%)	Predicted Mass Loss (WIT/nF)100 (%)	Actual Steel Area A_{st}, (cm^2)	Steel Density,(D) (g/cm^2)	Corroded Steel Area A= A_{st}- W/(D*L) (cm^2)	Penetration Rate $R=8.76x10^4$ W/(A T D) (mm/ year)
OBN_{30}	274	269.8	144	428.4	4.2	1.533	6.444	1.131	7.85	1.115	292.04
OBR_{30}	282	274.5	384	285.6	7.5	2.660	11.456	1.131	7.85	1.102	197.86
OBE_{30}	276	265.5	576	193.8	10.5	3.804	11.660	1.131	7.85	1.090	186.66
OBA_{30}	278.3	272.8	432	112.2	5.5	1.976	5.063	1.131	7.85	1.109	128.06
OSN_{30}	271.3	265.4	240	285.6	5.9	2.175	7.160	1.131	7.85	1.108	247.62
OSR_{30}	281.3	274.9	360	190.4	6.4	2.275	7.160	1.131	7.85	1.106	179.39
OSE_{30}	275	267.2	480	129.2	7.8	2.836	6.478	1.131	7.85	1.100	164.79
OSA_{30}	276.8	269.6	648	74.8	7.2	2.601	5.063	1.131	7.85	1.103	112.44
PBN_{30}	274	268	258	292.0	6.0	2.190	7.869	1.131	7.85	1.1075	234.34
PBR_{30}	266.3	261	330	182.5	5.3	1.990	6.291	1.131	7.85	1.1102	161.43
PBE_{30}	271	263.2	570	138.7	7.8	2.878	8.258	1.131	7.85	1.1004	138.77
PBA_{30}	275	267.8	666	109.5	7.2	2.618	7.618	1.131	7.85	1.1028	109.40
PSN_{30}	287	281.5	282	188.0	5.5	1.916	5.538	1.131	7.85	1.1094	196.18
PSR_{30}	275	266	594	117.5	9.0	3.273	7.291	1.131	7.85	1.0957	154.31
PSE_{30}	274	266.2	642	89.3	7.8	2.847	5.989	1.131	7.85	1.1004	123.21
OSA_{30}	276	269	738	70.5	7.0	2.536	5.435	1.131	7.85	1.1035	95.92

Table E-03: Measurement of Corrosion Level (%) & Penetration Rate (mm/year) for 45 Degree Specimens

Sample Name	Initial Wt. (W_i) (g)	Final Wt. (W_f) (g)	Elapsed Time , T (hour)	Corrosion Current, I (μA)	Weight loss, W= (W_i- W_f) (g)	Measured Mass Loss (W_i-W_f)* 100/W_i (%)	Predicted Mass Loss (WIT/nF)100 (%)	Actual Steel Area A_{st}, (cm^2)	Steel Density,(D) (g/cm^2)	Corroded Steel Area A= A_{st}- W/(D*L) (cm^2)	Penetration Rate $R=8.76x10^4$ W/(A T D) (mm/ year)
OBN_{45}	276	266.6	228	567.0	9.4	3.406	13.504	1.131	7.85	1.094	420.49
OBR_{45}	286	276.8	336	378.0	9.2	3.217	13.267	1.131	7.85	1.095	279.06
OBE_{45}	280	271.0	372	256.5	9.0	3.214	9.967	1.131	7.85	1.096	246.40
OBA_{45}	278	270.3	432	148.5	7.7	2.770	6.701	1.131	7.85	1.101	180.69
OSN_{45}	280	272.5	216	357.0	7.5	2.679	8.055	1.131	7.85	1.102	351.74
OSR_{45}	284	276.5	336	238.0	7.5	2.641	8.353	1.131	7.85	1.102	226.12
OSE_{45}	278	267.5	468	161.5	10.5	3.777	7.895	1.131	7.85	1.090	229.73
OSA_{45}	271	262.9	504	93.5	8.1	2.989	4.922	1.131	7.85	1.099	163.16
PBN_{45}	273	262.8	264	403.2	10.2	3.736	11.119	1.131	7.85	1.091	395.19
PBR_{45}	275	264.3	432	268.8	10.7	3.891	12.130	1.131	7.85	1.089	253.80
PBE_{45}	274	267.0	336	182.4	7.0	2.555	6.402	1.131	7.85	1.104	210.67
PBA_{45}	273	265.5	468	105.6	7.5	2.747	5.162	1.131	7.85	1.102	162.34
PSN_{45}	273	263.0	336	273.0	10.0	3.663	9.582	1.131	7.85	1.092	304.20
PSR_{45}	274	264.5	456	182.0	9.5	3.467	8.669	1.131	7.85	1.094	212.56
PSE_{45}	284	272.1	552	123.5	11.9	4.190	7.121	1.131	7.85	1.084	221.86
OSA_{45}	283	274.8	612	71.5	8.2	2.898	4.571	1.131	7.85	1.099	136.07

Table E-04: Measurement of Corrosion Level (%) & Penetration Rate (mm/year) for 60 Degree Specimens

Sample Name	Initial Wt. (W_i) (g)	Final Wt. (W_f) (g)	Elapsed Time , T (hour)	Corrosion Current, I (μA)	Weight loss, W= (W_i- W_f) (g)	Measured Mass Loss (W_i-W_f)* 100/W_i (%)	Predicted Mass Loss (WIT/nF)100 (%)	Actual Steel Area A_{st}, (cm^2)	Steel Density,(D) (g/cm^2)	Corroded Steel Area A= A_{st}- W/(D*L) (cm^2)	Penetration Rate $R=8.76x10^4$ W/(A T D) (mm/ year)
OBN_{60}	281	271.1	180	655.2	9.9	3.523	12.319	1.131	7.85	1.092	561.96
OBR_{60}	279	269.2	264	436.8	9.8	3.513	12.045	1.131	7.85	1.093	379.15
OBE_{60}	283	271.5	372	296.4	11.5	4.064	11.517	1.131	7.85	1.086	317.69
OBA_{60}	268	255.1	480	171.6	12.9	4.813	8.604	1.131	7.85	1.080	277.58
OSN_{60}	276	266.6	192	436.8	9.4	3.406	8.760	1.131	7.85	1.094	499.33
OSR_{60}	274	264.2	288	291.2	9.8	3.577	8.760	1.131	7.85	1.093	347.55
OSE_{60}	278	266.8	360	197.6	11.2	4.029	7.431	1.131	7.85	1.087	319.37
OSA_{60}	275	262.2	516	114.4	12.8	4.655	6.166	1.131	7.85	1.081	256.12
PBN_{60}	273	260.6	288	478.8	12.4	4.5421	14.404	1.131	7.85	1.082	443.90
PBR_{60}	275	261.5	456	319.2	13.5	4.9091	15.204	1.131	7.85	1.078	306.45
PBE_{60}	274	261	480	216.6	13.0	4.7445	10.860	1.131	7.85	1.080	279.84
PBA_{60}	273	259.8	648	125.4	13.2	4.8352	8.488	1.131	7.85	1.079	210.63
PSN_{60}	273	262.4	264	319.2	10.6	3.8828	8.802	1.131	7.85	1.089	411.28
PSR_{60}	274	261	480	212.8	13.0	4.7445	10.670	1.131	7.85	1.080	279.84
PSE_{60}	284	271.4	480	144.4	12.6	4.4366	7.240	1.131	7.85	1.082	270.83
OSA_{60}	283	273.1	528	83.6	9.9	3.4982	4.611	1.131	7.85	1.092	191.58